PREDICTION OF P-Y CURVES
FROM FINITE ELEMENT ANALYSES

By

JAIRUS LAI YAN SHE

B.A.Sc., University of British Columbia, 1983

A THESIS SUBMITTED IN PARTIAL FULFILLMENT OF

THE REQUIREMENTS FOR THE DEGREE OF

MASTER OF APPLIED SCIENCE

in

THE FACULTY OF GRADUATE STUDIES

Department of Civil Engineering

We accept this thesis as conforming

to the required standard

THE UNIVERSITY OF BRITISH COLUMBIA

November 1986

In presenting this thesis in partial fulfilment of the requirements for an advanced degree at the University of British Columbia, I agree that the Library shall make it freely available for reference and study. I further agree that permission for extensive copying of this thesis for scholarly purposes may be granted by the head of my department or by his or her representatives. It is understood that copying or publication of this thesis for financial gain shall not be allowed without my written permission.

Department of Civil Engineering

The University of British Columbia
1956 Main Mall
Vancouver, Canada
V6T 1Y3

Date December 18, 1986

ABSTRACT

The prediction of P-Y curves for undrained clay and sand based on the results of finite element analyses is presented in this thesis.

A higher-ordered finite element program was used in the analyses. The ability of the program to accurately model the undrained soil condition was verified by comparing predicted load-deflection responses with closed form solutions for the cylindrical cavity expansion problem.

Pressuremeter curves were predicted from plane strain axisymmetric finite element analyses. The effect of pressuremeter size on the predicted results was examined.

P-Y curves were predicted for plane strain and plane stress conditions. Values for the initial slope and P_{ult} of the curves were obtained. The curves were normalized for comparison, and simplified methods presented for determining P-Y curves.

Finite element predictions for the pressuremeter and laterally loaded pile problems were also compared. Factors were determined from these comparisons to generate P-Y curves from pressuremeter curves.

TABLE OF CONTENTS

LIST OF TABLES

LIST OF FIGURES

LIST OF FIGURES - Continued

LIST OF FIGURES - Continued

LIST OF FIGURES - Continued

LIST OF FIGURES - Continued

ACKNOWLEDGEMENTS

I thank my supervisor, Dr. P.M. Byrne, for his guidance and interest during this research. Thanks also to Dr. W.D.L. Finn and Dr. Y.P. Vaid, for their review of this manuscript and their helpful comments. My appreciations to my colleagues, U. Atukorala, H. Cheung (where are you?), F. Salgado, and H. Vaziri, for their assistance, and especially to C. Lum, for being my "Vancouver connection".

Appreciation is extended to Ms. E. Seymour-G., for the typing of this manuscript.

Financial support provided by the Natural Sciences and Engineering Research Council is acknowledged with deep appreciation.

Special thanks to Maple, for her "distance" support and encouragement.

Above all, I am grateful to the Lord, for His sovereign control in guiding me to the completion of this research.

CHAPTER 1

INTRODUCTION

1.1 INTRODUCTION

The problem of a pile subjected to lateral loads is one which requires the analysis of the interaction between soil and structural member. The behaviour of the structural member (the pile) is governed by its strength and stiffness properties and those of the surrounding soil. Of prime concern are the bending moments, shear stresses, and displacements of the laterally loaded pile. The ultimate load is generally determined by the maximum moment and shear stress that develop in the pile, while the working load is commonly governed by lateral displacements. The accurate determination of these quantities is therefore essential for pile foundation design.

The behaviour of a laterally loaded pile is a three-dimensional problem. A complete analysis of the problem requires an examination of the complex stress-strain behaviour of the soil surrounding the pile. Near the ground surface, displacements of the soil are three-dimensional. Soil behind the pile may separate from the pile surface, leaving a gap. Stresses at these shallow depths are essentially two-dimensional. At depths greater than several pile diameters, stresses are three-dimensional and strains two-dimensional, with all displacements occurring in the horizontal plane (Scott, 1981). At intermediate depths, both stresses and strains are three-dimensional.

To facilitate the analysis of this complex problem, simplified soil models were considered. Depending on the soil model, methods for predicting the behaviour of laterally loaded piles can be classified

into three categories (Atukorala & Byrne, 1984):

1. The Winkler Foundation Approach: the soil is represented by a set of independent linear or non-linear springs distributed along the length of the pile.
2. The Elastic Continuum Approach: the soil is idealized as a linear elastic, isotropic and homogeneous continuum.
3. The Finite Element Approach: the surrounding soil is discretized into finite elements, each possessing the stress-strain properties of the soil.

At present, the Winkler approach is most commonly used for analysing the response of a laterally loaded pile. With this method, the soil surrounding the pile is replaced by discrete springs. Soil resistance to pile deflection is represented by the load-deflection characteristics of the springs and are specified by "P-Y" curves, where P is the soil resistance to lateral pile displacement per unit length of pile at a given depth, and Y is the corresponding horizontal pile deflection at that depth. A typical P-Y curve is shown in Figure 1.1. Since P-Y curves are defined by soil resistance, they can be expected to vary for different soil properties. The size and shape of the pile section, and the roughness of the pile surface can also affect the P-Y relationship.

The key to the laterally loaded pile problem, then, lies in the accuracy of the P-Y curves. Aside from instrumented pile loading field tests, which are both costly and time-consuming, methods for determining P-Y curves based on the results of pressuremeter expansion

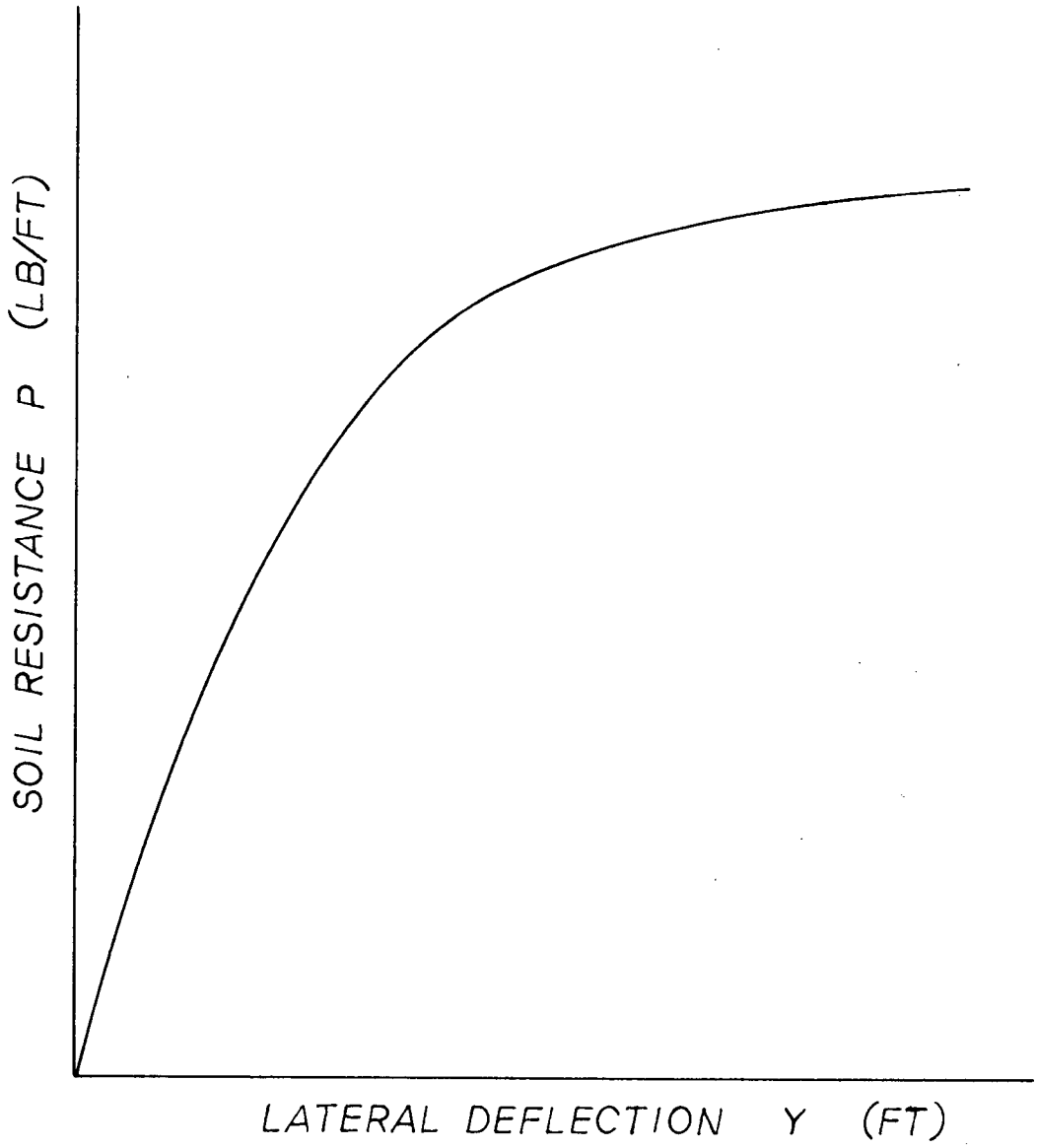

FIGURE 1.1: TYPICAL P-Y CURVE

tests, centrifuge tests, and finite element analyses have been proposed.

Analysis of the laterally loaded pile problem by the Winkler approach with the use of P-Y curves can be performed by the finite difference method. The method and its formulation are described by Focht & McClelland (1955). Computer programs employing this technique were developed by Reese (1977) and Reese & Sullivan (1980) to perform the analyses. The use of the programs are facilitated by the recent introduction of interactive graphics. A modified version of Reese & Sullivan's program (COM624) with graphic input and output capabilities is currently in use at the University of British Columbia (Byrne & Grigg, 1982).

1.2 SCOPE OF THESIS

The purpose of the research is to predict P-Y relationships for laterally loaded piles using finite element analyses. P-Y curves predicted for both cohesive and cohesionless soils using non-linear elastic soil models are presented.

A recently-developed higher-ordered two-dimensional finite element program was used in the study. The program was not tested for the type of analyses performed to predict P-Y curves. Consequently, to verify the accuracy of the P-Y results, load-deflection responses for uniaxial compression of test elements and cavity expansion in infinite elastic-plastic media were predicted and compared with closed form solutions.

Load-deflection responses for pressuremeter expansion were also predicted using the plane strain axisymmetric finite element model

used in the cavity expansion analyses. The effect of pressuremeter size was examined.

P-Y curves were determined for both cohesive and cohesionless soils. The sensitivity of the P-Y predictions to various parameters in the finite element method were also examined. The predicted curves were normalized with respect to soil strength and pile size, and simplified methods devised to generate P-Y curves from fundamental soil properties. Finally, P-Y predictions were compared with pressuremeter results to determine factors for converting pressuremeter curves to P-Y curves.

1.3 ORGANIZATION OF THE THESIS

This thesis consists of twelve chapters. A brief review of previous research, highlighting the methods and the results, is given in Chapter 2.

Chapter 3 contains a discussion of the formulation of the finite element model for analysing the laterally loaded pile problem to predict P-Y curves. The validity of the formulation is considered in light of previous research on the problem.

The importance of interface elements is discussed in Chapter 4. Results of previous work involving the use of these special elements to model the behaviour of the soil-pile interface are presented. A simplified formulation for the interface elements used in this study is given.

The finite element program used in the research is discussed briefly in Chapter 5. Results of uniaxial compression and cavity expansion analyses performed to verify the capabilities of the program

are presented in Chapters 6 and 7.

Chapter 8 deals with the pressuremeter problem. Analyses were performed by modelling pressuremeter expansion as an axisymmetric cylindrical cavity expansion problem.

The P-Y curve problem is considered in Chapters 9 to 11. Plane strain and plane stress P-Y curves were predicted for both undrained clay and sand. The effects of pile diameter and mesh size on the predicted P-Y responses were examined. Normalized P-Y curves based on the results of Chapter 9 are shown in Chapter 10. Simplified methods for determining P-Y curves were derived from the normalized curves. In Chapter 11, predicted P-Y curves are compared with pressuremeter curves determined in Chapter 8. Factors for converting pressuremeter curves to P-Y curves were determined.

A summary of the research and the conclusions is presented in Chapter 12.

CHAPTER 2

REVIEW OF PREVIOUS WORKS

2.1 INTRODUCTION

The prediction of P-Y curves for the design of laterally loaded piles has been the subject of much research over the past 10 or 15 years. With the advent of offshore structures for oil exploration and recovery, and the increasing importance of seismic design for foundations, the laterally loaded pile problem was brought to the foreground of research. Indeed, the interest of oil companies has led to their funding of much of the research. An annual conference, the Offshore Technology Conference, now in its eighteenth year, was established for the exchange of information related to offshore design and construction. Proceedings of the annual conferences fill many volumes, a sizeable portion of which deals with offshore piling problems.

The successful design of pile foundations subjected to lateral forces, whether they be ice, wave, wind, or seismic, is contingent on the accuracy of P-Y relationships describing the resistances of foundation soils to lateral pile displacements. Methods for predicting the P-Y curves, based on empirical, mathematical, and analytical solutions, were proposed by various authors. A brief review of these methods and their results is given in Section 2.2. The finite element method of analysis is discussed in greater detail in Chapter 3.

2.2 REVIEW OF PREVIOUS WORK

2.2.1 Empirical Method

Of the various methods developed to predict P-Y curves, the empirical approach is the most widely used in industry. Empirical curves based on P-Y relationships derived from instrumented full-scale pile load tests were developed by Matlock (1970) for soft clays, Reese & Welch (1975) and Reese et al. (1975) for stiff clays, and Reese et al. (1974) for sands. Though simple to use, these methods require estimates of the ultimate lateral soil resistances, P_{ult}, and reference strain values, ε_{50}, corresponding to one-half of the maximum deviator stresses. Values for ε_{50} can be obtained from laboratory stress-strain curves, or estimated from tables of representative values if no stress-strain curves are available (Reese & Sullivan, 1980, and Reese et al., 1975). Values of P_{ult} are calculated from equations derived by Matlock (1970) and Reese et al. (1974, 1975), assuming passive wedge-type failure near the ground surface and failure by lateral soil flow around the pile at greater depths. Matlock's equation for clay is

$$P_{ult} = N_p c D \qquad 2.1$$

$$N_p = 3 + \frac{\sigma_v'}{c} + J\frac{H}{D}, \qquad 3 \leq N_p \leq 9$$

where

c = undrained strength

D = pile diameter

σ_v' = overburden effective stress at depth H

J = coefficient ranging from 0.25 to 0.5, depending on the soil. A value of 0.5 is applicable for the soft offshore clay of the Gulf of Mexico, and 0.25 is valid for stiffer clays.

For sand, the theoretical ultimate lateral resistance for wedge-type failure at shallow depths is given by

$$P_{ct} = \gamma H \left[\frac{K_o H \tan\phi' \sin\beta}{\tan(\beta-\phi') \cos\alpha} + \frac{\tan\beta}{\tan(\beta-\phi')} (D + H \tan\beta \tan\alpha) + K_o H \tan\beta (\tan\phi' \sin\beta - \tan\alpha) - K_a D \right] \qquad 2.2$$

And for lateral flow at greater depths,

$$P_{cd} = \gamma HD \left[K_a(\tan^8\beta - 1) + K_o \tan\phi' \tan^4\beta \right] \qquad 2.3$$

where

γ = effective unit weight of the sand

K_o = coefficient of lateral pressure at rest

K_a = coefficient of active lateral pressure

$= \tan^2(45^o - \phi'/2)$

ϕ' = internal friction angle of the sand

$\beta = 45^o + \phi'/2$

$\alpha = \phi'/2$

Agreement between the theoretical P_c values and the values obtained from the pile load tests was poor, and consequently, P_c was adjusted by a factor A according to

$$P_{ult} = A\ P_c \qquad 2.4$$

Values for the adjustment factor, A, were determined by dividing the experimental ultimate resistances by the theoretical P_c values. The values for A are shown in Figure B.2 in Appendix B.

2.2.2 Centrifuge Tests

The laterally loaded pile problem was also studied under controlled laboratory conditions. Centrifuge tests on model pipe piles driven in saturated sand were conducted by Barton et al. (1983). Modelling a prototype pile with a diameter of 25 inches, bending moments (M) were measured at points along the length of the model pile subjected to lateral loads at the pile head. Cubic spline interpolatory functions were fitted to the data and double integrations and differentiations performed to obtain values for Y and P. The mathematical relationships for Y and P are

$$Y = \iint (M/EI)dz \qquad 2.5$$

and

$$P = d^2M/dz^2 \qquad 2.6$$

where

EI = stiffness of the pile

z = depth

The accuracy of P values determined according to Equation 2.6 is questionable. Derivatives of the cubic spline function are very sensitive to the curve shape and the errors are greatly multiplied by the double differentiation. Consequently, considerable errors may

exist in the P-Y curves developed by this method.

The results of the centrifuge tests suggest that P_{ult} values determined from Reese's equations (2.2 to 2.4) overestimate soil resistances at large depths and underestimate resistances near the ground surface. P_{ult} was underestimated by factors of approximately 1.9, 1.6 and 1.1 at depths of 2, 4 and 6 feet, respectively. Values of P_{ult} were not obtained from the centrifuge tests for depths greater than 6 ft.

The shape of the centrifuge P-Y curves also differs markedly from the shape of Reese's empirical curves. The initial slopes of the empirical curves are much steeper than those of the centrifuge curves, and the curves flatten out much quicker than the centrifuge predictions at shallow depths. Overall, there is little resemblance between the P-Y curves predicted by the two methods.

2.2.3 Finite Element Method

The finite element method of analysis was used by a number of researchers to predict P-Y curves for sand and undrained clay. Plane stress finite element formulations were used to analyse the problem for shallow depths while plane strain formulations were used for greater depths. The models and formulations used by the researchers are similar and are described in Chapter 3.

P-Y curves for undrained clay were predicted by Yegian & Wright (1973), Thompson (1977), and Atukorala & Byrne (1984). A wide range of values for P_{ult} were obtained by the researchers.

Using interface elements to model soil-pile interface behaviour, and assuming a soil-pile adhesion factor, f_c, of 0.3

($c_a = f_c c_u$; see Section 4.2.2), a P_{ult} value of approximately 12cD was obtained by Yegian for plane strain analysis. Similarly, a value of 6.6cD was determined from plane stress analyses.

Thompson, following the work of Yegian, performed P-Y analyses for a wide range of soil-pile interface conditions. P_{ult} values ranging from about 6cD for complete soil-pile separation behind the pile to 11cD for no separation were obtained for plane strain analysis. Likewise, values ranging from 3.1cD to 6.1cD were determined from plane stress analyses. Neither Thompson nor Yegian made any conclusions regarding the initial slopes and shapes of the P-Y relationships.

P-Y curves for sand were also predicted by Barton et al. (1983) using the finite element method. The predicted curves were compared with experimental curves from centrifuge tests (see Section 2.2.2). Good agreement exists between the computed curves and centrifuge curves at shallow depths. For depths exceeding 3 ft, however, the finite element predictions were considerably less stiff than the centrifuge curves. No values were determined for P_{ult}, nor was any conclusion drawn regarding the initial slopes of the P-Y curves.

Plane strain P-Y analyses performed by Atukorala produced results similar to those of the other researchers. Matlock's empirical curves for soft clay were shown to underestimate P_{ult} while Reese's curves for sand drastically overestimate P_{ult}, perhaps by as much as 6 times.

Results of research conducted by the various authors yielded one common observation: Matlock's and Reese's empirical curves for soft clay and saturated sand do not agree with finite element

predictions. Large discrepancies exist in the initial slope, shape, and ultimate soil resistance of the P-Y relationships predicted by the two methods. Since the empirical curves were developed from limited pile load tests, their applicability for soils other than those in which the tests were conducted is questionable. On the other hand, many factors that could affect the predicted results (ie: mesh size, boundary conditions, pile diameter, interface properties, soil disturbances) were not considered in the finite element analyses. Consequently, the validity of the numerical P-Y curves is also in doubt.

The ultimate proof of the validity of the finite element predictions lies in their ability to predict field data. Bending moments, shear stresses, and deflections of piles determined by using finite element P-Y curves in conjunction with finite difference programs such as COM624 (see Section 1.1) can be compared with results obtained from field pile load tests. Reasonable agreement between predicted and actual values serves to validate the finite element approach to P-Y prediction. Little work, however, has been done in this respect. Much additional research is warranted to fully study the laterally loaded pile problem.

CHAPTER 3

FINITE ELEMENT MODEL FOR LATERALLY LOADED PILE PROBLEM

3.1 INTRODUCTION

The prediction of P-Y curves for single laterally loaded piles from finite element analyses has received much attention in recent years. Previous studies of the problem were conducted by Yegian & Wright (1973), Thompson (1977), Barton & Finn (1983), and Atukorala & Byrne (1984). A review of their works is contained in Chapter 2.

The methods of analysis and the finite element models used by the researchers are similar. An overview of the finite element formulation is given in the following sections.

3.2 FINITE ELEMENT MESH

The finite element method for predicting P-Y curves requires the analysis of the pile and the surrounding soil. A horizontal cross-section of unit thickness is taken of the pile and soil as shown in Figure 3.1. At a sufficiently large distance, R, away from the pile, the soil is generally assumed to be unaffected by the pile in terms of displacements. A displacement boundary can then be inserted at this location and the outlying soil eliminated from further consideration. The selection of the correct value of R, however, is of importance and is discussed in Section 3.2.2. The resulting finite element mesh is a circular disk with the pile located at the centre. The outer boundary of the disk is fixed, assuming zero displacements.

Concentrated loads (P), representing lateral forces on the

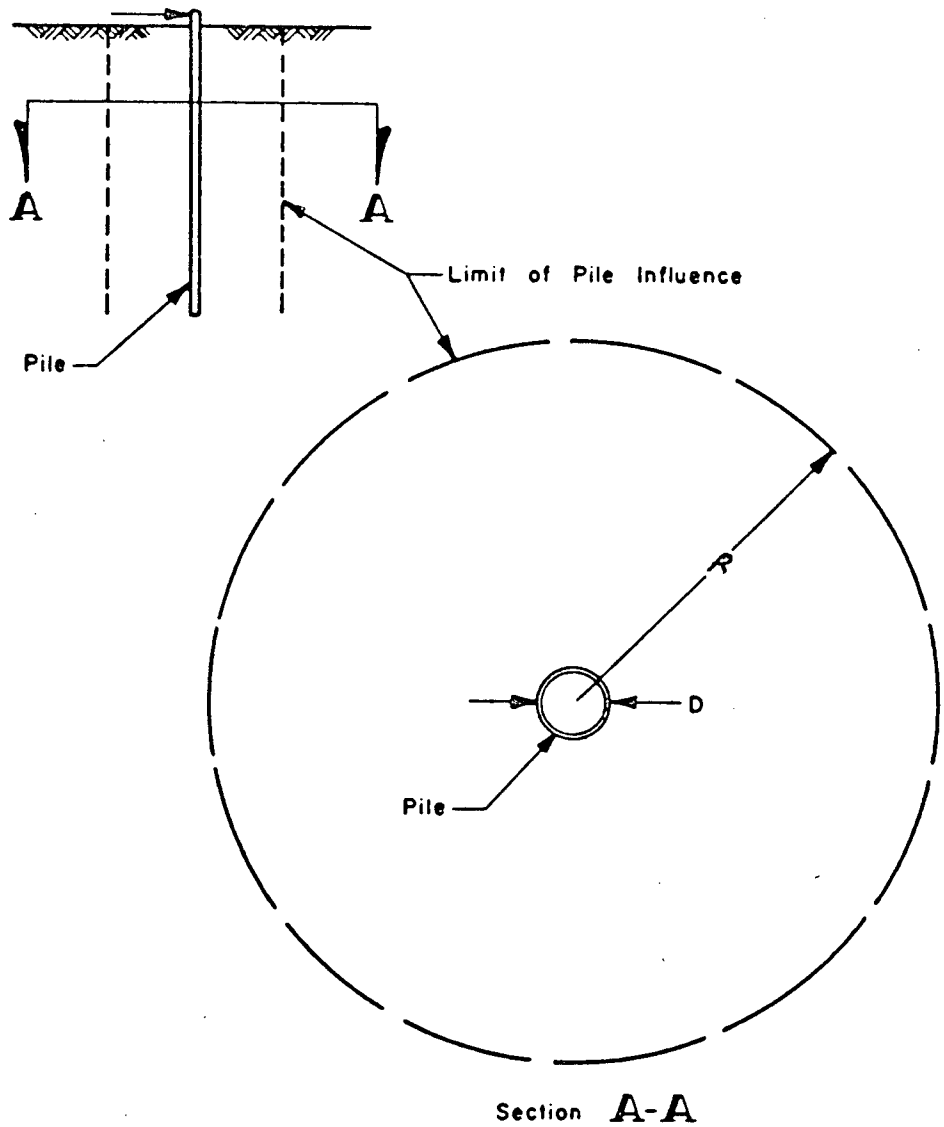

FIGURE 3.1: ZONE OF SOIL-PILE INTERACTION

(After Yegian & Wright, 1973, p. 673.)

pile, are applied to the pile centre. Pile deflections (Y) resulting from the applied loads produce the desired P-Y curves. Strictly speaking, P is the soil resistance per unit length of a pile subjected to a lateral displacement of Y. For the purpose of the finite element model, however, it is more convenient to consider P as the applied load. In any event, the two quantities are equivalent under an equilibrium load-deflection condition.

In all of the analyses, piles were assumed to be rigid. Accordingly, elements representing the piles were made 500 times stiffer than the surrounding soil elements to prevent significant pile deformations.

Since loads are applied to the pile along an axis of symmetry, only half of the mesh needs to be analysed, as illustrated in Figure 3.2. Rollers were placed along the symmetry boundary to ensure zero displacements perpendicular to the direction of loading.

In addition to the symmetry boundary, a line of anti-symmetry also exists, but only under the condition that stresses in the soil must not approach levels where tensile failure occurs and causes the soil to separate from the pile (Yegian & Wright, 1973). The use of this axis of anti-symmetry permits just one quadrant of the disk to be analysed for the problem. However, the required condition of no soil-pile separation may not be valid for large lateral loads or for analyses of pile sections at shallow depths (see also Sections 3.4 and 4.2.3). Consequently, the boundary of anti-symmetry was not considered and a half-disk was used in the analyses (Figure 3.2). In analysing only half of the disk, the horizontal load for a corresponding lateral displacement, Y, must be doubled to account for soil resistance on the

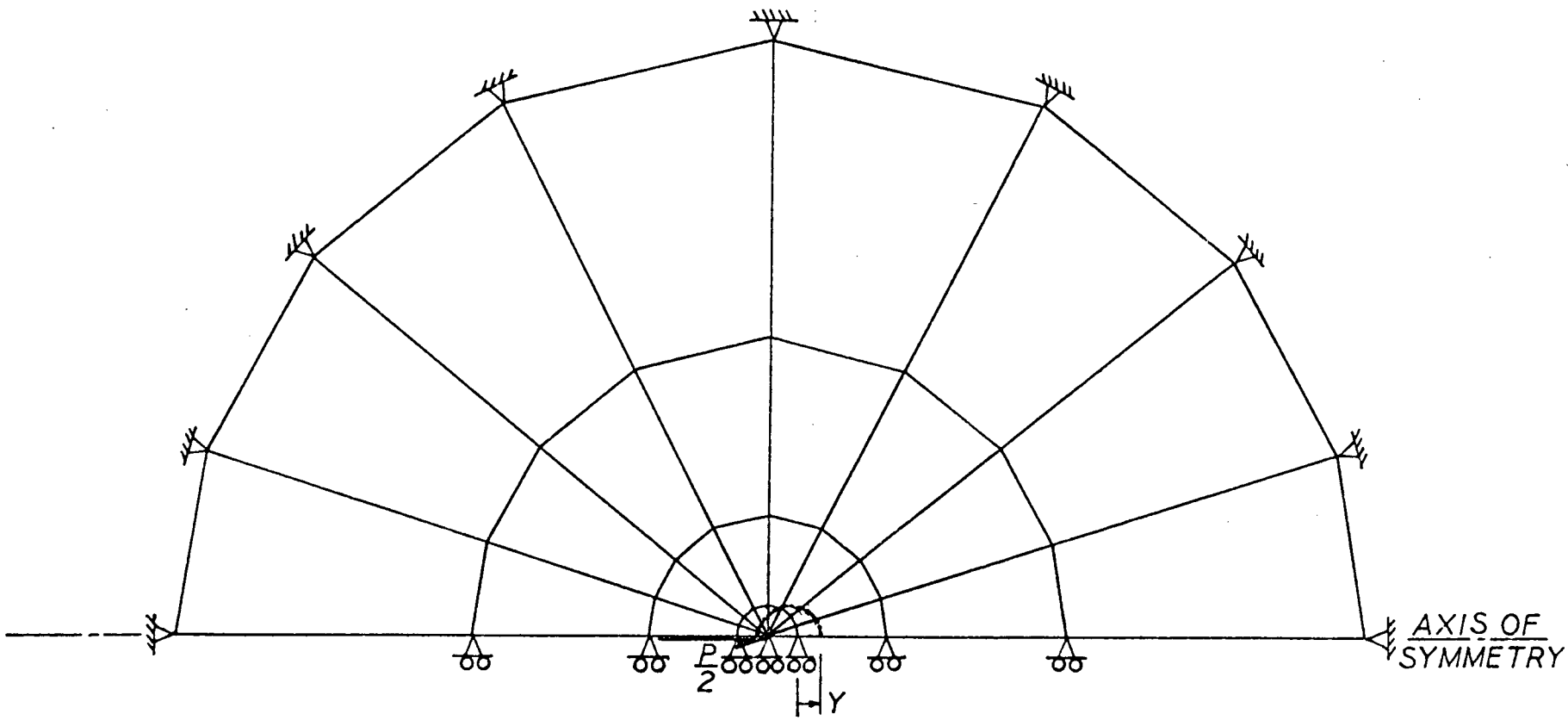

FIGURE 3.2: FINITE ELEMENT MESH FOR THE LATERALLY LOADED PILE PROBLEM

omitted half of the pile section.

3.2.1 Validity of the Disk Concept

In using a disk with fixed outer boundary to represent the soil in two-dimensional finite element analysis, a finite zone of influence is assumed. In reality, the boundary of this zone is at infinity. In three-dimensional analysis where vertical load-spreading and soil displacements are possible, the boundary can be moved in from infinity to some finite radius without significant error. But, if the soil is replaced by uncoupled disks, then pile displacements under lateral loads depend on the size of the disks. The problem then rests in the determination of the appropriate disk radius R to yield the correct pile displacements. In other words, errors introduced by using uncoupled disks can be compensated for by selecting an appropriate disk radius.

3.2.2 Mesh Radius

Based on comparisons of actual P-Y curves from field load tests and P-Y curves predicted using various values for R, a value of R = 8D (D = pile diameter) was determined by Yegian & Wright (1973). Thompson (1977), following the work of Yegian, concluded that zero lateral soil displacements beyond 20D, or about half the pile length, would be appropriate. Recent studies by Atukorala & Byrne (1984) attempted to model an outer boundary at infinity, using a disk radius of 20D with "infinity springs" as described by Byrne & Grigg (1980). The use of "infinity springs" for the laterally loaded pile problem is incorrect, however, since soil is displaced laterally rather than radially.

In his research, Thompson noted that the use of different mesh radii did not affect the predicted value of P_{ult}, but did affect the initial slope of the P-Y curve. Increases in mesh radius resulted in decreases in the slope, as illustrated in Figures 3.3 and 3.4. It is apparent from Thompson's results that as R tends to infinity, the slope of the P-Y curve approaches zero.

The results of Thompson's research on the effects of varying the mesh radius are supported by theoretical analyses. Baguelin et al. (1977) examined the lateral reaction of piles in an elastic-plastic medium, assuming plane strain condition and perfect soil-pile adhesion. In this two-dimensional study using a rigid circular pile section and a fixed outside boundary at radius R from the pile centre, pile displacement (Y) is given by

$$Y = \frac{P}{8\pi E} \frac{1 + \mu}{1 - \mu} \left[(3 - 4\mu) \ln\left[\frac{R^2}{r^2}\right] - \left[\frac{R^2 - r^2}{R^2 + r^2}\right]\left[\frac{2}{3 - 4\mu}\right] \right] \qquad 3.1$$

where

P = lateral force (per unit length) on pile

μ = Poisson's ratio

r = radius of pile = D/2

Clearly, displacement depends on R, and tends to infinity as R tends to infinity.

The results given by Equation 3.1, though valid for a two-dimensional problem, are unrealistic for actual pile behaviour. A three-dimensional study was therefore conducted by Baguelin et al. to determine the value of R for the two-dimensional model that will give

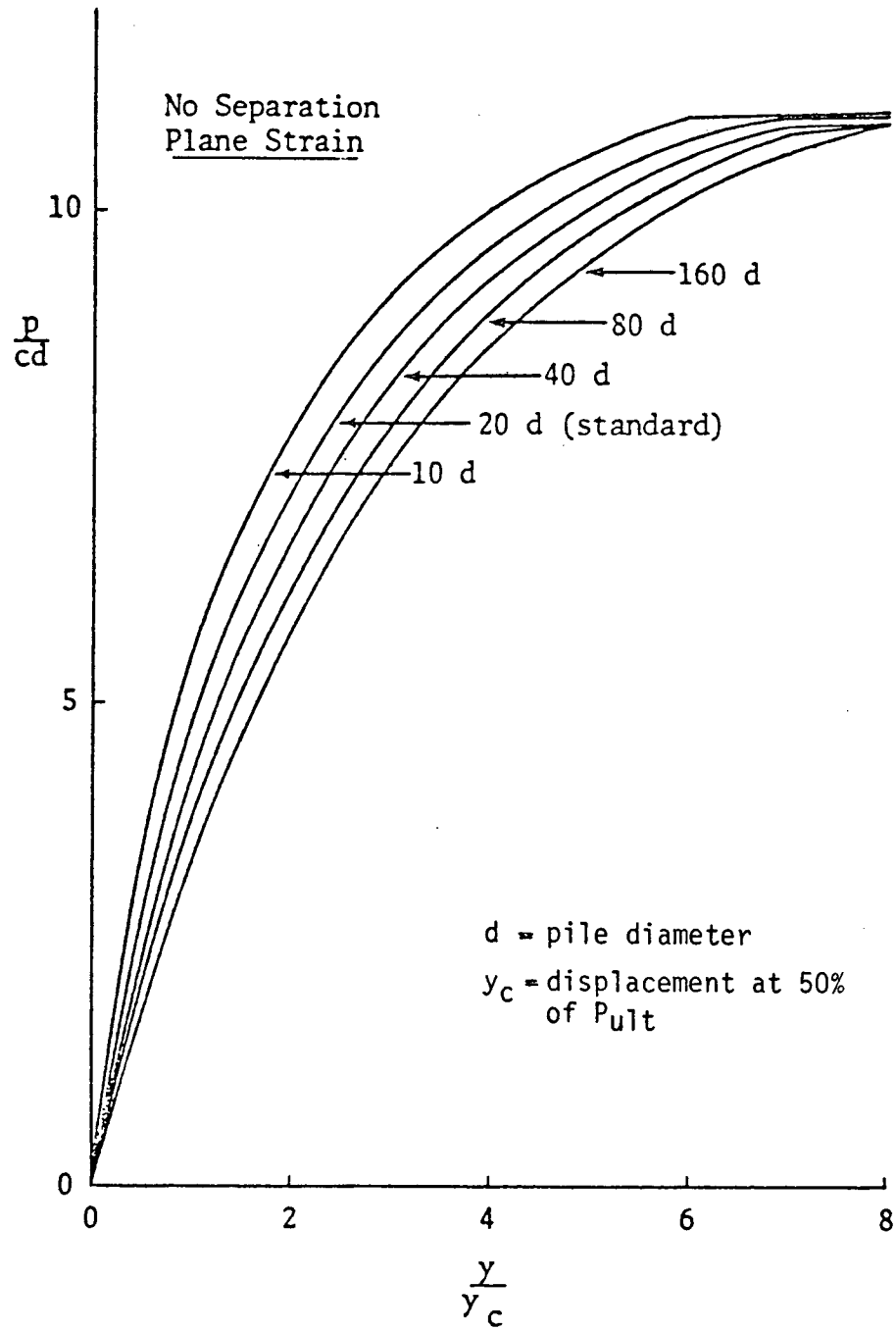

FIGURE 3.3: EFFECT OF MESH RADIUS ON PLANE STRAIN P-Y CURVE PREDICTIONS

(After Thompson, 1977, p. 172.)

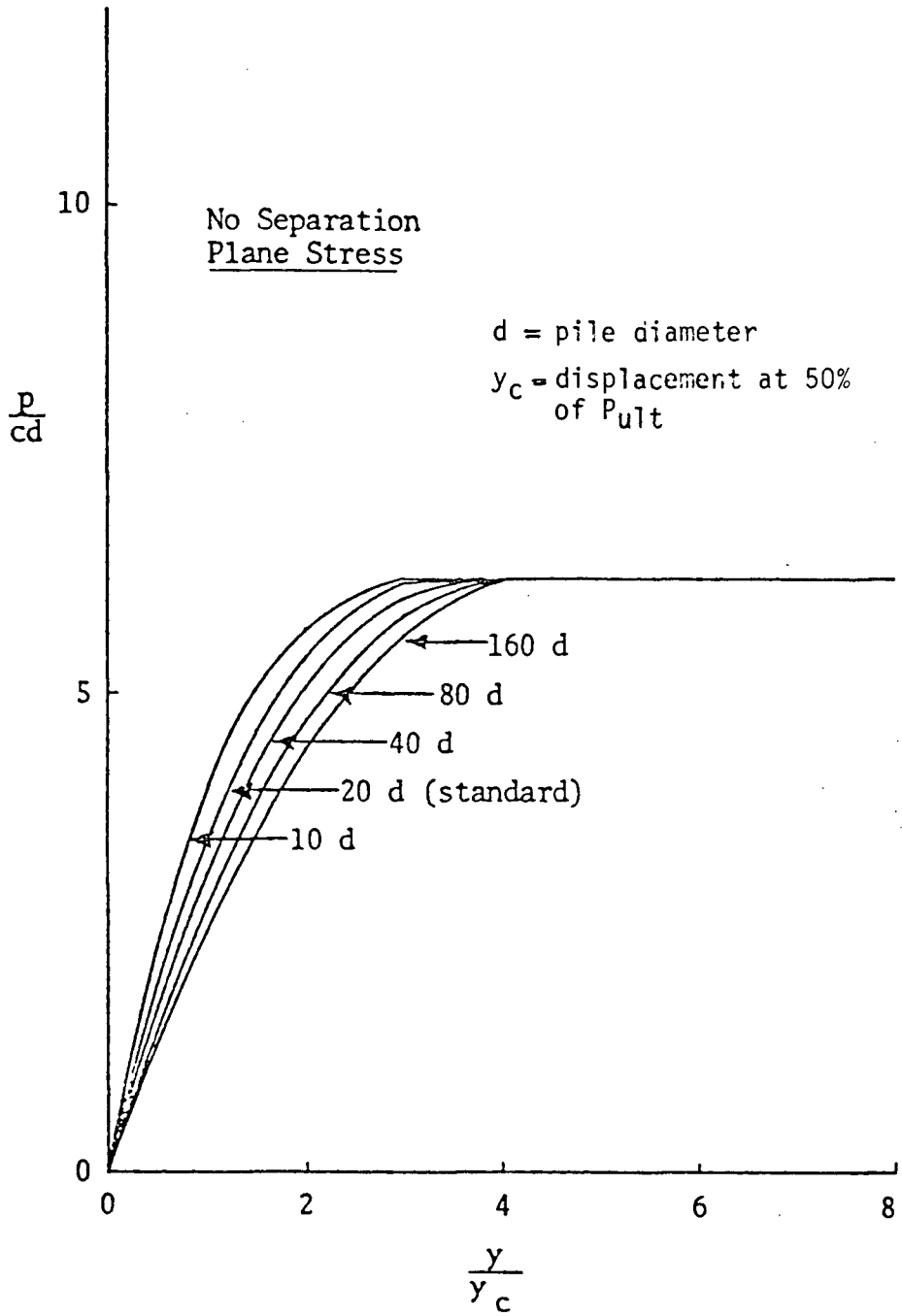

FIGURE 3.4: EFFECT OF MESH RADIUS ON PLANE STRESS P-Y CURVE PREDICTIONS

(After Thompson, 1977, p. 173)

displacements representative of actual pile behaviour.

In this study, the soil surrounding the pile was divided into two zones. For soil within a radius r_a, plane strain condition was assumed. Beyond r_a, soil behaviour is three-dimensional. Deformations along the plane of loading for the two-dimensional model (outer radius R) and three-dimensional model were compared. The value of R was chosen to give equal two-dimensional and three-dimensional displacements at the boundary r_a, as illustrated in Figure 3.5. Values of R thus derived for piles with free heads subjected to horizontal loads at the top are:

For flexible piles $(h/l_o > 7/3)$: $R = 7l_o$

For rigid piles $(h/l_o < 7/3)$: $R = 3h$ 3.2

where

h = embedded length

l_o = soil-pile stiffness factor = $4E_pI_p/E_{so}$

E_p = pile modulus

I_p = moment of inertia for pile section

= $1/4\pi r^4$ for circular pile

E_{so} = initial soil modulus

Equation 3.2 was used to determine the mesh radius for the P-Y curve finite element analyses. Although the equations were derived for an elastic-plastic medium and assumed perfect soil-pile adhesion, they are, nonetheless, valid for the initial elastic behaviour of "real" soils prior to soil-pile separation. Consequently, the initial portion of the P-Y responses can be predicted with accuracy. Moreover, as

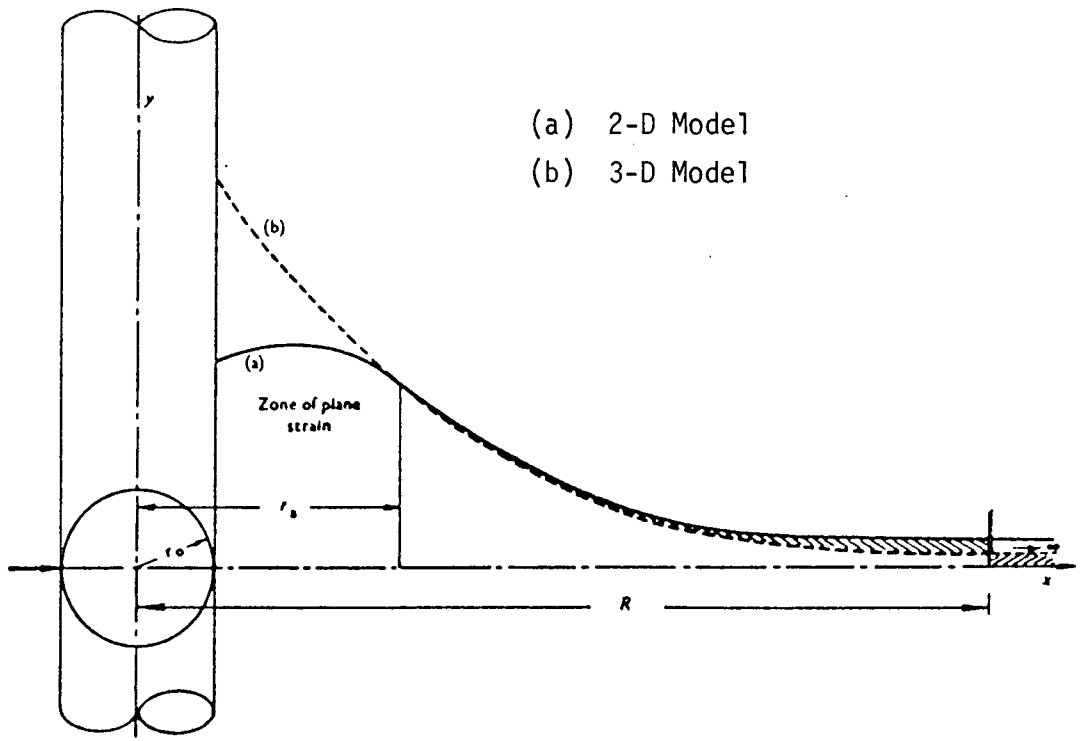

FIGURE 3.5: 2-D AND 3-D DEFORMATIONS ALONG THE LOADING AXIS

(After Baguelin et al., 1977, p. 424)

shown by Thompson, the mesh radius does not affect the value of P_{ult}, and has only a moderate influence on the shape of the P-Y curve (see Figures 3.3 and 3.4). Overall, in the absence of soil-pile separation, fairly accurate P-Y curves should be predicted by using values of R determined from Equation 3.2. Where soil-pile separation does occur, softer P-Y responses and lower values of P_{ult} can be expected.

3.3 PLANE STRESS AND PLANE STRAIN ANALYSES

In using two-dimensional finite element models to predict P-Y curves, a plane strain formulation was used for analyses at large depths, and a plane stress formulation for analyses at shallow depths.

At large depths, the plane strain assumption is justifiable on the basis that pressures from soil above and below are sufficiently large to prevent vertical displacements. Consequently, displacements are restricted to the horizontal plane with soil flowing around the pile as the pile is displaced laterally under loads.

For analyses at shallow depths, the plane strain formulation is invalid. At the ground surface, vertical stress is zero and displacements are three-dimensional. Consequently, the two-dimensional plane stress formulation is appropriate. A transition zone, consisting of three-dimensional stresses and strains, exists between the plane stress condition at the surface and the plane strain condition at greater depths.

Reese (1958) used a passive wedge failure condition to estimate P_{ult} near the surface of a saturated clay. For P_{ult} at large depths, a block flow model was used. These failure conditions are

illustrated in Figure 3.6. A similar method was used to determine P_{ult} for sand (Reese et al., 1974).

Based on Reese's results, Thompson (1977) determined that the depth at which plane strain becomes applicable for saturated clay is between 1.5 and 3.0 pile diameters, depending on the pile roughness and soil-pile adhesion. Thompson further concluded that the transition from plane stress to plane strain is gradual and may be approximated by a linear combination of the responses produced by the two deformation conditions.

3.4 SOIL-PILE ADHESION

As mentioned in Section 3.2, soil-pile adhesion affects the displacement and failure characteristics of the laterally-loaded pile and soil system. The ultimate soil resistance, P_{ult}, is also a function of the degree of soil-pile adhesion.

Figures 3.7 and 3.8 shows the results obtained by Thompson (1977) for plane stress and plane strain conditions. Using various values of σ/c (ratio of initial horizontal stress σ to undrained shear strength c) to represent different degrees of insitu soil confinement or soil depths, normalized P-Y curves were predicted for saturated clays. Using a constant value for c, results for adhesion conditions ranging from complete soil-pile separation at zero depth (σ=0) to no separation at large depths were obtained. Separation was assumed when stress changes (decreases) behind the pile exceeded the initial confining stress σ. Increases in P_{ult} with increasing adhesion are shown by the graphs.

Randolph & Houlsby (1984), using plasticity theory, presented

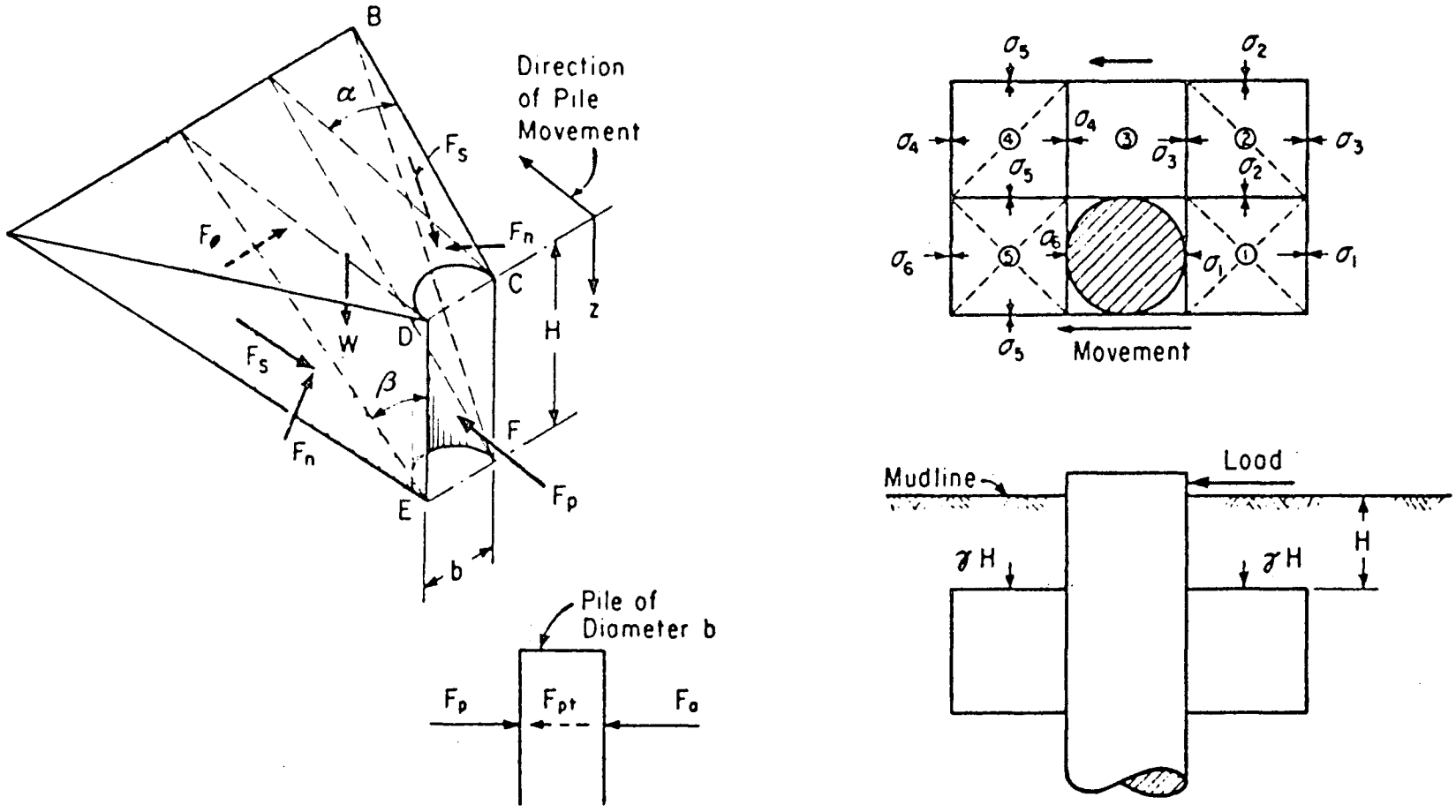

a) Passive Wedge

b) Lateral Flow

FIGURE 3.6: ASSUMED FAILURE MECHANISMS FOR LATERALLY LOADED PILE PROBLEM

(After Reese et al., 1974, p. 481)

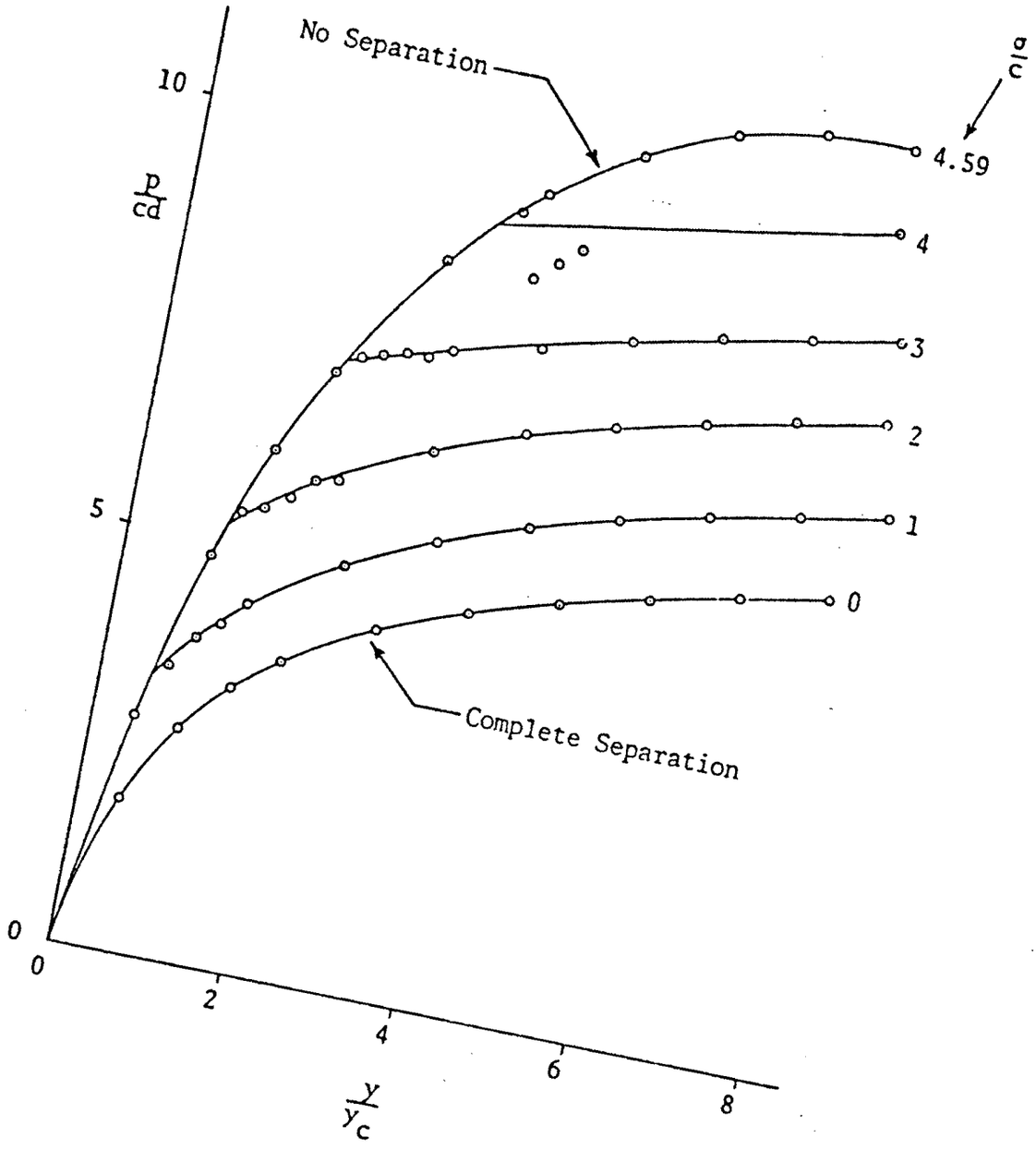

FIGURE 3.7: EFFECT OF SOIL-PILE ADHESION ON PLANE STRAIN P-Y CURVE PREDICTIONS

(After Thompson, 1977, p. 82)

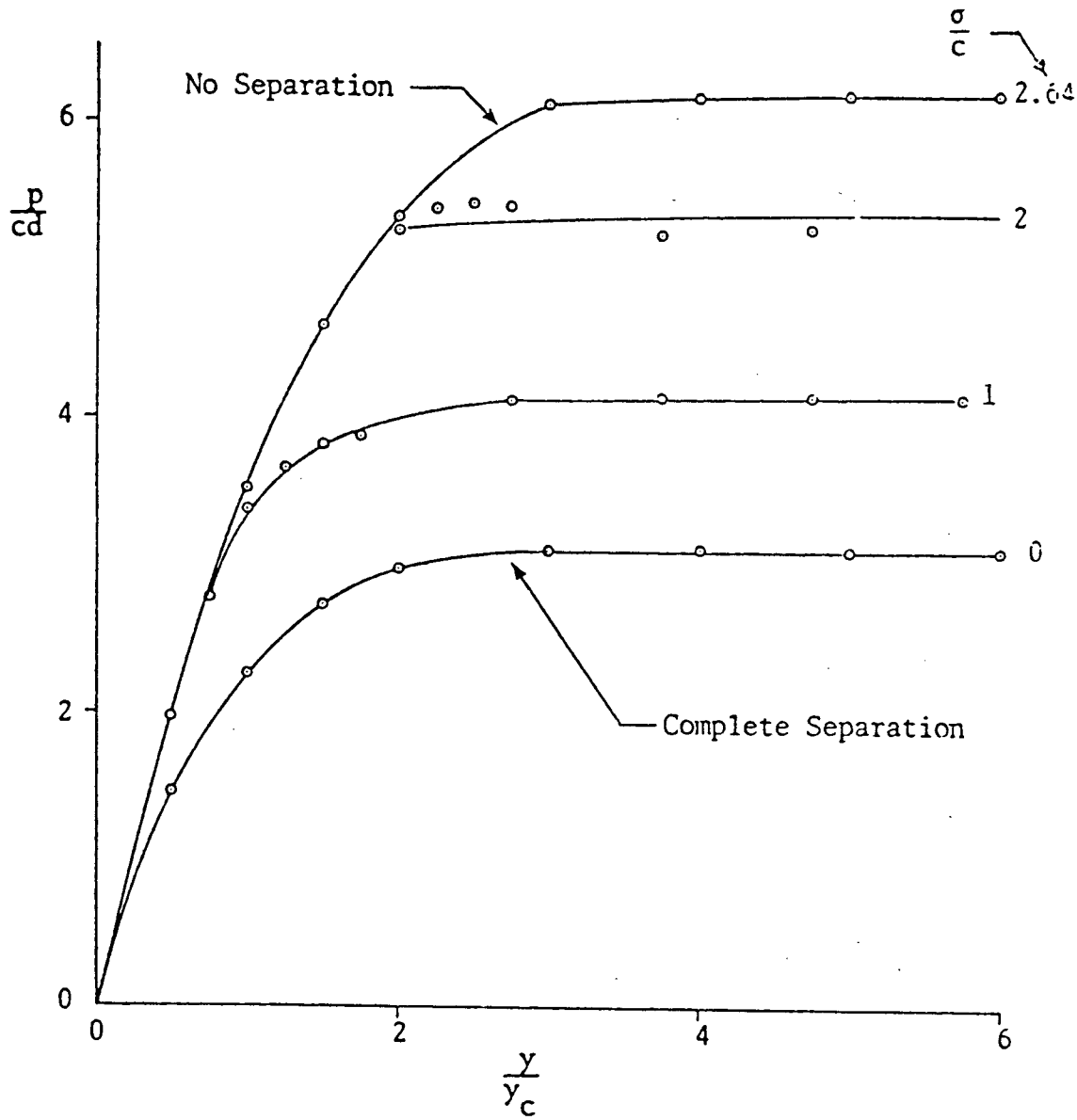

FIGURE 3.8: EFFECT OF SOIL-PILE ADHESION ON PLANE STRESS P-Y CURVE PREDICTIONS

(After Thompson, 1977, p. 81)

solutions for P_{ult} for various values of α, the coefficient of adhesion (ie: $c_a = \alpha c$ as discussed in Section 4.2.3). Upper and lower bound solutions determined were shown to be identical, thus indicating an exact solution. Their results for the plane strain deformation of an undrained cohesive soil are presented in Table 3.1. Again, a clear trend of increasing P_{ult} with increasing adhesion (ie: α) is indicated.

In the finite element analyses performed to predict P-Y curves in Chapters 9 to 11, interface elements were used to model the soil-pile adhesion characteristics of the problem. The interface elements and their properties are discussed in Chapter 4.

TABLE 3.1

EFFECT OF SOIL-PILE ADHESION ON P_{ult} FOR PLANE STRAIN ANALYSIS OF UNDRAINED CLAY

α	P_{ult}/cd
0·0	9·142
0·1	9·527
0·2	9·886
0·3	10·220
0·4	10·531
0·5	10·820
0·6	11·088
0·7	11·336
0·8	11·563
0·9	11·767
1·0	11·940

(After Randolph & Houlsby, 1984, p. 617)

CHAPTER 4

INTERFACE ELEMENTS

4.1 INTRODUCTION

To properly model the lateral movement of a pile section through the soil, elements exhibiting the appropriate soil-pile interface behaviour are needed. Figure 4.1 illustrates diagrammatically the response of the soil to lateral pile displacement. In the absence of interface elements, the soil is bound to the pile surface (Figure 4.1b). Movement of the pile forces the surrounding soil to deform, inducing large shear stresses along the side of the pile and tension stresses behind the pile. The presence of large shear stresses, however, will likely cause slippages along the interface. Tensile stresses may result in the development of a cavity behind the pile, or gapping. If interface slippages and gapping are neglected in developing P-Y relationships, soil resistances and the stiffness of the load-deflection responses may be over-predicted.

A better model of the soil-pile interaction allows for soil movements at the interface. As the pile is displaced laterally, high stresses develop in front of the pile while stress reductions occur at the back (Reese et al., 1974). This situation is illustrated in Figure 4.2. At large depths where the initial confining pressure is high (Figure 4.2b), tension stresses will not develop during loading. The resulting stress distribution may be as shown in Figure 4.2c. Under these circumstances, soil adjacent to the pile flows around the pile from front to back with no separation taking place (Randolph & Houlsby, 1984, and Yegian & Wright, 1973). At shallower depths,

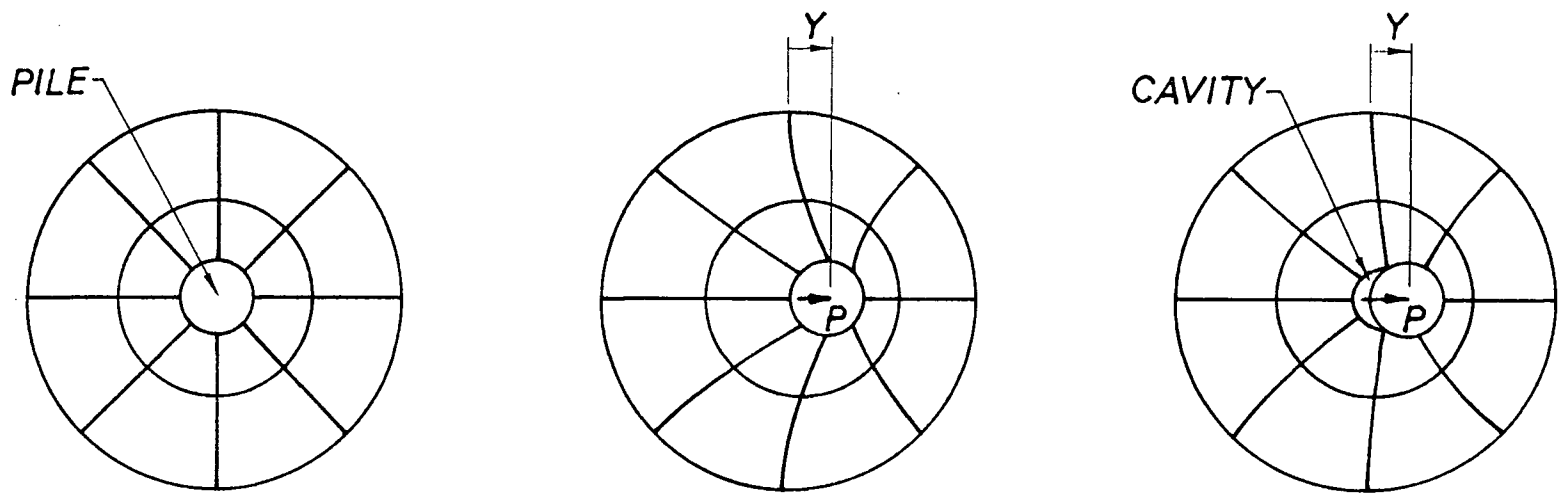

a) Finite Element Mesh Prior to Loading

b) Mesh During Loading: Soil Bound to Pile Surface - Large Soil Deformation and Resistance

c) Mesh During Loading: Soil Allowed to Separate and Shear Along Side of Pile - Less Soil Deformation and Resistance

FIGURE 4.1: DEFORMATION OF FINITE ELEMENT MESH DURING LATERAL PILE LOADING

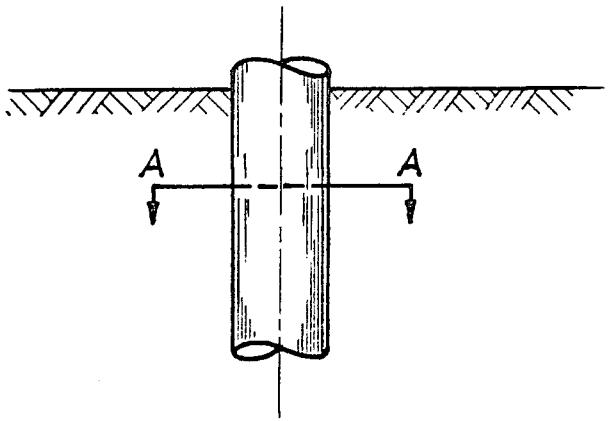

a) Laterally Loaded Pile

SECTION A-A

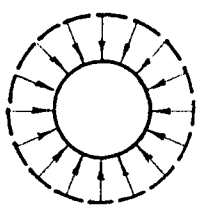

b) Soil Pressure Distribution Prior to Loading (Assuming Perfect Pile Installation)

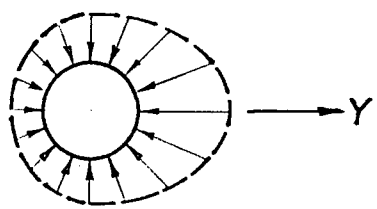

c) Soil Pressure Distribution During Lateral Loading - No Tension Stress Development

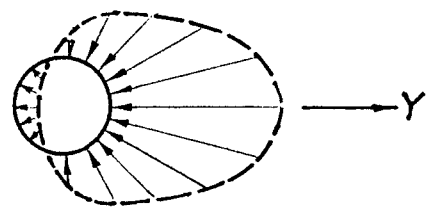

d) Soil Pressure Distribution During Lateral Loading - With Development of Tension Stresses Behind Pile

FIGURE 4.2: SOIL PRESSURE DISTRIBUTIONS AROUND LATERALLY LOADED PILES

(Adapted from Reese et al., 1974, p. 481)

however, the development of tension stresses behind the pile is possible (Figure 4.2d). Subsequent failure of the soil in tension leads to the formation of a cavity as illustrated in Figure 4.1c. In this situation, soil flows around the front of the pile and separates from the pile at some point along the back (Pyke & Beikae, 1984).

A proper representation of the interface behaviour requires the use of special elements. These elements must allow the soil to shear along the surface of the pile if the pile skin friction is exceeded. There must also be soil-pile separation if sufficiently large tension stresses develop during loading.

Interface, or slip, elements were developed by Goodman et al. (1968) to model the behaviour of jointed rock masses. These elements were subsequently adapted for use in soil mechanics. Yegian & Wright (1973) employed curved interface elements in their finite element analysis of the laterally loaded pile problem. Interface properties were shown to have a noticeable effect on the predicted value of the ultimate soil resistance. More recently, the curved interface elements were used by Thompson (1977) in developing P-Y curves for saturated clays (see Figures 3.7 and 3.8). Results similar to those of Yegian were obtained.

As a simple alternative to the interface elements developed by Yegian, normal elements with special modulus properties were used. The properties and their formulations are described in the following sections.

4.2 PROPERTIES OF INTERFACE ELEMENTS

4.2.1 Geometry

In the finite element mesh, the interface soil was represented by a thin ring of elements encompassing the pile. The elements were given a thickness of 0.005D (D = pile diameter) as indicated in Figure 4.3. Instability problems were not encountered in using the thin interface elements despite their high aspect ratio of about 39.

4.2.2 Shearing Behaviour

A bi-linear model, shown in Figure 4.4, was used to describe the shear stress-shear strain relationship at the interface. The shear modulus of the soil, G, remains constant during shearing until τ_s, the maximum allowable shear stress, is reached. The value of G is determined from the initial elastic and bulk modulii of the soil. The value of τ_s is a function of the properties of the soil and pile surface, reflecting the maximum skin friction that can develop during loading. The corresponding strain at τ_s is given by γ_c. For strains beyond γ_c, the soil deforms at constant stress. Consequently, G=0. A "zero" value, however, cannot be assigned to G in practice due to instability problems within the finite element program associated with the stress-strain matrix [D]. To maintain stability, the shear modulus at failure was defaulted to 0.001 of its initial value.

In general, the strength of a soil is characterized by c and ϕ, the cohesion and internal friction angle. Similarly, the strength of the soil-pile interface can be represented by the adhesion, c_a, and

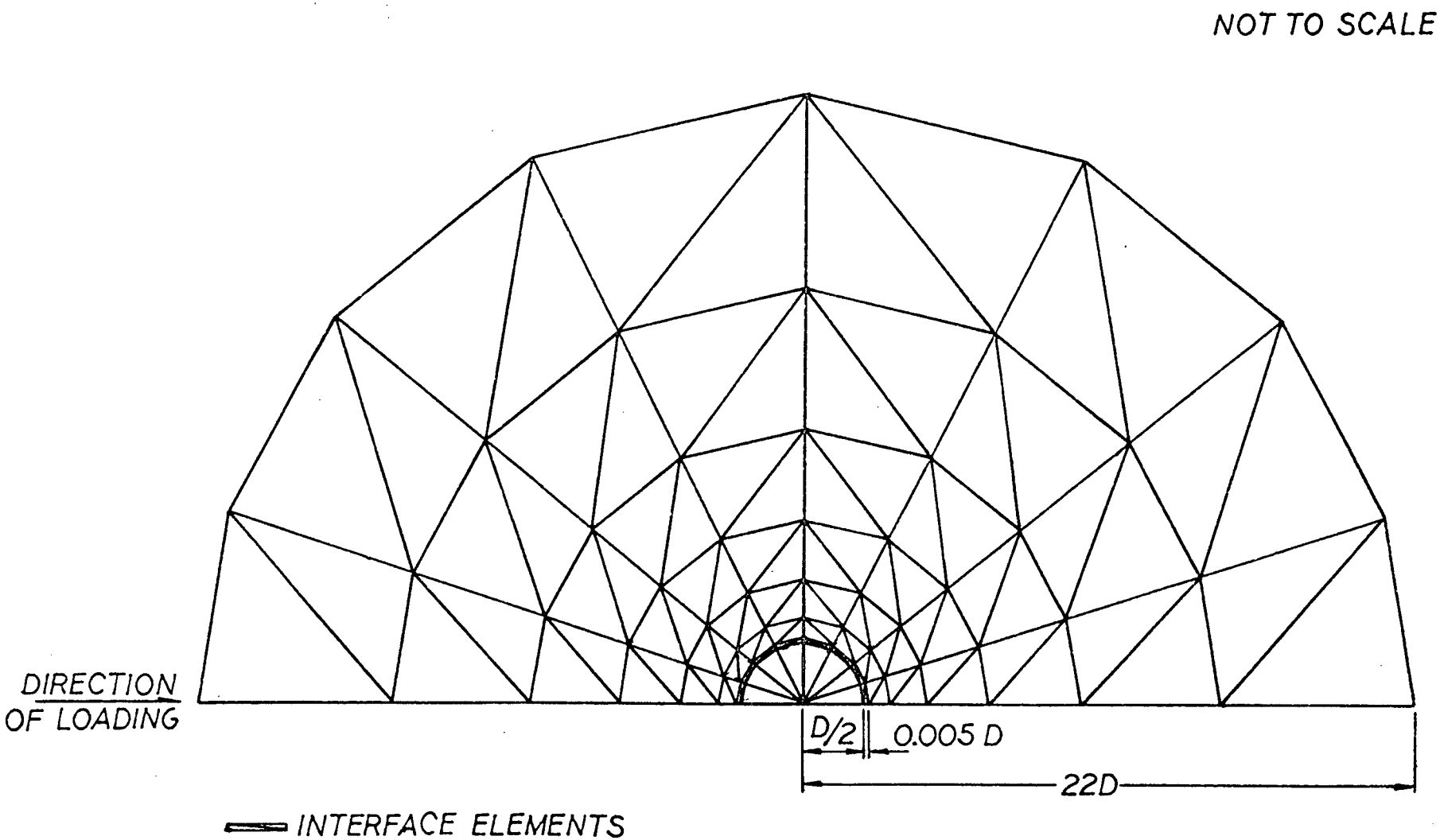

FIGURE 4.3: FINITE ELEMENT MESH WITH INTERFACE ELEMENTS

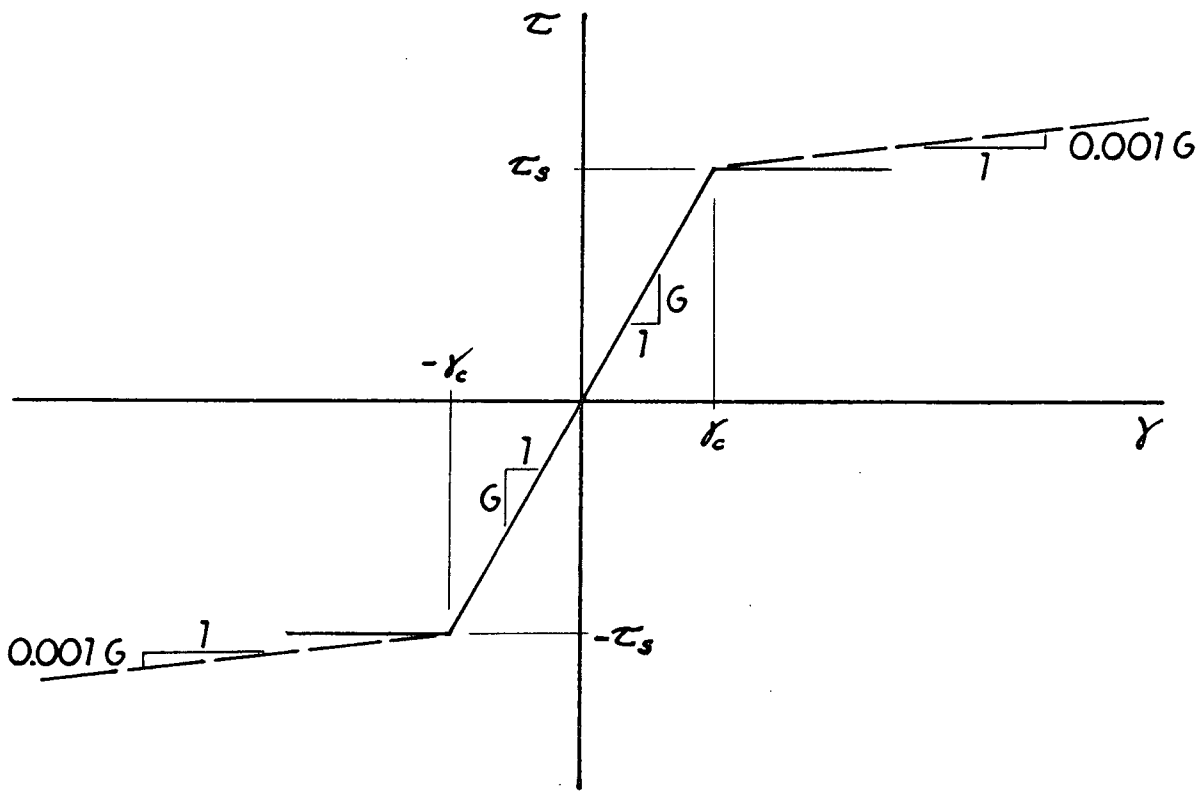

FIGURE 4.4: STRESS-STRAIN RELATIONSHIP FOR SHEAR ALONG THE SOIL-PILE INTERFACE

the friction angle, δ. Using these parameters, the maximum skin friction was determined based on the Mohr-Coulomb failure criterion:

$$2\tau_s = \frac{2c_a \cos\delta + 2\sigma_3 \sin\delta}{1 - \sin\delta} \qquad 4.1$$

where σ_3 is the minor principal stress.

Potyondy (1961) has shown that c_a and δ can be expressed as fractions of c and ϕ, respectively. In general,

$$c_a = \alpha c \qquad 4.2$$

and $$\delta = \beta\phi \qquad 4.3$$

Experimental values of α and β determined by Potyondy for various materials under different testing conditions are given in Table 4.1. Based on these recommended values, $\alpha = \beta = 0.50$ was selected for use with rough steel pile surfaces in clay, and $\beta = 0.80$ for piles in sand.

4.2.3 Soil-Pile Separation

The second consideration of interface behaviour is soil-pile separation. At shallow depths where the initial confining stresses are low, negative stresses may develop behind the pile during loading, resulting in the formation of cavities.

Although cohesive soils may be subjected to small tension stresses without failure, with the magnitudes of the stresses limited possibly by the soil cohesion (c) or the soil-pile adhesion (c_a),

TABLE 4.1

Proposed coefficients of skin friction between soils and construction materials

[$f\phi = \delta/\phi$, $fc = \frac{c_a}{c}$, $fc\max = \frac{c_a \max}{c\max}$; without factor of safety]

Construction material			Sand		Cohesionless silt			Cohesive granular soil		Clay		
			$0{\cdot}06 < D < 2{\cdot}0$ mm		$0{\cdot}002 < D < 0{\cdot}06$			50% Clay + 50% Sand		$D \leqq 0{\cdot}06$ mm		
	Surface finish of construction material		Dry	Sat.	Dry	Sat.		Consist. I. = 1·0–0·5		Consist. Index: 1·0–0·73		
			Dense		Dense	Loose	Dense					
			$f\phi$	$f\phi$	$f\phi$	$f\phi$	$f\phi$	$f\phi$	fc	$f\phi$	fc	$fc\max$
Steel	Smooth	Polished	0·54	0·64	0·79	0·40	0·68	0·40	—	0·50	0·25	0·50
	Rough	Rusted	0·76	0·80	0·95	0·48	0·75	0·65	0·35	0·50	0·50	0·80
Wood	Parallel to grain		0·76	0·85	0·92	0·55	0·87	0·80	0·20	0·60	0·4	0·85
	At right angles to grain		0·88	0·89	0·98	0·63	0·95	0·90	0·40	0·70	0·50	0·85
Concrete	Smooth	Made in iron form	0·76	0·80	0·92	0·50	0·87	0·84	0·42	0·68	0·40	1·00
	Grained	Made in wood form	0·88	0·88	0·98	0·62	0·96	0·90	0·58	0·80	0·50	1·00
	Rough	Made on adjusted ground	0·98	0·90	1·00	0·79	1·00	0·95	0·80	0·95	0·60	1·00

Note: $f_c \equiv \alpha$

$f_\phi \equiv \beta$

(After Potyondy, 1961, p. 352)

the stresses likely cannot be sustained for static loadings. Consequently, as a somewhat conservative measure, soil-pile separation was allowed whenever negative stresses developed in the interface elements.

To model the possible formation of cavities behind the piles, both the shear and the bulk modulii were reduced by a factor of 1000 upon tension failure. The low shear modulus prevents any further significant changes in shear stress while the low bulk modulus allows large volume changes to occur.

4.2.4 Failure Criteria

To achieve the desired behaviour of the interface elements, the above criteria were used to define soil failure. The interface elements were considered to have failed whenever the maximum shear stress, given by $\sigma_d/2$, exceeded the skin friction, τ_s, or whenever the minor principal stress, σ_3', became negative. Upon shear failure, the shear modulus was reduced to 0.001 of its initial value. Upon tension failure, both the shear and the bulk modulii were reduced to 0.001 of their initial values. The low modulii allow large shear deformations and volume changes to occur to model both the shearing of soil along the pile surface and the development of a tension cavity behind the pile.

CHAPTER 5

FINITE ELEMENT PROGRAM

A new higher-ordered finite element program was used in the analyses of the cavity expansion, pressuremeter, and laterally loaded pile problems. The program, CONOIL, was developed by Hans Vaziri at the University of British Columbia.

The program is divided into two parts: a geometry program and the main finite element program. The geometry program inputs mesh geometry data, rearranges the order of the nodes to minimize the bandwidth, processes the data, and creates a LINK file to transfer the information to the main program. The advantages of this system is obvious. Program users can number the nodes the way they desire and the geometry program will do the work to minimize the bandwidth. Moreover, if the same mesh geometry is used for more than one analysis, savings in computing time can be achieved by processing the geometry information only once.

The main finite element program contains several useful features. The program analyses two types of higher-ordered elements: 6-noded Linear Strain Triangles (LST), and 15-noded Cubic Strain Triangles (CST). Examples of the elements are shown in Figure 5.1. LST elements were found to produce accurate results when compared with theoretical stress-strain and cavity expansion theories (Chapters 6 and 7). These elements were used for all subsequent analyses. Load-deflection responses were slightly stiffer than the theoretical predictions but is to be expected as a result of the incremental elastic method of analysis used in the program. Trial analyses

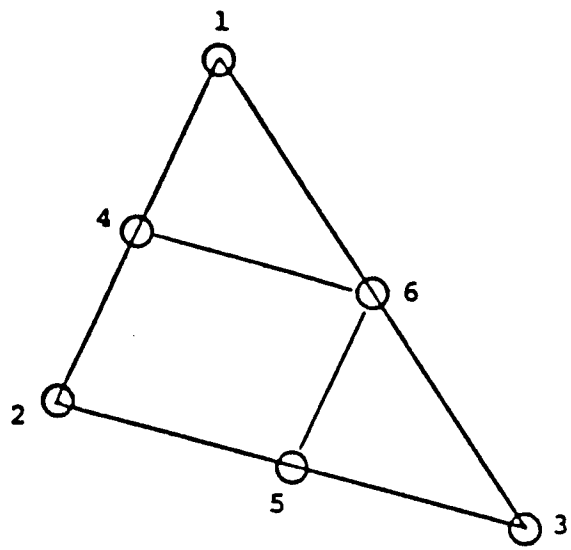

a) Linear Strain Triangular Element
6 Nodes, 12 D.O.F.

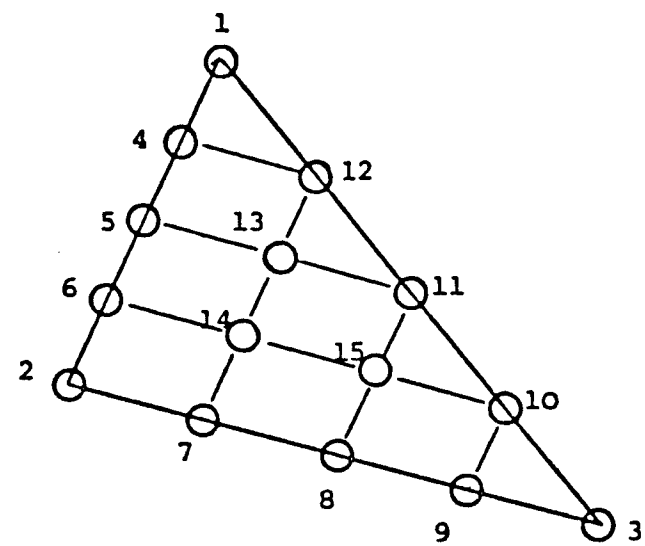

b) Cubic Strain Triangular Element
15 Nodes, 30 D.O.F.

FIGURE 5.1: HIGHER-ORDERED ELEMENTS

(After Vaziri, 1985)

performed with CST elements produced better results. The improvements, however, were small and did not warrant the high computing costs incurred by using the CST elements.

Another advantage of CONOIL is its ability to handle high Poisson's ratios. Values as high as 0.499 were used without encountering instability problems. The high values were useful in simulating undrained conditions (no volume change) for cohesive soils.

Other special features of CONOIL are its ability to perform consolidation and load-shedding analyses. These options were not used in dealing with the present problems. A complete documentation of the finite element program is given by Vaziri in his doctoral dissertation (1985).

CHAPTER 6

STRESS-STRAIN RELATIONSHIP

6.1 INTRODUCTION

The stress-strain relations of soil are complex, being non-linear, inelastic, and stress level dependent. In the finite element program CONOIL, a simple incremental linear elastic and isotropic stress-strain model is used. The model is described by Duncan et al. (1980).

To verify the ability of the finite element program to correctly model the complex stress-strain behaviour of soil, a group of 4 linear strain triangular elements was tested. The test elements and the boundary constraints are shown in Figure 6.1. Uniformly distributed pressure loads, $\Delta\sigma_y$, were applied to the top of the elements and the corresponding axial (Y) deflections computed. The elements were tested under both plane strain and plane stress conditions.

6.1.1 Stress-Strain Relationship

The incremental stress-strain relationship used in CONOIL can be written as follows:

$$\{\Delta\sigma\} = [\ D\ ]\ \{\Delta\varepsilon\} \qquad 6.1$$

where

$\{\Delta\sigma\}$ is the incremental stress vector

$\{\Delta\varepsilon\}$ is the incremental strain vector

$[\ D\ ]$ is the stress-strain matrix

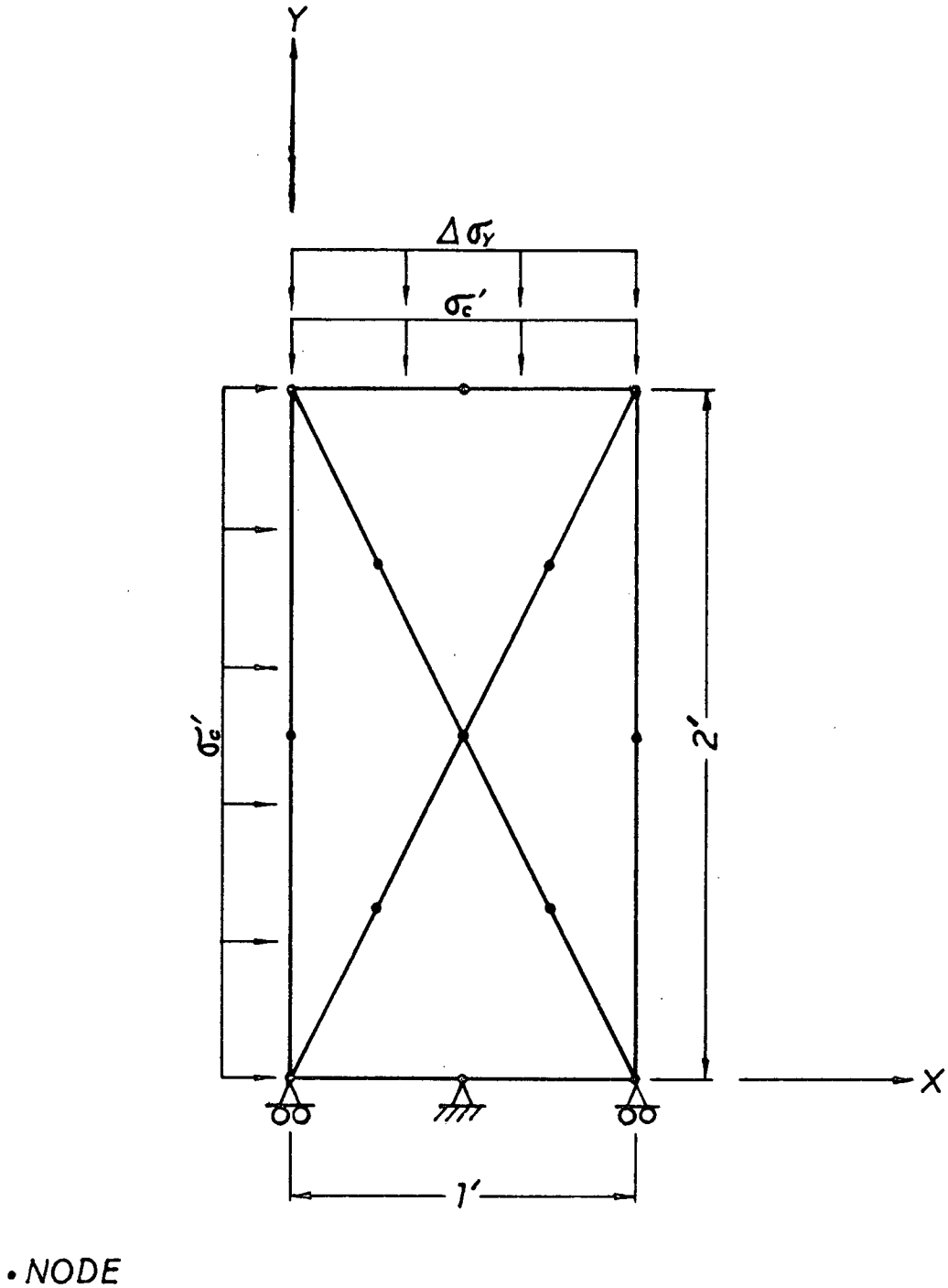

FIGURE 6.1: TEST ELEMENTS

[D] is a function of the tangent Young's and bulk modulii, E_t and B_t:

$$E_t = E_i(1 - R_f(\sigma_d/\sigma_{df})^2 \qquad 6.2$$

$$B_t = k_{Bt}P_a(\sigma_3/P_a)^m \qquad 6.3$$

where

E_i = initial Young's modulus = $k_E P_a(\sigma_3/P_a)^n$

k_E = Young's modulus number

n = Young's modulus exponent

k_{Bt} = tangent bulk modulus number

m = tangent bulk modulus exponent

P_a = atmospheric pressure

σ_3 = minor principal stress

R_f = failure ratio

σ_d = deviator stress

σ_{df} = deviator stress at failure

6.2 PLANE STRAIN CONDITION

6.2.1 Stress-Strain Relations

The stress-strain relationship below was derived for the plane strain uniaxial loading condition:

$$\varepsilon_y = \frac{(9B - E_s)(3B + E_s)}{36B^2E_s}\,\sigma_y \qquad 6.4$$

where

ε_y = axial strain corresponding to the applied stress σ_y

E_s = secant Young's modulus

B = bulk modulus = $k_B P_a(\sigma_3/P_a)^m$

k_B = bulk modulus number

m = bulk modulus exponent

E_s for the hyperbolic stress-strain model is given by Duncan & Chang (1970) as

$$E_s = E_i[1 - R_f(\sigma_y/\sigma_{df})] \qquad 6.5$$

where

$$\sigma_{df} = \text{deviator stress at failure} = \frac{2c\cos\phi + 2\sigma_3\sin\phi}{1 - \sin\phi}$$

The derivation of the stress-strain relationship is contained in Appendix A.

6.2.2 Comparison of Finite Element Results with Closed Form Solution

Finite element tests were performed for both cohesive (ϕ=0) and frictional (c'=0) materials. Soil parameters employed in these analyses are tabulated in Table 6.1. The properties listed for the cohesive material correspond to those of a normally consolidated undrained clay (based on Atukorala & Byrne, 1984) while the frictional material properties are appropriate for a sand with a relative density of 75% (Byrne & Eldridge, 1982).

The results of the analyses are shown in Figure 6.2 for the undrained clay, and in Figure 6.3 for the sand. Good agreements exist

TABLE 6.1

SOIL PARAMETERS USED IN STRESS-STRAIN ANALYSES

PARAMETER	MATERIAL	
	COHESIVE SOIL (Undrained Clay)	FRICTIONAL SOIL (Sand)
k_E	72.1	750.0
n	0.0	0.5
k_B	24.0	600.0
m	0.0	0.5
R_f	0.9	0.9
μ	0.0	0.29
c (Psf)	305.0	0.0
ϕ_1 (deg)	0.0	39.0
$\Delta\phi$ (deg)	0.0	4.0
ϕ_{cv} (deg)	0.0	33.0
γ_{sat} (Pcf)	123.4	122.4
Depth (ft)	20.0	20.0
σ_c' (Psf)	1220.0	1200.0
P_{atm} (Psf)	2116.2	2116.2

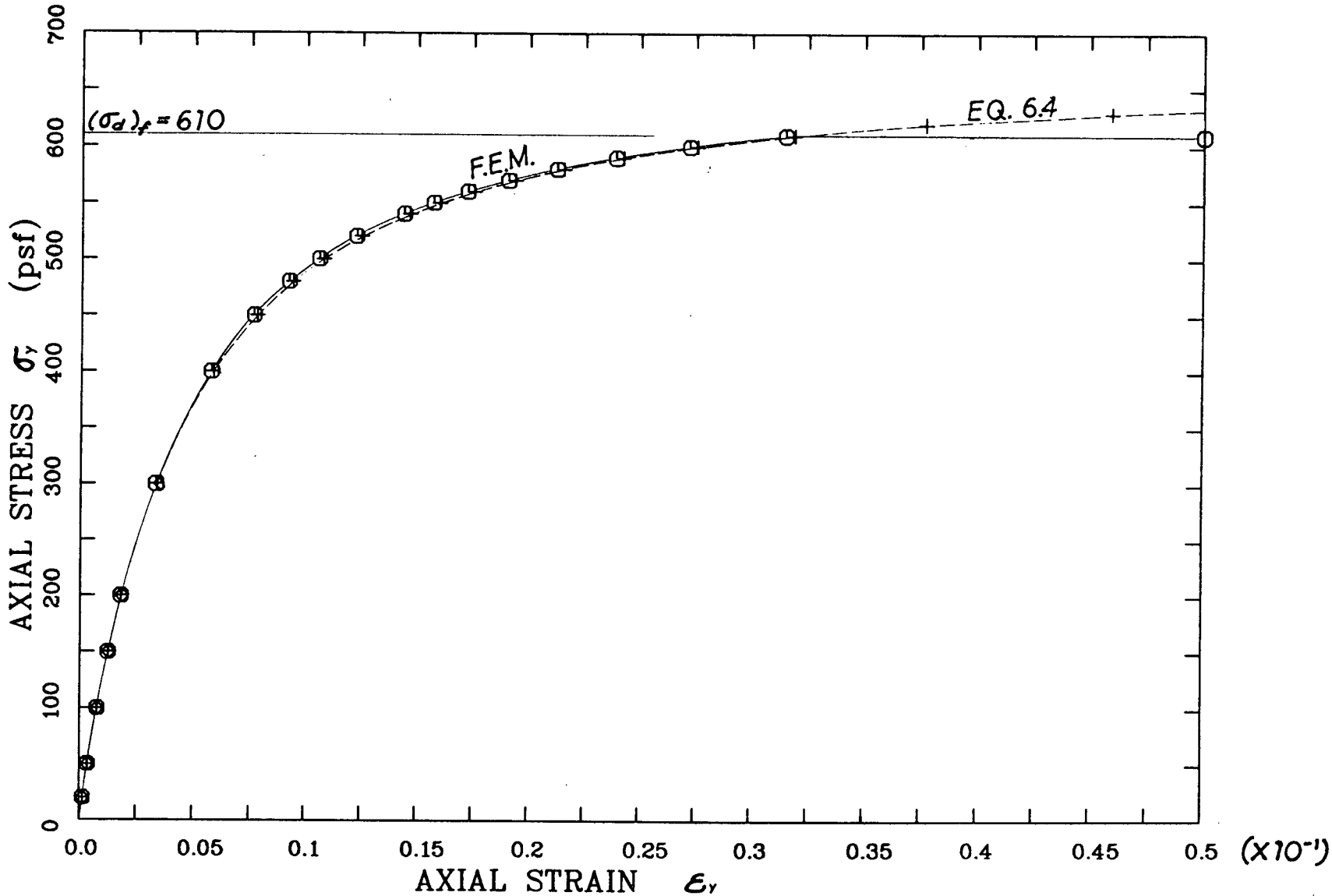

FIGURE 6.2: PLANE STRAIN STRESS-STRAIN RELATIONSHIPS FOR UNDRAINED CLAY

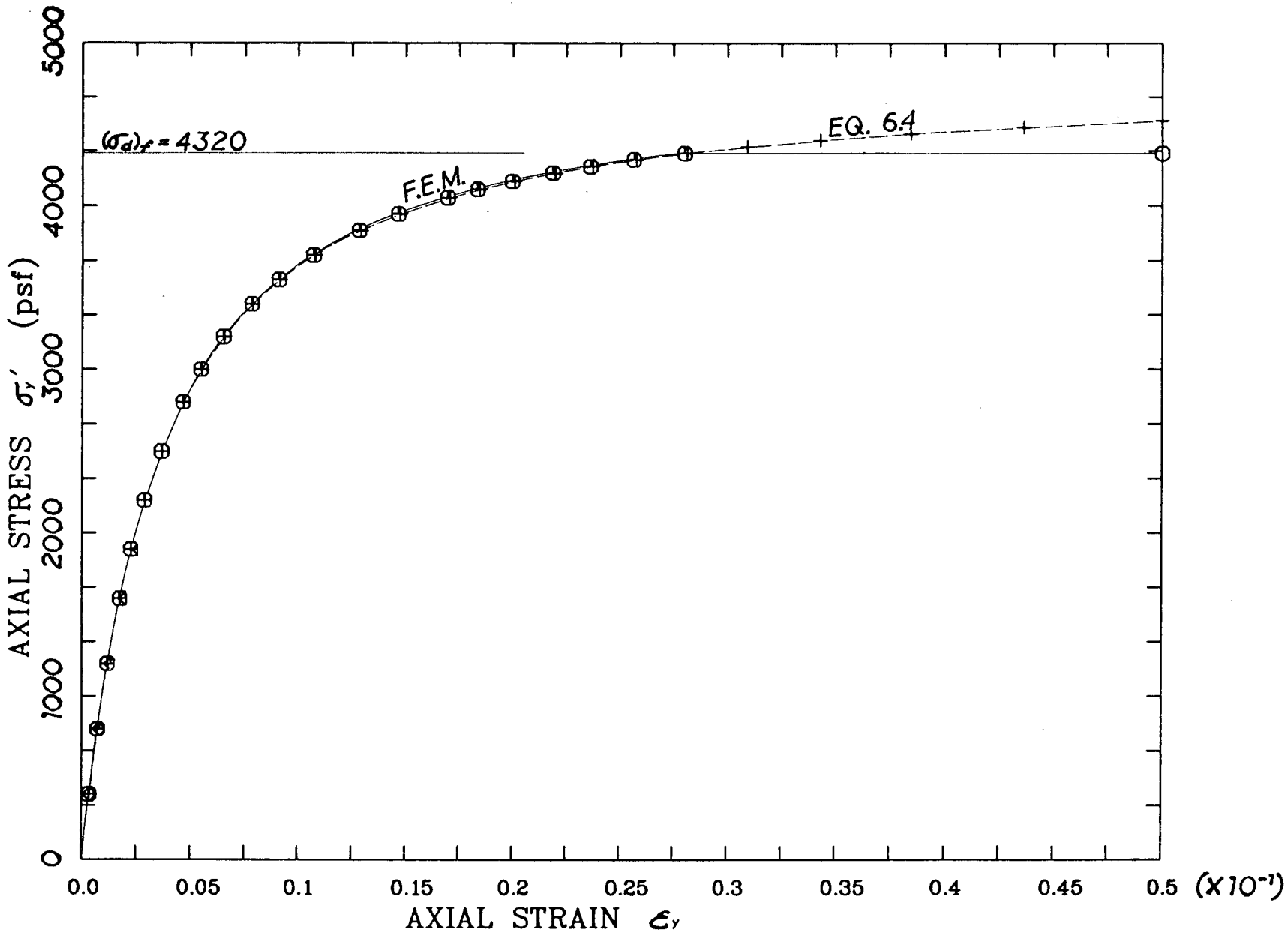

FIGURE 6.3: PLANE STRAIN STRESS-STRAIN RELATIONSHIPS FOR SAND

between the finite element predictions and the theoretical curves given by Equation 6.4.

The finite element curves are truncated at stresses corresponding to the failure condition where $\sigma_y/\sigma_{df} = 1$. Upon failure, the shear modulus was reduced to 0.001 of its initial value. This reduction of the shear modulus allows for large deformations on subsequent stress increases and yields the flat portions of the curves shown.

The computed stress-strain curves are, in general, slightly stiffer than the theoretical curves predicted by Equation 6.4. This stiffness is expected, however, due to the inherent nature of the incremental elastic method employed in the finite element program. Better agreements could have been obtained by using smaller stress increments, but was deemed unnecessary. The computed results clearly demonstrate the finite element program's ability to model the non-linear stress-strain behaviour of soil under plane strain condition.

6.3 PLANE STRESS CONDITION

6.3.1 Stress-Strain Relations

For the loading conditions illustrated in Figure 6.1, a stress-strain relationship was derived for the plane stress case. As shown in Appendix A, this relationship can be expressed as

$$\varepsilon_y = \frac{\sigma_y}{E_s} = \frac{\sigma_y}{E_i[1 - R_f(\sigma_y/\sigma_{df})]} \qquad 6.6$$

where E_i and σ_{df} are as given in Equation 6.5. The remaining parameters are as defined in Section 6.2.1.

6.3.2 Comparison of Finite Element Results with Closed Form Solution

The theoretical and computed stress-strain curves for the undrained clay and sand (material properties given in Table 6.1) are plotted in Figures 6.4 and 6.5. Again, good agreements exist between the numerical results and the theoretical relationships. As in the plane strain case, the finite element predictions are slightly stiffer than the theoretical curves. The differences, however, are negligible. Once again, the results verify the ability of the program to model the stress-strain behaviour of soil under plane stress condition.

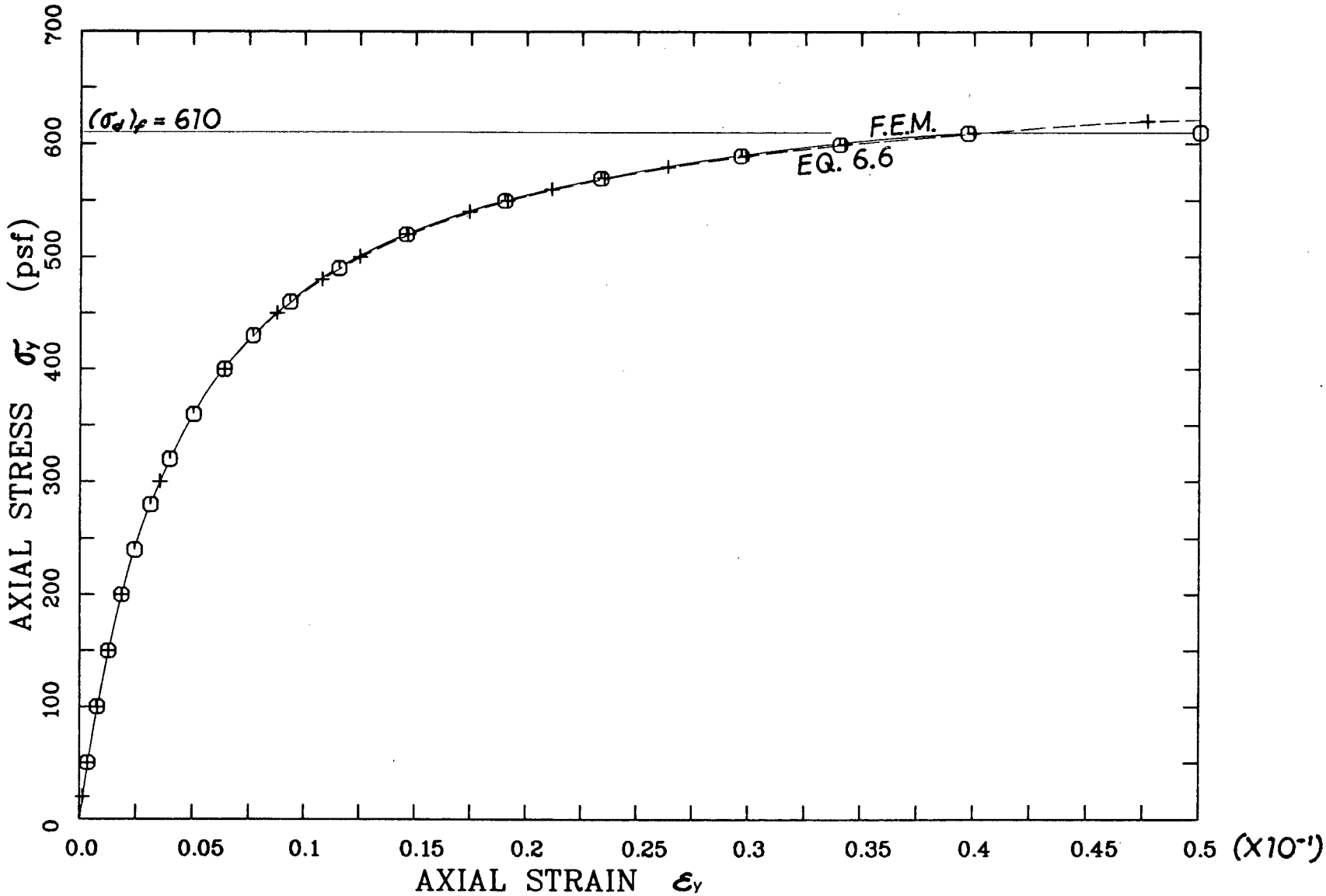

FIGURE 6.4: PLANE STRESS STRESS-STRAIN RELATIONSHIPS FOR UNDRAINED CLAY

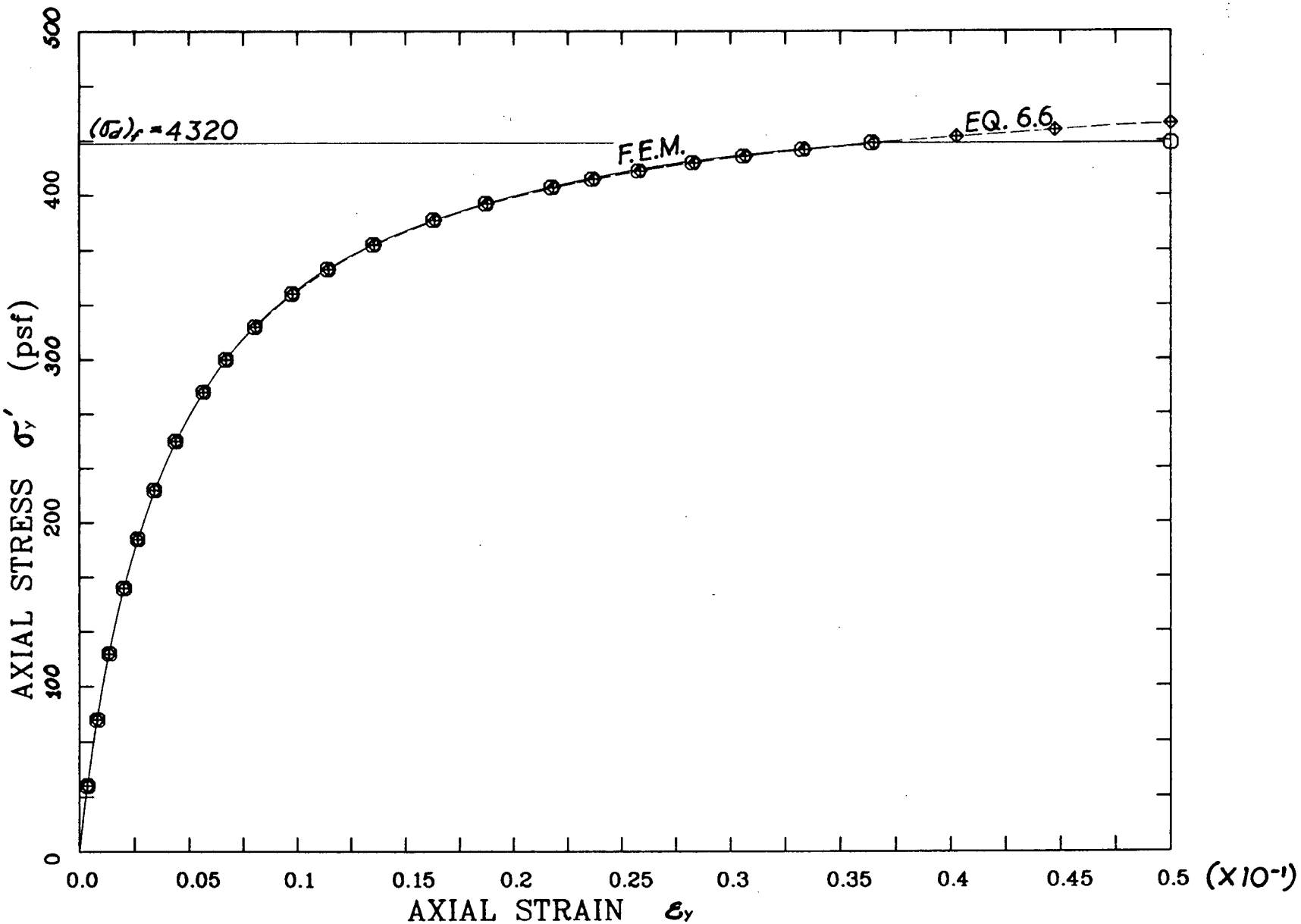

FIGURE 6.5: PLANE STRESS STRESS-STRAIN RELATIONSHIPS FOR SAND

CHAPTER 7

CYLINDRICAL CAVITY EXPANSION

7.1 INTRODUCTION

The cylindrical cavity expansion problem bears some similarities to the laterally loaded pile situation. At depths away from the ground surface, soil displacements upon the expansion of a cavity are confined to the radial plane (Hughes et al., 1977, and Robertson, 1982). The problem can thus be treated as plane strain. Similarly, plane strain deformations are assumed for the laterally loaded pile problem at large depths. In both instances, the lateral passive resistance of the soil is mobilized.

Although no mathematical solution exists for the lateral pile problem, closed form solutions for cavity expansion are readily available. Consequently, to validate the method of analysis for the laterally loaded pile problem, finite element analyses for the expansion of cylindrical cavities were performed. The results are compared with closed form solutions developed for the expansion of infinitely long cylindrical cavities in infinite media.

Finite element analyses for the cavity expansion problem were performed using two different mesh geometries, the two-dimensional plane strain quadrant shown in Figure 7.1, and the plane strain axisymmetric domain in Figure 7.2. Taking into account small discrepancies in the results due to the different sizes and, to a lesser degree, the pattern or geometry of the elements, both mesh geometries yielded approximately the same pressure-deflection responses. Although the quadrant mesh is suited for validating the

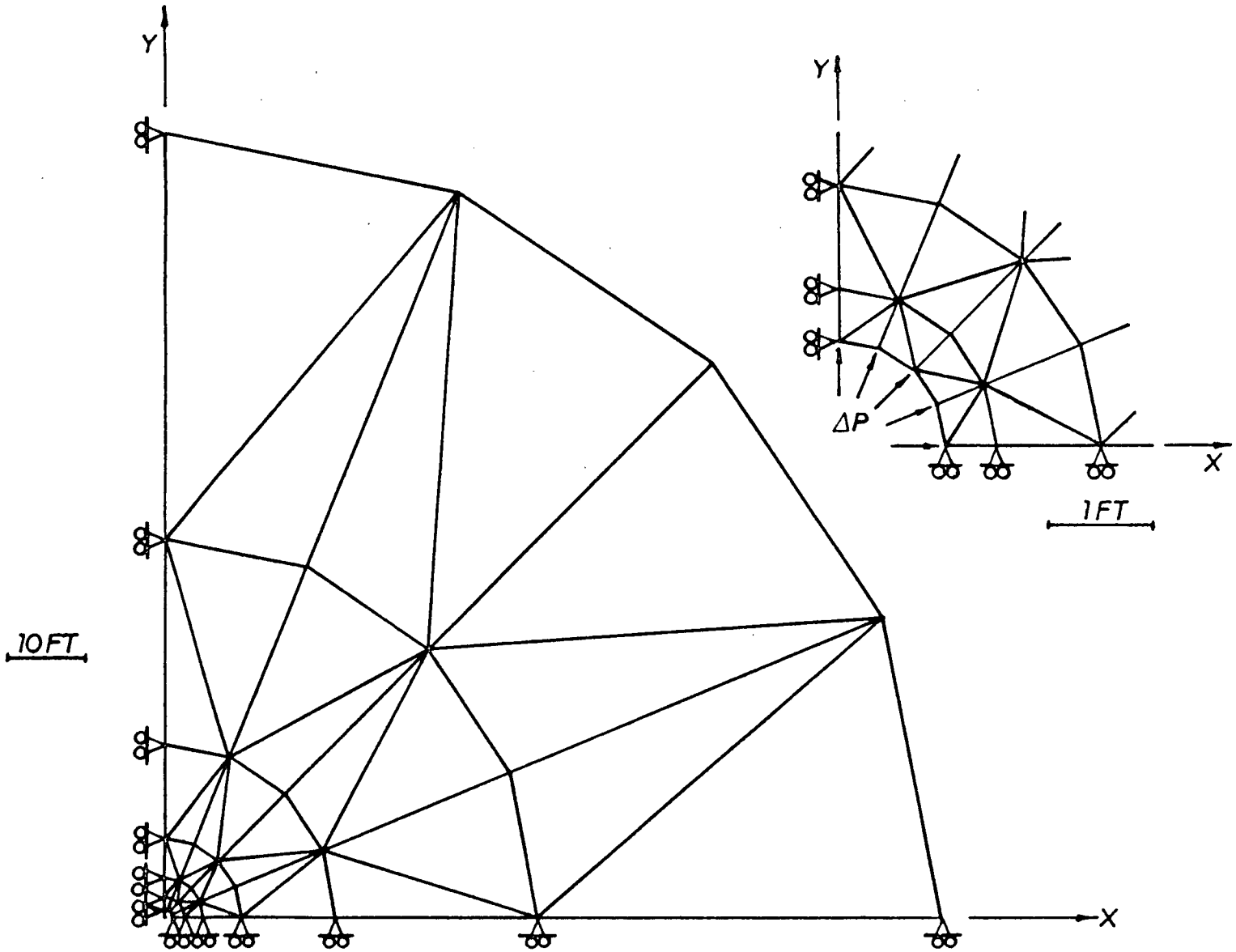

FIGURE 7.1: FINITE ELEMENT MESH FOR PLANE STRAIN CAVITY EXPANSION ANALYSIS

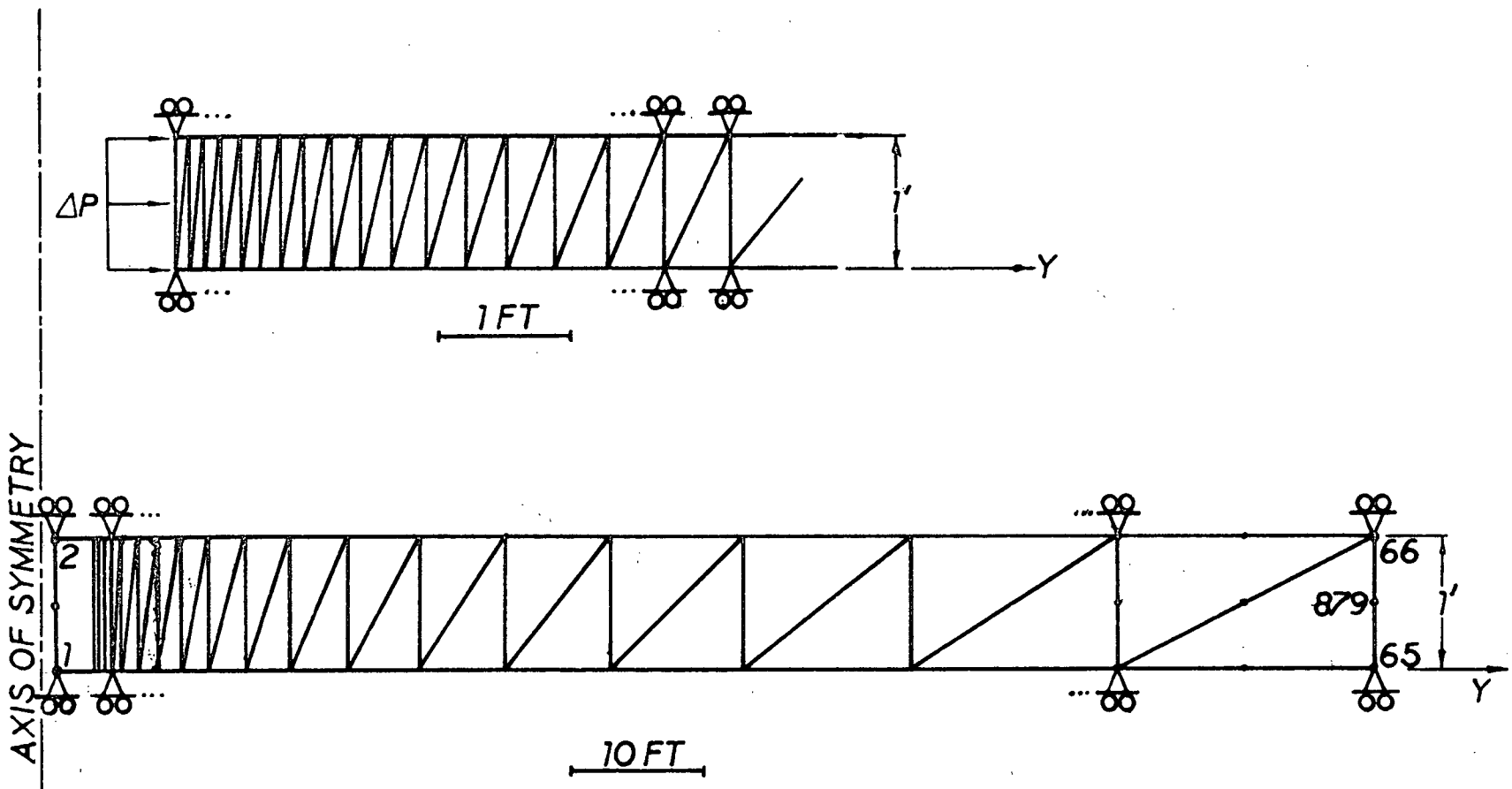

FIGURE 7.2: FINITE ELEMENT MESH FOR PLANE STRAIN AXISYMMETRIC CAVITY EXPANSION ANALYSIS

pile results because of its similarity to the mesh used in the laterally loaded pile problem (see Figures 3.2 and 4.3), the axisymmetric mesh was chosen because of its simplicity, which permitted the use of smaller, and therefore, more elements in the domain without incurring excessive computing costs. Since soil failure progresses out radially from the centre of the mesh in the cavity expansion problem, greater accuracy in predicting deflection responses was achieved with the use of smaller elements.

Finite element predictions were obtained for both elastic-plastic and non-linear elastic material properties. The results are compared with elastic-plastic closed form solutions. Both cohesionless (sand) and cohesive (clay) soil properties were used in the comparisons.

7.2 COHESIVE SOIL

Finite element analyses and the elastic-plastic closed form solution for an undrained clay were compared. The soil properties are tabulated in Table 7.1. These values are appropriate for a normally consolidated clay and are based on Atukorala & Byrne (1984). The R_f value of 0.0006 given for the elastic-plastic case serves only as a flag to indicate the material type and is of no consequence in subsequent calculations. A K_o value of 1.0 was used for the isotropic consolidation condition assumed in the closed form solution.

7.2.1 Elastic-Plastic Closed Form Solution

The closed form solution for a purely cohesive material was derived by Hughes (1979) based on the assumptions of expansion in an

TABLE 7.1

MATERIAL PROPERTIES FOR UNDRAINED CLAY

PARAMETER	MATERIAL	
	ELASTIC-PLASTIC	NON-LINEAR ELASTIC
k_E	144.1	144.1
n	0.0	0.0
k_B	24021.0	24021.0
m	0.0	0.0
R_f	0.0006	0.9
c_u (Psf)	610.0	610.0
ϕ_1 (deg)	0.0	0.0
$\Delta\phi$ (deg)	0.0	0.0
ϕ_{cv} (deg)	0.0	0.0
μ	0.499	0.499
γ_{sat} (Pcf)	123.4	123.4
Depth (ft)	40.0	40.0
σ_{vo}' (Psf)	2440.0	2440.0
K_o	1.0	1.0
P_{atm} (Psf)	2116.2	2116.2

infinite medium and a Tresca failure criterion (ie: $1/2(\sigma_r - \sigma_\theta) = c_u$). In addition, soil in the plastic zone was assumed to deform at constant volume. Although no volumetric strain constraint was placed on the deformation of soil in the elastic zone, Hughes showed that $\Delta\sigma_r = -\Delta\sigma_\theta$ during cavity expansion. Moreover, in the case of an infinitely long cylindrical cavity, $\Delta\sigma_z = 0$. Consequently, the mean normal stress, σ_m, is constant during expansion and no change in volumetric strain occurs. The overall effect is that of constant volume deformation, applicable to the case of an undrained clay. Hughes' solution for small strains is given below:

$$P_r = P_o + c_u\left(1 + \ln\left(\frac{\Delta r}{r_o}\frac{2G}{c_u}\right)\right) \qquad 7.1a$$

or

$$P_r = P_o + c_u\left(1 + \ln\left(\frac{\Delta r}{r_o}\frac{1}{c_u}\frac{6BE}{9B - E}\right)\right) \qquad 7.1b$$

where

P_r = pressure on wall of cavity

P_o = initial pressure on wall of cavity

Δr = deflection of cavity wall

r_o = initial radius of cavity

B, G and E = initial modulus values

In the equations given above, P_r tends to infinity as Δr tends to infinity, and no limiting pressure can be determined. Clearly, this relationship breaks down for large deformations. Gibson & Anderson (1961) have derived an equation for large strains as follows:

$$P_r = P_o + c_u\left(1 + \ln\left(\frac{\Delta r}{r}\frac{2G}{c_u}\right)\right) \qquad 7.2$$

where

r = current radius of cavity = $r_o + \Delta r$

For this equation, as r tends to infinity, $\Delta r/r$ approaches 1, and a limiting pressure, based solely on material properties, is achieved:

$$P_L = P_o + c_u[1 + \ln(2G/c_u)] \qquad 7.3$$

Assuming $E = 500c_u$ for an undrained clay (μ=0.5), $P_L = P_o + 6.8c_u$.

The theoretical elastic-plastic curve based on Equation 7.1a for the material properties given in Table 7.1 is shown in Figure 7.3. For $\Delta r < 0.001103$ ft, or $\ln[(\Delta r/r_o)(2G/c_u)] < -1$, $\Delta P = P_r - P_o$ is negative. This apparent error is caused by the 'log' term in the closed form solution and reflects the linear elastic behaviour of the soil prior to the start of plastic failure. Consequently, the small strain or initial elastic portion of the curve is given by the linear elastic closed form solution (Byrne & Grigg, 1980):

$$P_r = P_o + 2G(\Delta r/r_o) \qquad 7.4$$

From Figure 7.3, plastic failure can be seen to begin at ΔP = 605 Psf where the two curves meet.

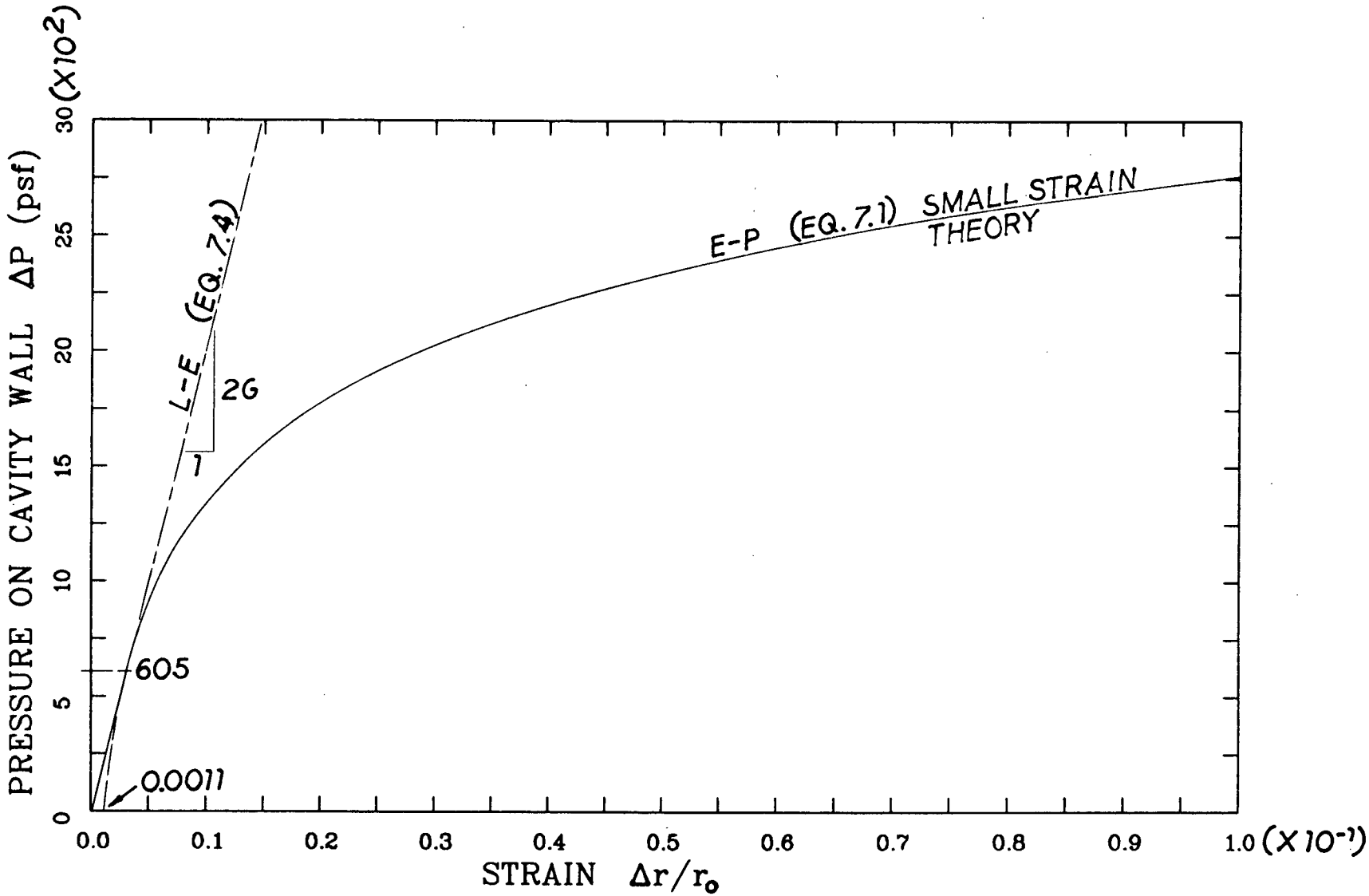

FIGURE 7.3: CLOSED FORM SOLUTIONS FOR CAVITY EXPANSION IN UNDRAINED CLAY

7.2.2 Finite Element Predictions and Comparison with Closed Form Solution

The result of the finite element analyses are presented in Figure 7.4. Good agreement with the closed form solution was obtained for the elastic-plastic curves.

The cavity expansion curve for non-linear elastic material properties is also shown in the graph. As expected, the initial linear elastic behaviour of the elastic-plastic curves is absent and the overall pressure-deflection response is considerably softer.

7.2.2.1 Boundary Conditions

Although the inherent nature of incremental elastic analysis is to predict responses somewhat stiffer than the actual behaviours, the elastic-plastic finite element curve in Figure 7.4 shows an initial response slightly softer than that of the close form solution. At larger deflections, the curve stiffens as expected and matches the theoretical curve for deflections greater than about 0.15 ft.

The behaviour of the finite element curve can be explained by the boundary conditions. Since undrained clay deforms at constant volume, the expansion of a cavity in a finite medium is physically impossible. To illustrate, a separate analysis was performed using the mesh in Figure 7.2 but with the outer boundary pinned at nodes 65, 66 and 879 to model a finite medium. The resulting pressure-deflection curve is shown in Figure 7.5. Although this curve deviates from an expected vertical line and indicates an increase in deflection with increasing pressure, the response is much stiffer than that predicted by Equation 7.1. The calculated deflections were found to be the

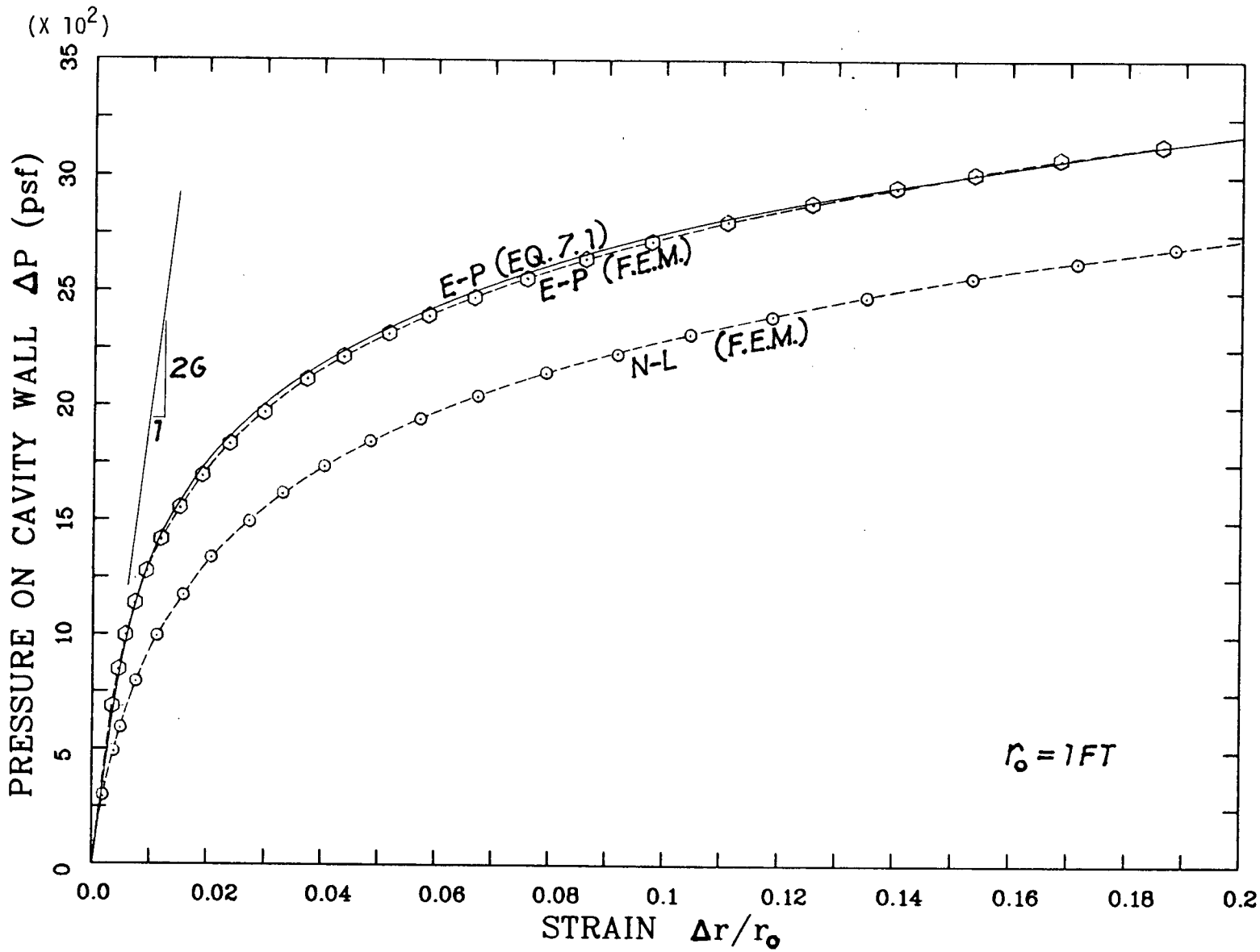

FIGURE 7.4: CAVITY EXPANSION CURVES FOR UNDRAINED CLAY

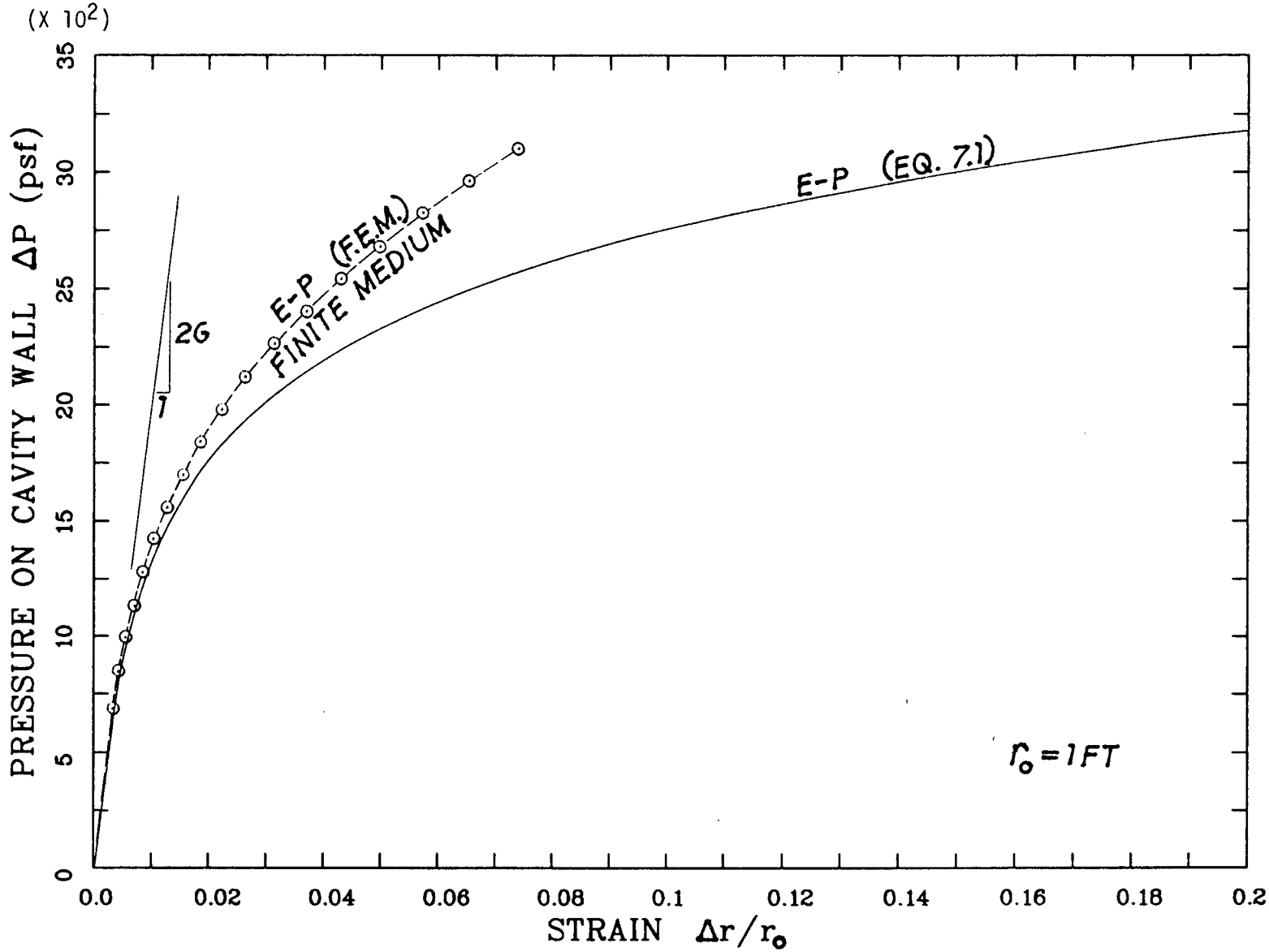

FIGURE 7.5: CAVITY EXPANSION IN A FINITE MEDIUM FOR AN ELASTIC-PLASTIC UNDRAINED CLAY

results of small volumetric strains ($\varepsilon_v < 0.5\%$) in the mesh elements owing to the inability to use $B = \infty$, and the similarity in initial slope between the predicted curve and the theoretical relationship is coincidental. The use of a finite element mesh with a different radius would have produced a curve with a different initial slope. To model expansion in an infinite medium, the outer boundary was permitted to deflect in the radial direction as shown in Figure 7.2, creating a stress boundary where $\Delta\sigma_r = 0$. The expansion curve predicted by this method is presented in Figure 7.4.

In using the stress boundary method, the resisting force of the soil beyond the radius of 100 ft is omitted. As shown in Figure 7.6, the radial stress, σ_r, decreases with radial distance from the cavity according to the equation derived by Hughes (1979):

$$\sigma_r = P_r(a^2/r^2) \qquad 7.5$$

where

P_r = pressure (or change in pressure) on wall of cavity

a = radius of cavity

r = radial distance from centre of cavity

In the above analysis for an initial cavity radius of 1 ft, the resisting pressure omitted at the outer boundary (r = 100 ft) increased from a value of 0.069 Psf at the start of plastic failure at ΔP = 690 Psf (a = 1.0034 ft) to 0.416 Psf at ΔP = 3060 Psf (a = 1.166 ft). The omission of this resisting pressure is thought to be the cause of the slightly soft response of the finite element curve at low strains ($\Delta r/r_o < 0.14$) in Figure 7.4. Although this error could have been reduced by extending the radius of the finite element mesh,

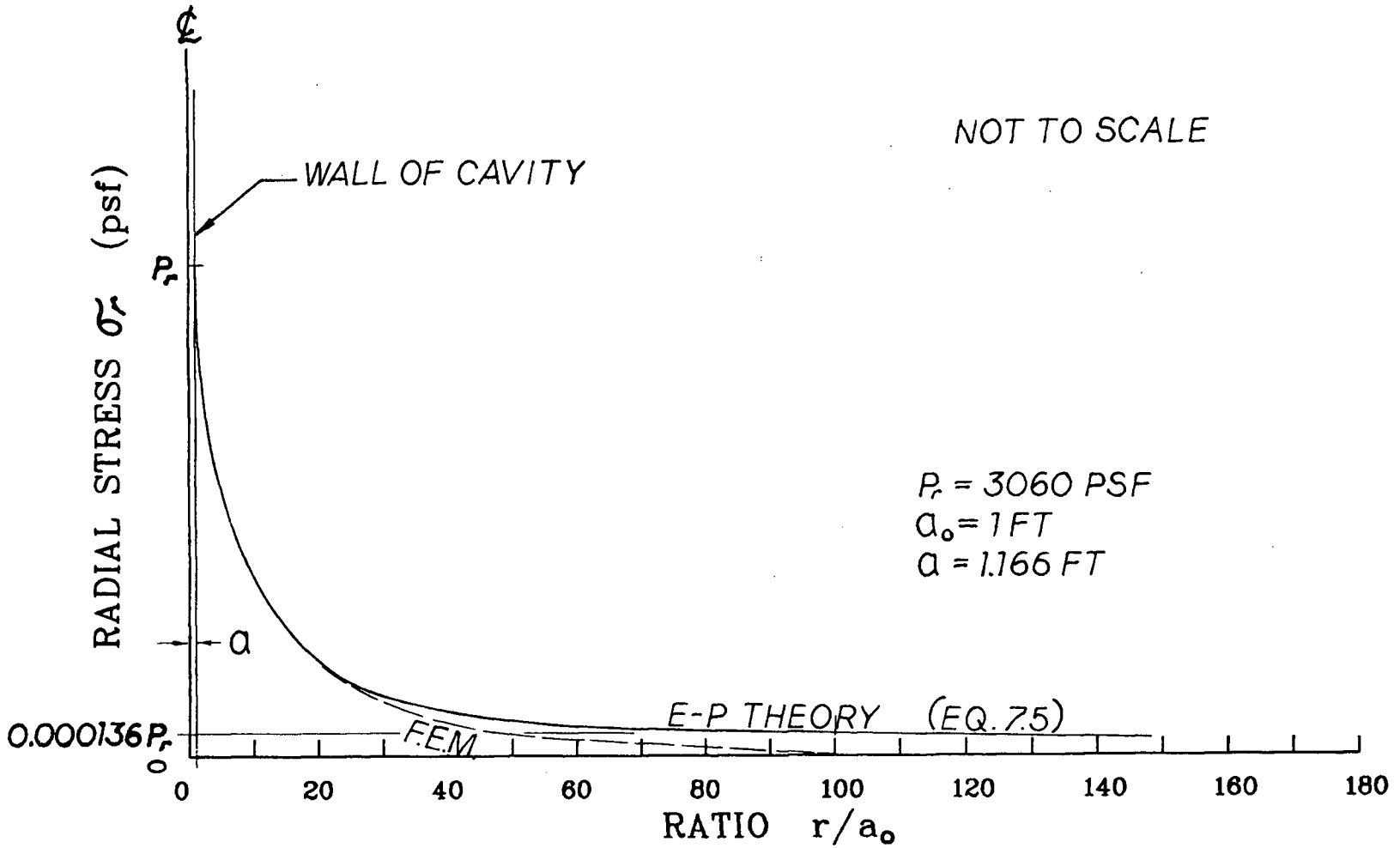

FIGURE 7.6: VARIATION OF RADIAL STRESS WITH DISTANCE FROM CAVITY

it was not considered necessary since the error introduced by using a mesh radius of 100 ft is relatively small and insignificant. Volumetric strains calculated for the stress boundary (infinite medium) analysis were approximately 150 times less than those obtained in the finite medium analysis (Figure 7.5). Consequently, deflection errors resulting from volume changes can be discounted.

7.3 COHESIONLESS SOIL

In the case of a cohesionless soil, finite element analyses were performed using only non-linear elastic material properties for a dense sand.

7.3.1 Elastic-Plastic Materials

Difficulties arise in the analysis of elastic-plastic materials due to the variation of shear strength with the minor principal stress, σ_3', as follows:

$$\sigma_{df} = 2\tau_{max} = \frac{2\,\sigma_3'\,\sin\phi'}{1 - \sin\phi'} \qquad 7.6$$

and

$$\tau_f = \frac{\sigma_3'\,\sin\phi'\,\cos\phi'}{1 - \sin\phi'} \qquad 7.7$$

Moreover, ϕ' varies with σ_3' as given by Duncan et al. (1980):

$$\phi' = \phi_1' - \Delta\phi\,\log(\sigma_3'/P_a) \qquad 7.8$$

As increasing loads are applied to a soil element, σ_3'

varies, resulting in changes in the shear strength, stress level (σ_d/σ_{df}), and modulus values. Problems arise as the soil approaches failure. The reduction of modulus values at failure to 0.01 or 0.001 of their initial values causes σ_d/σ_{df} to fluctuate above and below the failure value of 1.0, leading to erratic soil behaviour. An illustration of the problem was presented by Eldridge (1983) and is shown in Figure 7.7. Because of this erratic behaviour, elastic-plastic analyses were not performed. Instead, a comparison was made between the non-linear elastic finite element prediction and the elastic-plastic closed form solution.

7.3.2 Elastic-Plastic Closed Form Solution

An elastic-plastic closed form solution for the expansion of a cylindrical cavity in an infinite cohesionless medium was derived by Hughes et al. (1977) assuming a Mohr-Coulomb failure criterion. A complete derivation of the solution, including dilation effects, was presented by Eldridge (1983). The following relationship was obtained:

$$P_r = P_o\,(1 + \sin\phi')\left[\frac{E}{1+\mu}\,\frac{\Delta r}{r}\,\frac{1}{nP_o\,\sin\phi'}\right]^{(1-N)/(1+n)} \qquad 7.9$$

and $N = (1 - \sin\phi')/(1 + \sin\phi')$

$n = (1 - \sin\nu)/(1 + \sin\nu)$

where

ϕ' = friction angle of the cohesionless material

ν = dilation angle

E = initial Young's modulus = $k_E P_a(\sigma_3'/P_a)^n$

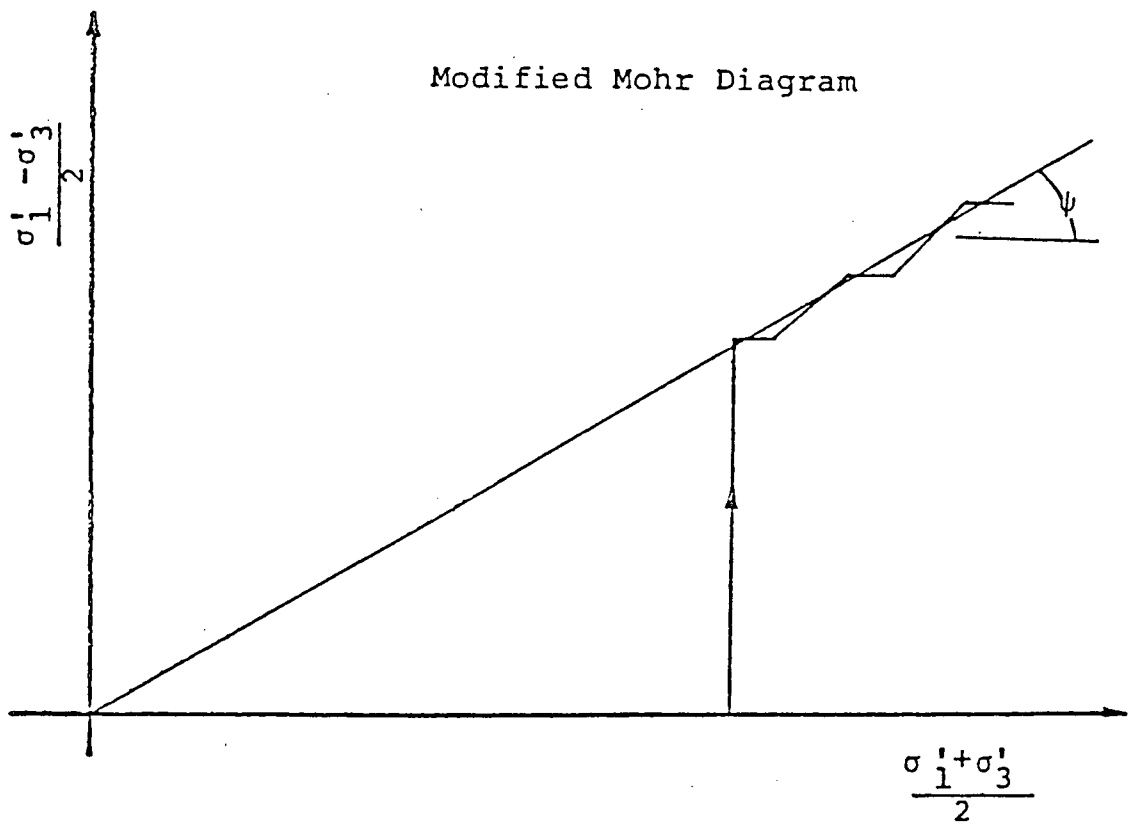

FIGURE 7.7: STRESS PATH FOR FAILED SAND ELEMENT

(Adapted from Eldridge, 1983, p. 90)

P_r, P_o, r and Δr are as defined in Equations 7.1 and 7.2. Volumetric strain due to dilation effects is given by

$$\Delta \varepsilon_v = -\Delta \gamma \sin \nu \qquad 7.10$$

For the condition of constant volume deformation, $\nu = 0$ and Equation 7.9 reduces to

$$P_r = P_o\ (1 + \sin\phi')\left[\frac{E}{1+\mu}\ \frac{\Delta r}{r}\ \frac{1}{P_o\ \sin\phi'}\right]^{(1-N)/2} \qquad 7.11$$

As in the case of the solution for cohesive materials, as Δr tends to infinity, $\Delta r/r$ approaches 1, and the limiting pressure is given by

$$P_L = P_o\ (1 + \sin\phi')\left[\frac{2G}{P_o\ \sin\phi'}\right]^{(1-N)/2} \qquad 7.12$$

The above closed form solution does not take into account the variation of ϕ' with σ_3' given by Equation 7.8, nor does it consider the effect of σ_3' on the initial modulus values according to

$$E_i = k_E P_a (\sigma_3'/P_a)^n \qquad 7.13$$

$$G = k_G P_a (\sigma_3'/P_a)^m \qquad 7.14$$

Since σ_3' may vary considerably during loading, omitting its influences may lead to significant errors. Consequently, the

elastic-plastic solution given by Equations 7.9 to 7.12 is, at best, only an approximation of the real problem.

The closed form solution for a dense sand is shown in Figure 7.8. The assumption of $\nu = 0$ was made for constant volume expansion. Material properties for the sand are based on Byrne & Eldridge (1982) and are tabulated in Table 7.2. As in the case of the cohesive soil, the initial linear elastic portion of the curve is given by Equation 7.4. Plastic failure is shown to begin at $\Delta P = 1400$ Psf.

7.3.3 Finite Element Prediction

The results of a plane strain axisymmetric finite element analysis and the corresponding elastic-plastic closed form solution ($\nu = 0$) are shown in Figure 7.9. An outer stress boundary was used in the analysis, as discussed in Sec. 7.2.2.1. Material properties are given in Table 7.2. An unusually high k_B value of 1250.0 was used in order to limit volume changes and to facilitate comparison with the constant volume closed form solution. K_o was taken as 1.0 to model the isotropic consolidation condition assumed in the closed form solution.

The initial slope of the two curves is 2G, as predicted by the elastic closed form solution in Equation 7.4. The expansion curve for non-linear material properties, however, lacks the initial linear elastic behaviour and exhibits a much softer response. Although a softer response was anticipated, such a large difference between the two solutions was unexpected. The inaccuracy of the closed form solution in failing to take into account the effects of σ_3' as discussed in Section 7.3.2 may be the cause of the large discrepancy.

TABLE 7.2

MATERIAL PROPERTIES FOR SAND

PARAMETER	NON-LINEAR ELASTIC COHESIONLESS MATERIAL
D_r (%)	75
k_E	750.0
n	0.5
k_B	1250.0
m	0.5
R_f	0.9
c (Psf)	0.0
ϕ_1' (deg)	39.0
$\Delta\phi$ (deg)	4.0
ϕ_{cv}' (deg)	33.0
ν (deg)	0.0
μ_o	0.4
γ_{sat} (Pcf)	122.4
Depth (ft)	20.0
σ_{vo}' (Psf)	1200.0
K_o	1.0
P_{atm} (Psf)	2116.2

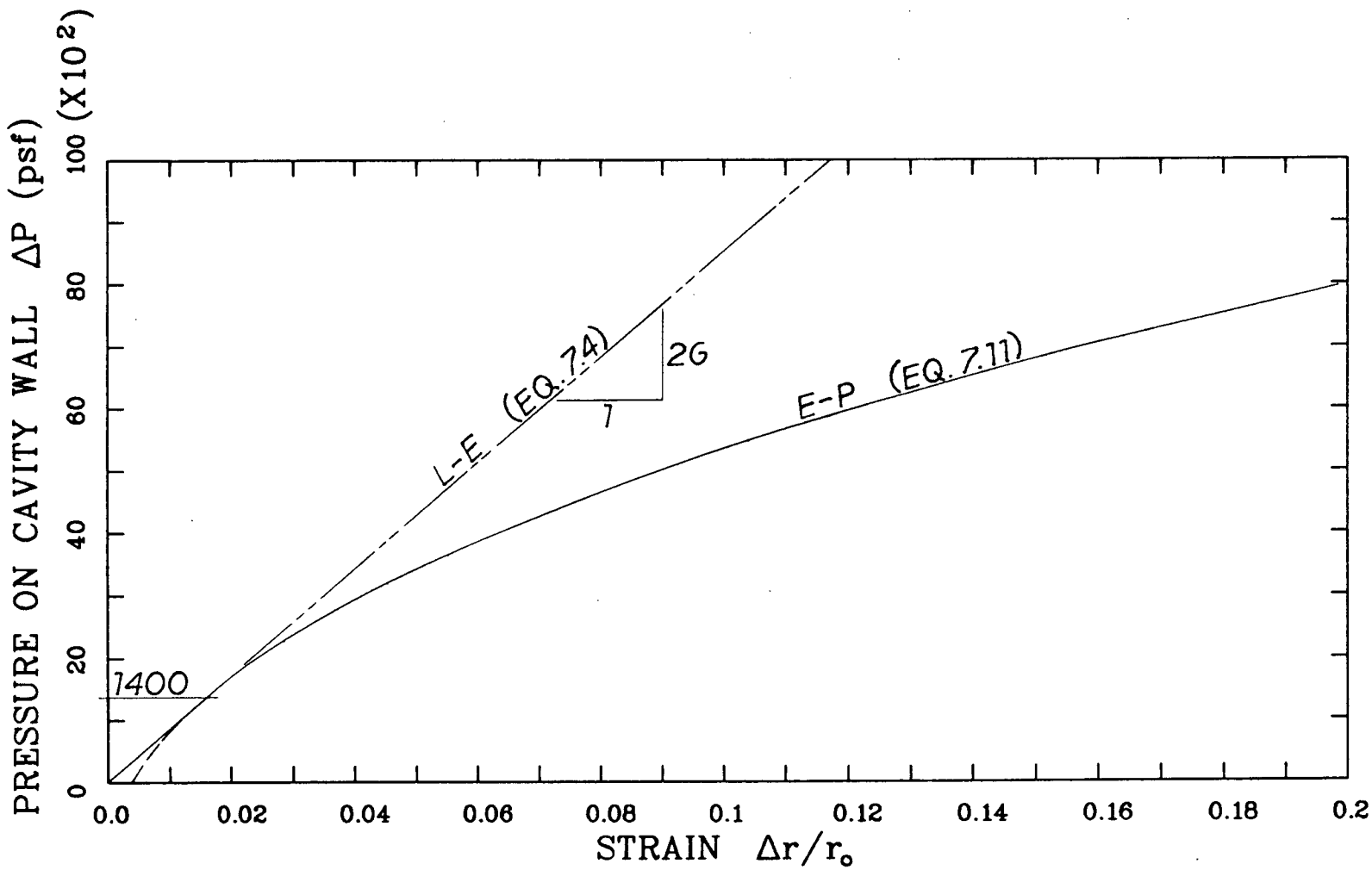

FIGURE 7.8: CLOSED FORM SOLUTION FOR CAVITY EXPANSION IN DENSE SAND

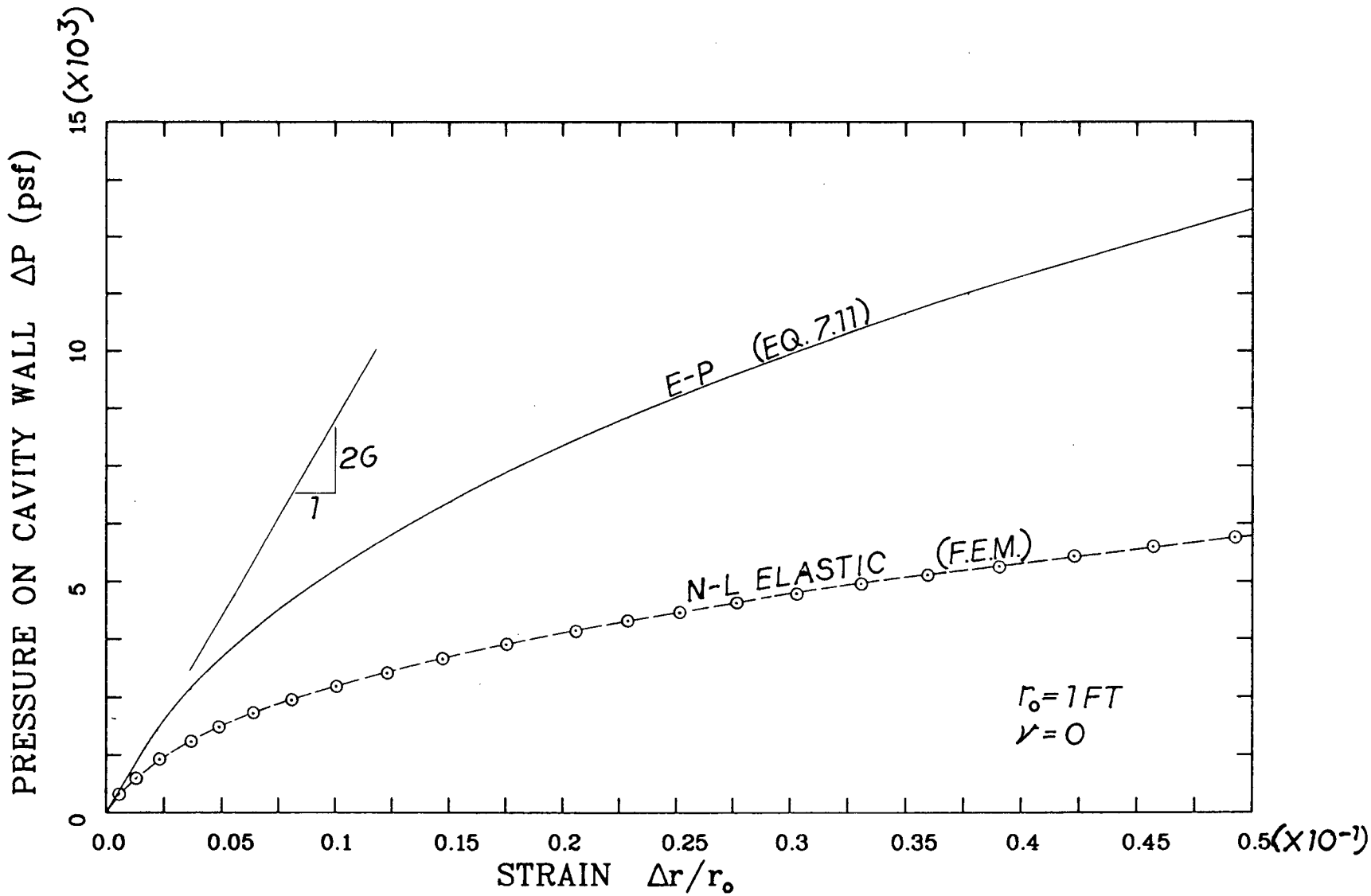

FIGURE 7.9: CAVITY EXPANSION CURVES FOR DENSE SAND

CHAPTER 8

PRESSUREMETER EXPANSION

8.1 INTRODUCTION

The pressuremeter is essentially an expandable tube which is either pushed into the soil or inserted into a pre-bored hole in the ground and inflated under controlled conditions (Robertson, 1982). Plots of Pressure vs. Volume Increase, referred to as pressure expansion curves, are obtained from the tests, from which values for soil parameters can be determined.

The foregoing plane strain axisymmetric cavity expansion analysis is generally considered to be a good model for pressuremeter expansion tests. Recent research by Yan (1986), using three-dimensional axisymmetric finite element analyses, has confirmed the validity of the plane strain cavity expansion model for pressuremeter analysis. For typical aspect ratios of pressuremeters ranging from about 6 to 8, pressure-deformation curves predicted from three-dimensional axisymmetric analyses were nearly identical to those obtained using the plane strain formulation described in Section 8.2. For simplicity, the cavity expansion formulation can be used to model pressuremeter expansion without significant errors.

The load-deflection relationship of pressuremeter expansion was analysed using the incremental elastic finite element method. Pressuremeter curves obtained from the analyses were compared with P-Y curves obtained in Chapters 9 and 10 to determine a rational method for deriving P-Y curves from pressuremeter curves. The results are presented in Chapter 11.

8.2 FINITE ELEMENT DOMAIN ANALYSED

To investigate the pressure-deflection response of the pressuremeter problem, plane strain axisymmetric analyses were performed using the finite element mesh shown in Figure 7.2. The placement of rollers along the top and bottom boundaries of the mesh ensured deformations only in the horizontal plane. The outer boundary was left unconstrained to simulate a boundary of zero stress change. Errors arising from the omission of pressures exerted along this boundary by soil outside the finite element domain were shown in Section 7.2.2.1 to be negligible. Pressure loads were applied to the side of the mesh over a length of one foot as indicated. Soil disturbances and stress changes due to the placement of the pressuremeter probe were ignored. An isotropic consolidation insitu stress condition was assumed for the entire mesh.

8.3 COHESIVE SOIL

The results of the analyses for a normally-consolidated undrained clay are presented in Figure 8.1. Soil parameters used in the study are given in Table 8.1 and were derived as follows:

Bulk unit weight of clay = 120 Pcf

Soil depth = H

Effective overburden stress, $\sigma_{vo}' = (120 - 62.4)\ H = 57.6\ H$

Undrained shear strength, $c_u = 0.265\ \sigma_{vo}' = 15.25\ H$

Initial Young's modulus, $E_i = 200\ c_u = 3050\ H$

For the undrained condition, $n = 0$ and $E_i = k_E P_{atm}$

therefore, $k_E = 1.44\ H$

TABLE 8.1

MATERIAL PROPERTIES FOR UNDRAINED N.C. CLAY

PARAMETER	NON-LINEAR ELASTIC COHESIVE SOIL	
	DEPTH = 10 FT	DEPTH = 20 FT
k_E	14.4	28.8
n	0.0	0.0
k_B	1200.0	2400.0
m	0.0	0.0
R_f	0.9	0.9
μ_o	0.498	0.498
c_u (Psf)	152.5	305.0
ϕ_1 (deg)	0.0	0.0
$\Delta\phi$ (deg)	0.0	0.0
ϕ_{cv} (deg)	0.0	0.0
γ_{sat} (Pcf)	120.0	120.0
Depth (ft)	10.0	20.0
σ_{vo}' (Psf)	576.0	1152.0
K_o	1.0	1.0
P_{atm} (Psf)	2116.2	2116.2

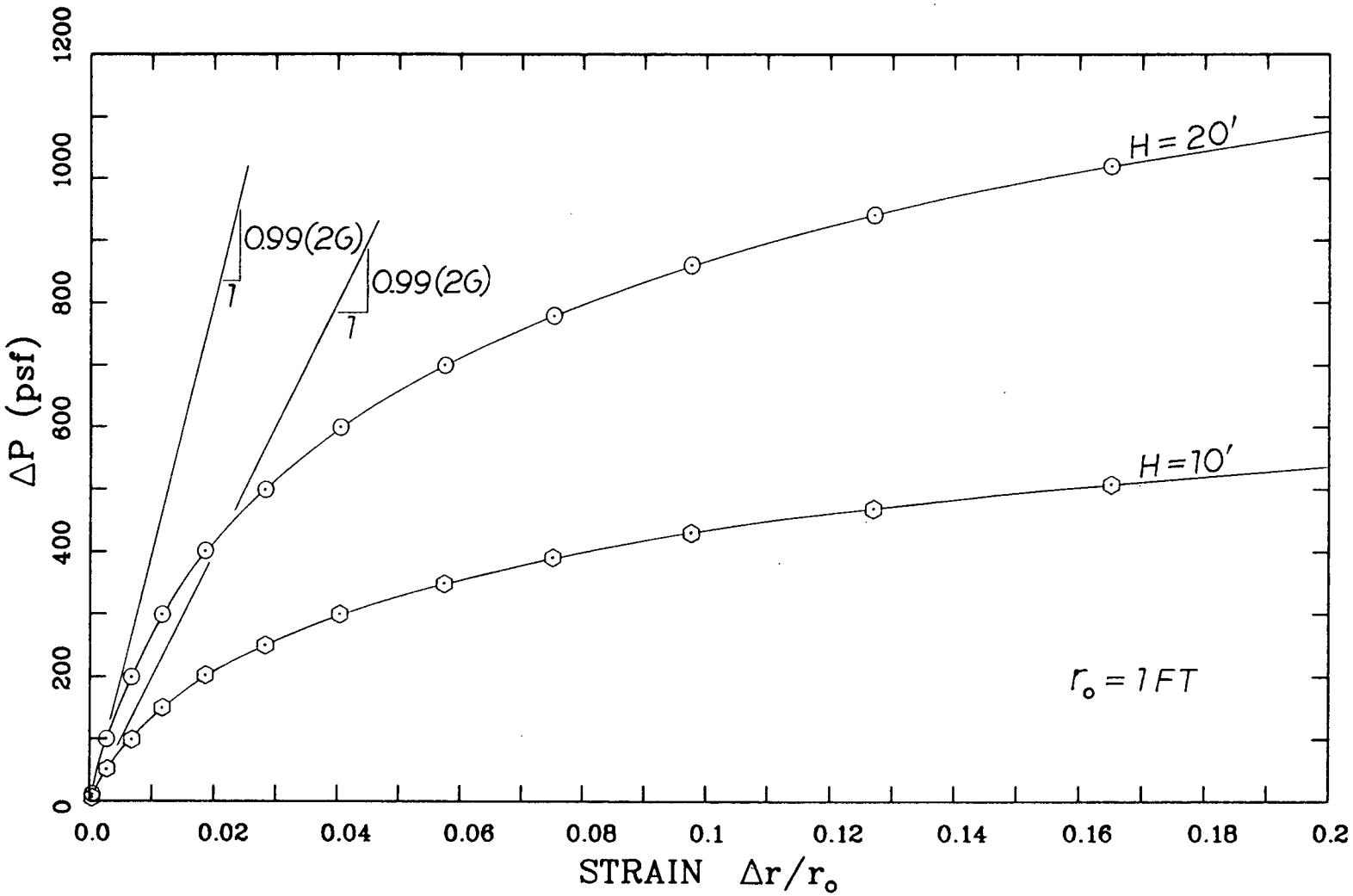

FIGURE 8.1: PRESSUREMETER CURVES FOR NON-LINEAR ELASTIC NORMALLY-CONSOLIDATED UNDRAINED CLAY FROM PLANE STRAIN AXISYMMETRIC FINITE ELEMENT ANALYSES

Taking μ_o = 0.498 for the undrained condition,

bulk modulus, $B = E_i/3(1 - 2\mu_o) = 83.3\ E_i$

and $B = k_B P_{atm}$ for m=0

therefore, $k_B = 83.3\ k_E = 120\ H$

Using H=10 ft and H=20 ft in the above equations yields the values shown in Table 8.1.

The initial slopes of the expansion curves are as expected. Values of approximately 0.99(2G) were obtained, compared to 2G predicted by the linear elastic closed form solution given by Equation 7.4. The results also show the H=20 ft curve to be merely a scaled-up version of the H=10 ft curve. The scaling factor of 2.0 indicated by the predicted load-deflection values corresponds to the differences in the values of c_u, k_E and k_B used in the two analyses.

8.4 COHESIONLESS SOIL

Finite element analyses were also performed for cohesionless soil using the mesh in Figure 7.2. The predicted pressuremeter curves for a dense sand are shown in Figure 8.2. Properties for the sand were determined from values given by Byrne & Eldridge (1982), and Byrne & Cheung (1984), and are summarized in Table 8.2.

Values of about 0.98(2G) were determined for the initial slopes of the pressuremeter curves, agreeing well with the theoretical value of 2G. The overall shape of the two curves are similar, the H=20 ft curve being a scaled-up version of the H=10 ft curve. A scaling factor of 1.66 was obtained for the range of strains shown.

Small irregularities can be observed in the predicted results.

TABLE 8.2

MATERIAL PROPERTIES FOR DENSE SAND

PARAMETER	COHESIONLESS SOIL	
	DEPTH=10 FT	DEPTH=20 FT
k_E	1000.0	1000.0
n	0.5	0.5
k_B	600.0	600.0
m	0.5	0.5
R_f	0.8	0.8
ϕ_1' (deg)	39.0	39.0
$\Delta\phi'$ (deg)	4.0	4.0
ϕ_{cv}' (deg)	33.0	33.0
D_r (%)	75	75
μ_o	0.222	0.222
u (Psf)	624.0	1248.0
γ_{sat} (Psf)	122.4	122.4
σ_m' (Psf)	330.0*	675.0*
K_o	1.0*	1.0*

* Values assumed for finite element analyses

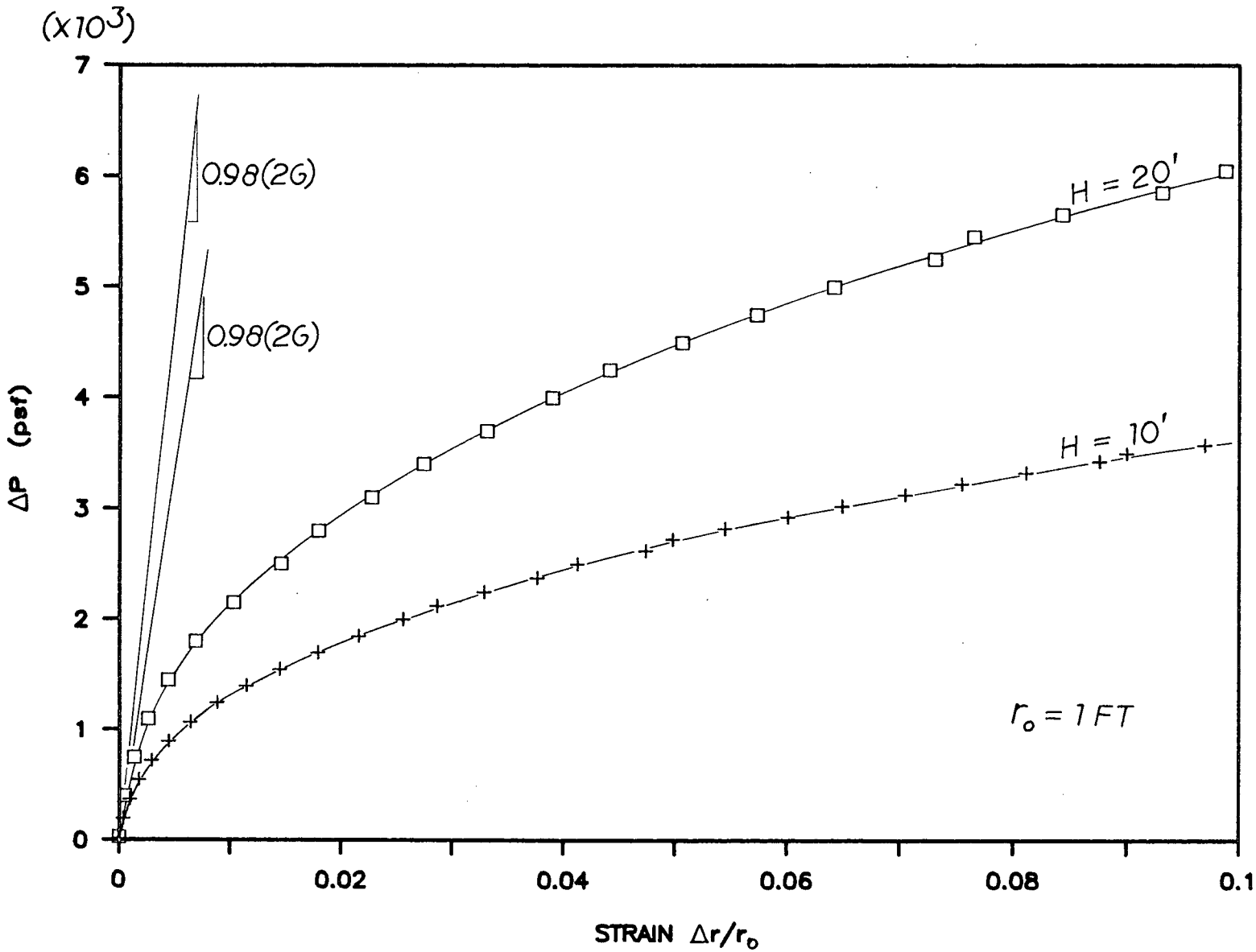

FIGURE 8.2: PRESSUREMETER CURVES FOR NON-LINEAR ELASTIC DENSE SAND FROM PLANE STRAIN AXISYMMETRIC FINITE ELEMENT ANALYSES

The load-deflection values plotted in Figure 8.2 do not describe smooth curves, but stray to either side of the best-fit relationships. These irregularities are the direct results of erratic soil behaviour at or near failure, where the strength of the soil varies with changes in σ_3', resulting in fluctuations in the stress level above and below the failure condition. A discussion of this problem is given in Section 7.3.1.

8.5 SIZE EFFECT

To simplify the conversion of radial displacements, Δr, into strain values, $\Delta r/r_o$, in the foregoing finite element analyses, an initial cavity radius of 1 ft was assumed. The actual radius of the pressuremeter cell, however, is in the neighbourhood of 1.5 inch. Analyses were performed to determine the existance of any size effect and to assess the validity of the pressuremeter results shown in Sections 8.3 and 8.4.

To examine the pressure-deflection relationship, an analysis was performed for the undrained clay using a mesh with an initial cavity diameter, D, of 3 inches. The mesh radius, R, was kept at 50D (150 in) as before. The width of the loaded area was also retained at 1 ft. Other boundary and loading conditions were kept the same as before. Soil parameters given in Table 8.1 for H = 20 ft were used.

Figure 8.3 shows the ΔP vs. Δr results of this analysis along with the curve for D = 2 ft (r_o = 1 ft). As expected, smaller displacements were obtained for the D = 3 inches case. A comparison of the ΔP vs. $\Delta r/r_o$ plots in Figure 8.4, however, shows that the results of the two analyses are identical. Consequently, size effects

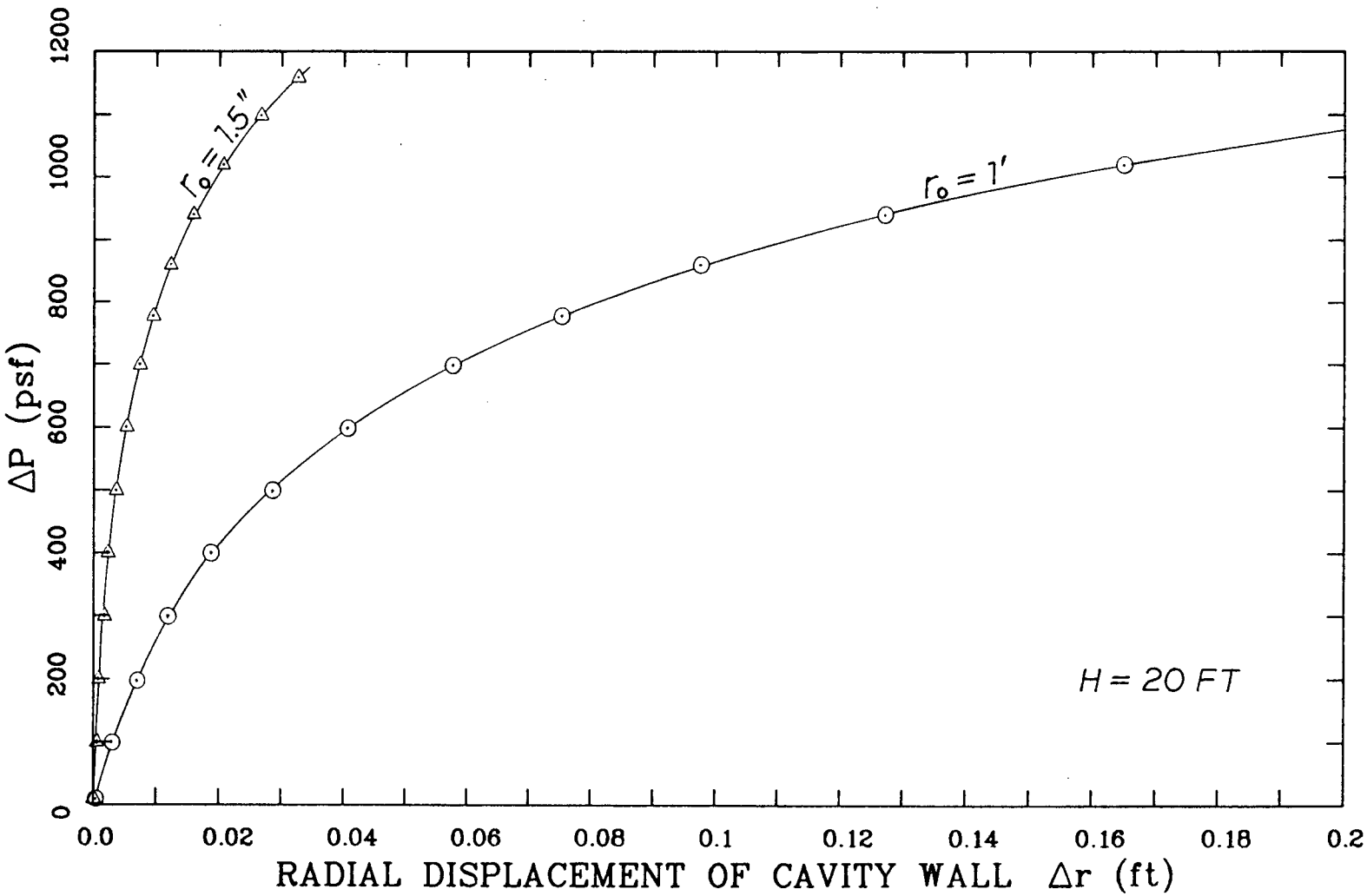

FIGURE 8.3: COMPARISON OF PRESSUREMETER CURVES PREDICTED USING DIFFERENT INITIAL CAVITY RADII

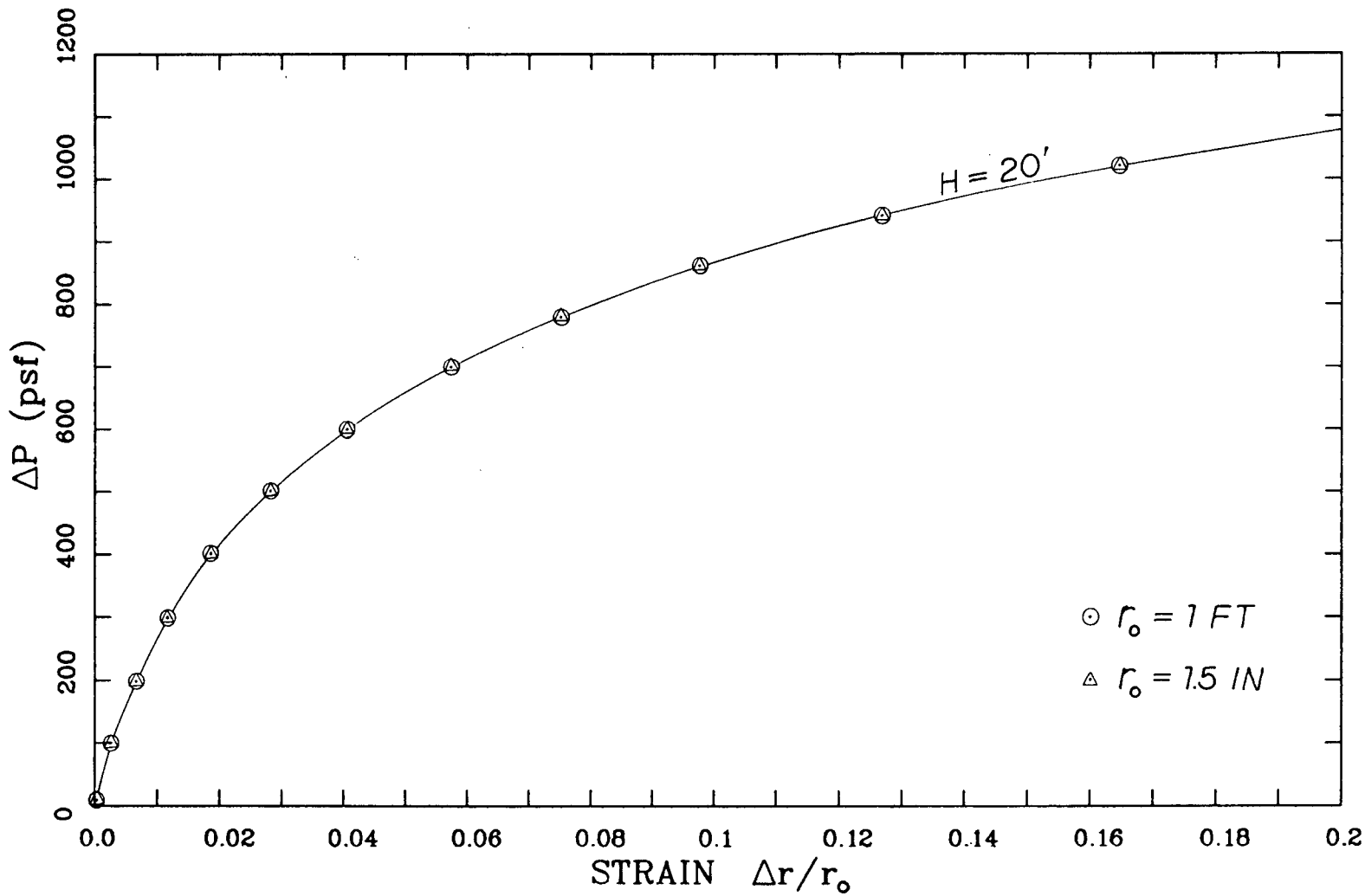

FIGURE 8.4: COMPARISON OF PRESSUREMETER CURVES PREDICTED USING DIFFERENT INITIAL CAVITY RADII

can be eliminated through the use of the circumferential strain, $\Delta r/r_o$, instead of deflection, Δr. Moreover, ΔP-Δr relationships can be obtained for pressuremeters of any size (aspect ratio > 6) simply by multiplying the $\Delta r/r_o$ values generated from any analysis by the new r_o values.

Based on the results shown in Figure 8.4, the initial cavity or cell diameter can be assumed to have no influence on the ΔP-$\Delta r/r_o$ relationship. This assumption, however, is valid only for self-boring pressuremeters installed with no soil disturbances. In practice, soil disturbance is unavoidable and its effects on the pressure-deflection relationship difficult to predict.

CHAPTER 9

PREDICTION OF P-Y CURVES

9.1 INTRODUCTION

P-Y curves for the laterally loaded pile problem were predicted using the finite element formulations described in Chapter 3. Plane strain and plane stress analyses for both undrained clay and sand were performed. The results are presented in the following sections. Additional analyses were performed to determine the effects of varying the mesh radius and the pile diameter. The P-Y curves were compared with the pressuremeter curves obtained in Chapter 8 to determine a method for deriving P-Y curves from pressuremeter curves. The results are presented in Chapter 11.

9.2 FINITE ELEMENT MESH

The finite element mesh used in the analyses is shown in Figure 9.1. As noted in Section 3.2, rollers were placed along the axis of symmetry to ensure zero displacement perpendicular to the loading direction. The outer mesh boundary was fixed at a radius of R determined from Equation 3.2. The value of R = 22D was calculated as follows:

Assuming flexible piles ($h > 7/3\ l_o$), $R = 7\ l_o$ applies.
To ensure that deformations of the pile elements are insignificant relative to soil deformations (ie: rigid pile section), take $E_p/E_{so} = 500$.
Also, $I_p = 1/4\pi r^4 = 1/64\pi D^4$

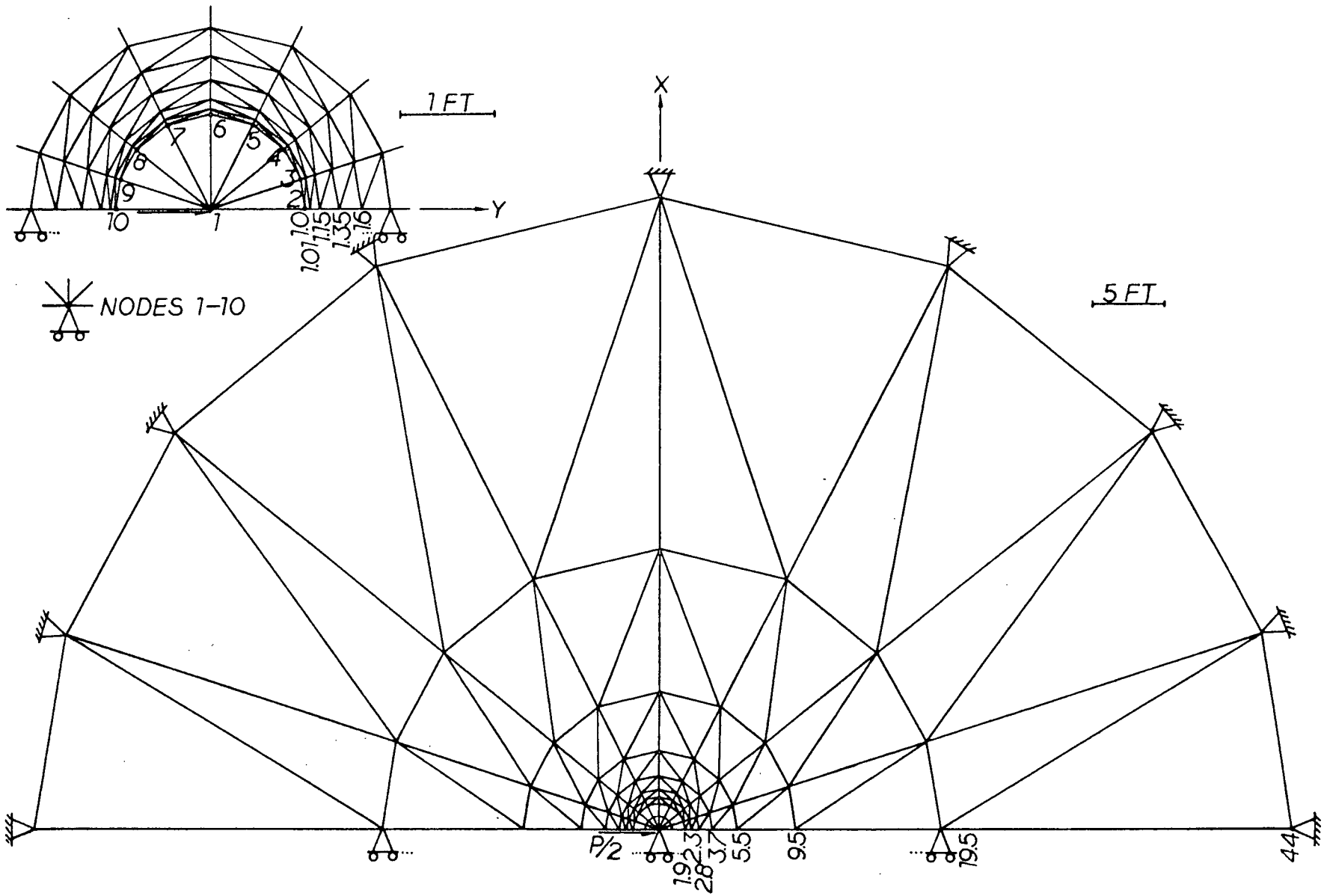

FIGURE 9.1: FINITE ELEMENT MESH FOR PLANE STRAIN OR PLANE STRESS P-Y CURVE ANALYSIS

And $l_o = [4(E_p/E_{so})I_p]^{1/4} = 3.148$ D

Finally, $R = 7\ l_o = 22.03$ D

Check: Embedded length of pile > $7/3\ l_o = 7.34$ D = 14.7 ft

for D = 2 ft.

Therefore, assumption of flexible pile is reasonable.

The mesh shown in Figure 9.1 is composed of triangular linear strain elements. A brief description of this element is given in Chapter 5. The higher-ordered 15-noded cubic strain elements were not used in the analyses due to the high computing costs involved. A trial analysis performed using the cubic strain elements produced results showing only a slight increase in sensitivity over the results obtained by using linear strain elements and the mesh in Figure 9.1. Computing costs, however, were increased by nearly 200%.

9.3 P-Y CURVES FOR UNDRAINED CLAY

Finite element analyses were performed for undrained normally-consolidated clay at various depths. The soil properties are given in Table 9.1, and are identical to those used in the pressuremeter expansion analyses in Chapter 8. The pile elements were treated as a linear elastic material. To limit deformations and to prevent failure of the pile elements, parameters 500 times greater than those of the soil were used.

TABLE 9.1

SOIL PARAMETERS FOR UNDRAINED N.C. CLAY

PARAMETER	VALUE
k_E	1.44 H
n	0
k_B	120 H
m	0
μ	0.498
R_f	0.9
c_u (Psf)	15.25 H
γ_{sat} (Pcf)	120.0
σ_v' (Psf)	57.6 H
σ_m' (Psf)	57.6 H
K_o	1.0

Note: H = depth (in feet)

9.3.1 Results

The predicted P-Y curves for various depths are shown in Figure 9.2 for plane strain analyses, and in Figure 9.3 for the plane stress condition. A pile diameter of 2 feet was assumed for the analyses.

The initial slopes of the four plane strain curves are identical, all with a value of $1.57E_i$. For μ_o=0.498, this is equal to 2.35(2G), considerably stiffer than the slope of 0.99(2G) obtained for the pressuremeter curves. Similarly, all three plane stress curves have the same initial slope of about $0.98E_i$, or 1.47(2G). These values were determined by computing the $\Delta P/\Delta Y$ ratio for very small load increments, roughly equal to 1% of P_{ult}. Slightly steeper slopes could probably have been obtained by using even smaller ΔP increments. Hence, for practical purposes, values of $1.6E_i$ (2.4(2G)) and $1.0E_i$ (1.5(2G)) are appropriate for the plane strain and plane stress conditions respectively.

None of the P-Y curves exhibit a well-defined peak value in soil resistance corresponding to P_{ult}. Instead, at large displacements (Y > 0.7 ft for plane strain, and Y > 0.4 ft for plane stress), the P-Y relationships are linear with P increasing slightly with Y. The load at which the P-Y curve becomes linear is taken as P_{ult}. Using this method, identical values of $P_{ult} = 12.1cD$ ($c \equiv c_u$) were obtained for the plane strain analyses. Likewise, consistent values of $P_{ult} = 6.1cD$ were determined for the plane stress curves.

The continuing small increases in P beyond P_{ult} is caused by the zero-displacement outer boundary. The use of the fixed boundary restricts soil displacement, which in turn limits the lateral movement of the pile. Consequently, the pile cannot displace infinitely at

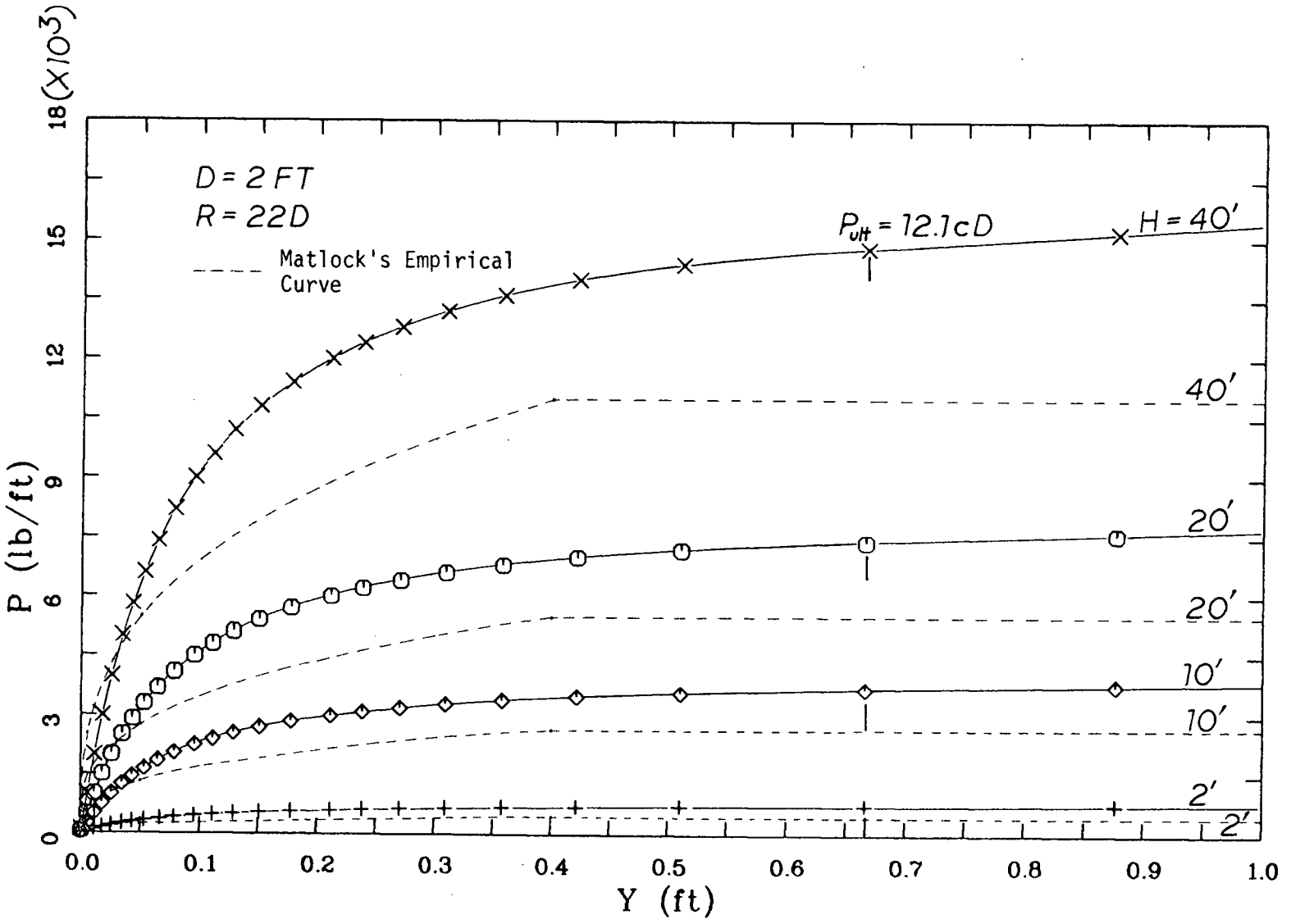

FIGURE 9.2: P-Y CURVES FOR UNDRAINED CLAY FROM PLANE STRAIN ANALYSES

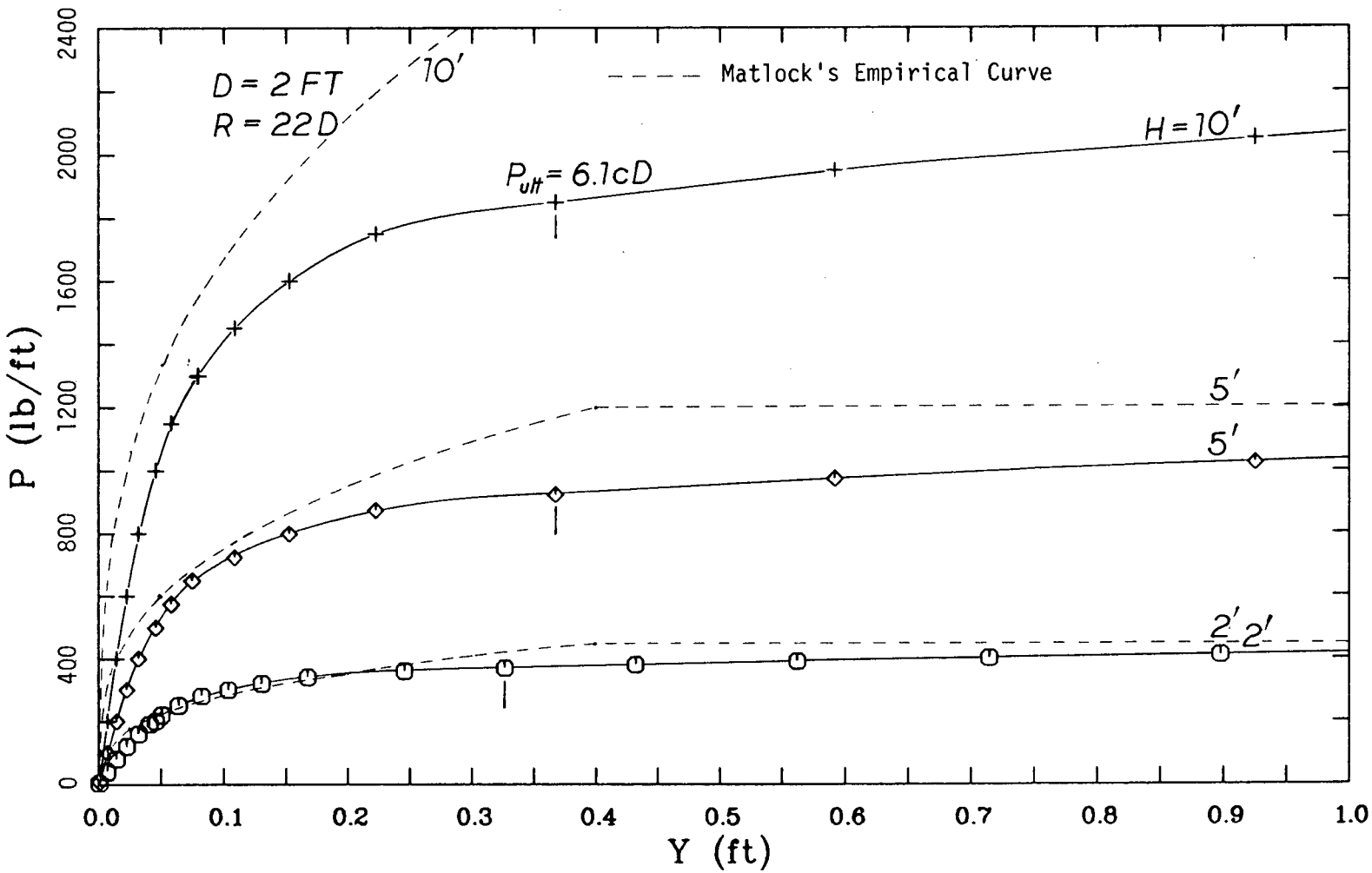

FIGURE 9.3: P-Y CURVES FOR UNDRAINED CLAY FROM PLANE STRESS ANALYSES

P_{ult}, and the P-Y curve does not flatten off as expected.

The P_{ult} value of 12.1cD obtained for the plane strain case is in reasonably good agreement with Randolph & Houlsby's (1984) results. As discused in Section 4.2.2, a soil-pile adhesion factor, α, of 0.5 was used in the finite element analyses for clay. Randolph's theoretical value of P_{ult} corresponding to $\alpha = 0.5$ is 10.82cD (Table 3.1), resulting in an error of about 12% for the finite element prediction.

9.3.1.1 Comparison with Empirical P-Y Curves

The finite element P-Y predictions are compared with empirical curves for soft clays. The empirical curves, shown as dashed lines in Figures 9.2 and 9.3, were determined using the method recommended by Matlock (1970). Calculations for determining the curves are contained in Appendix B.

P_{ult} for the empirical curves were determined by assuming a block flow failure mechanism at large depths (see Figure 3.5b). The value of 9cD obtained is considerably lower than the predicted value of 12.1cD for plane strain analyses. For three-dimensional deformations near the surface, a passive wedge failure mechanism was used (see Figure 3.5a), giving

$$P_{ult} = N_p cD \qquad 9.4$$

$$N_p = 3 + \sigma_v'/c + J\,H/D\,, \qquad 3 \leq N_p \leq 9$$

where

σ_v' = effective overburden stress

H = depth of soil

J = coefficient ranging from 0.25 to 0.5 depending on soil type

Assuming a conservative value of 0.25 for J, P_{ult} based on Equation 9.4 increases with depth, ranging from 3 at the surface to the maximum value of 9 at a depth of

$$H_c = \frac{6D}{(\sigma_v' D/cH) + 0.25} \qquad 9.5$$

For the plane stress curves shown in Figure 9.3, P_{ult} values determined from Equation 9.4 exceed the predicted values.

No initial slope value is predicted by Matlock's empirical curves. For lack of better information, the curves are drawn such that their slopes approach infinity for small lateral pile displacements. The overall agreement between empirical and predicted curves is poor, differing in both the initial slope and the P_{ult} values.

9.3.2 Effect of Pile Diameter

The results shown in Figures 9.2 and 9.3 were obtained for a pile diameter, D, of 2 ft. To determine the effect of D on the P-Y predictions, additional plane strain and plane stress analyses were performed using pile diameters of 1 and 4 ft. Soil parameters used in the plane strain analyses are for the clay at a depth of 20 ft. Parameters appropriate for a depth of 2 ft were used for the plane stress predictions. In keeping with the condition of Equation 3.2, a mesh radius of 22D was maintained for all the analyses. The same

number of elements were used for all the meshes, only the sizes of the elements were varied to accomodate the changing mesh size.

The predicted P-Y curves are shown in Figures 9.4 and 9.5. The results suggest that an increase in the pile diameter by an arbitrary factor of F_D would have the effect of increasing both P and Y by the same factor. In other words, plots of P/D vs. Y/D would yield a single curve for each of the plane strain and plane stress conditions, regardless of the value of D used in the analysis. Further discussions on normalized P-Y curves are given in Chapter 10.

9.3.3 Effect of Mesh Radius

The effect of the mesh radius, R, on the P-Y responses of laterally loaded piles were examined. As discussed in Section 3.2.2, previous work by Thompson (1977) has shown that the stiffness, but not the ultimate strength, of the P-Y curves depends on R. P-Y curves were generated for R = 10D, 20D and 50D to verify Thompson's results and to determine the sensitivity of the predicted curves to the mesh radius.

The results for plane strain analysis are shown in Figure 9.6. Plane stress P-Y curves for different values of R are presented in Figure 9.7. Soil parameters for the clay at depths of 20 ft and 2 ft were used in the plane strain and plane stress analyses, respectively.

The results obtained from the analyses confirm Thompson's observations. The stiffness, and hence, the initial slopes of the P-Y curves decrease with increasing R. Initial slopes of $2.16E_i$, $1.61E_i$, $1.57E_i$, and $1.22E_i$ were obtained for R = 10D, 20D, 22D, and 50D, respectively, for plane strain analyses. Slopes of $1.33E_i$, $0.98E_i$, and $0.77E_i$ were obtained for mesh radii of 10D, 22D, and 50D,

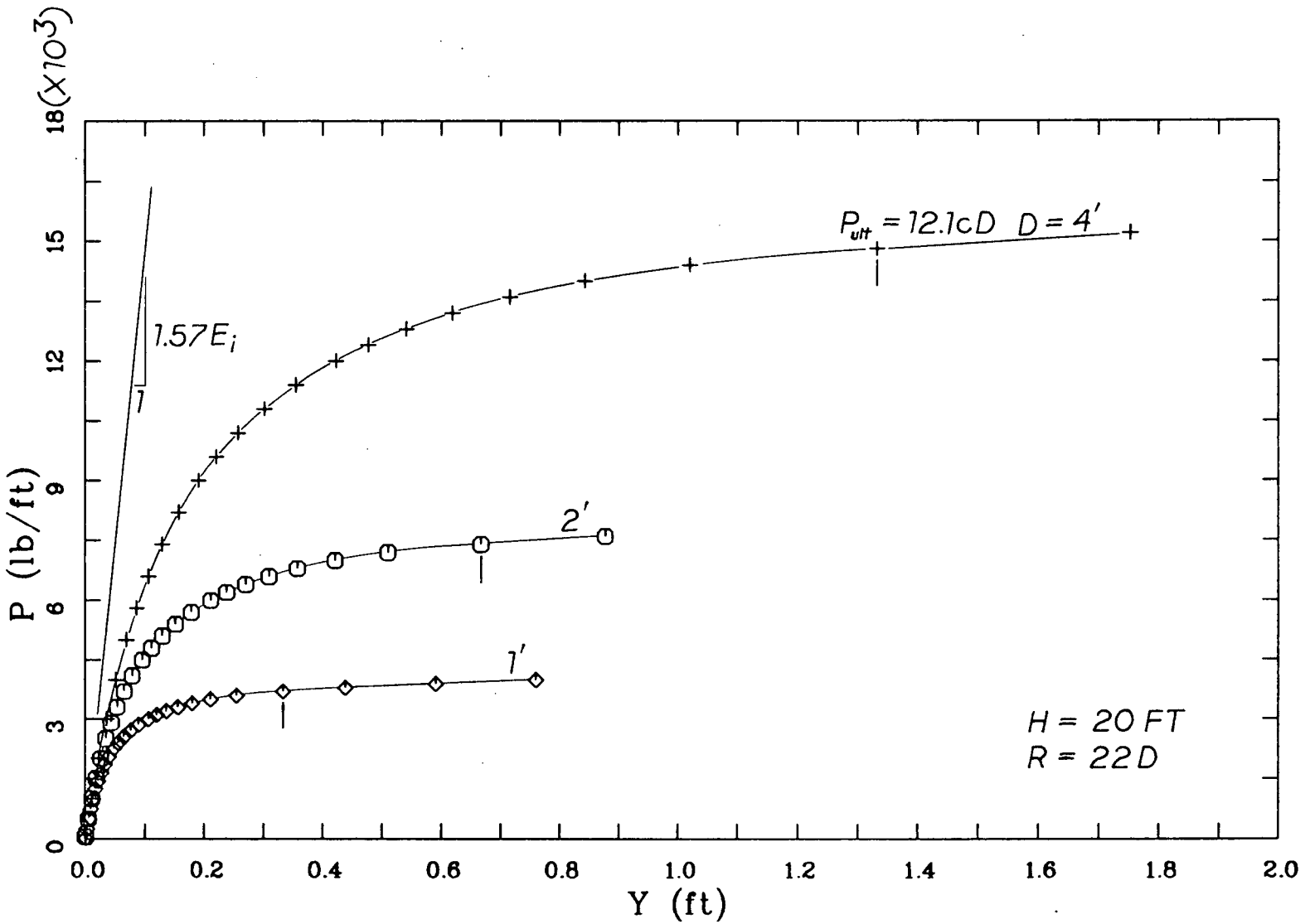

FIGURE 9.4: EFFECT OF PILE DIAMETER ON PLANE STRAIN P-Y CURVE PREDICTIONS FOR UNDRAINED CLAY

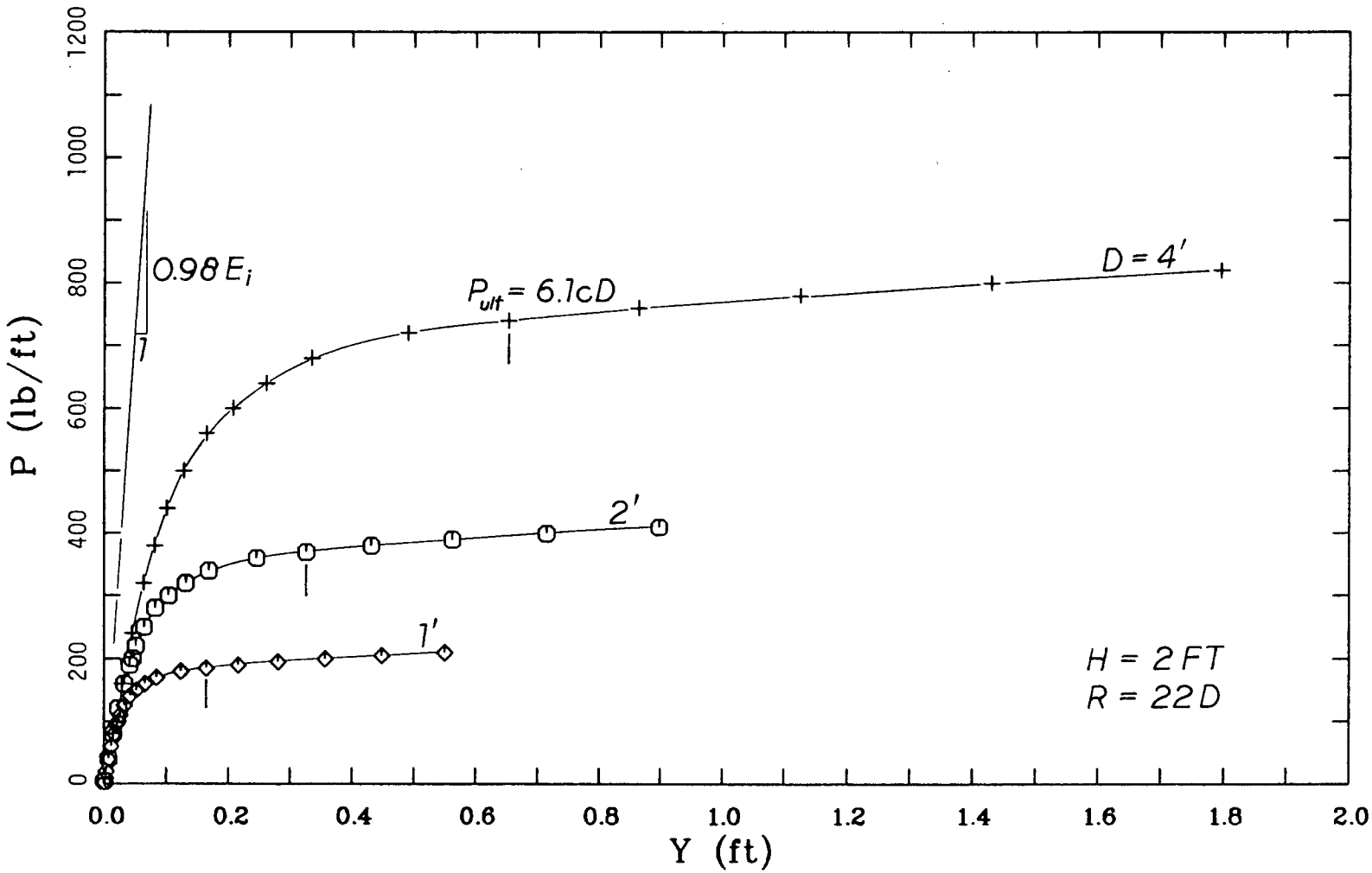

FIGURE 9.5: EFFECT OF PILE DIAMETER ON PLANE STRESS P-Y CURVE PREDICTIONS FOR UNDRAINED CLAY

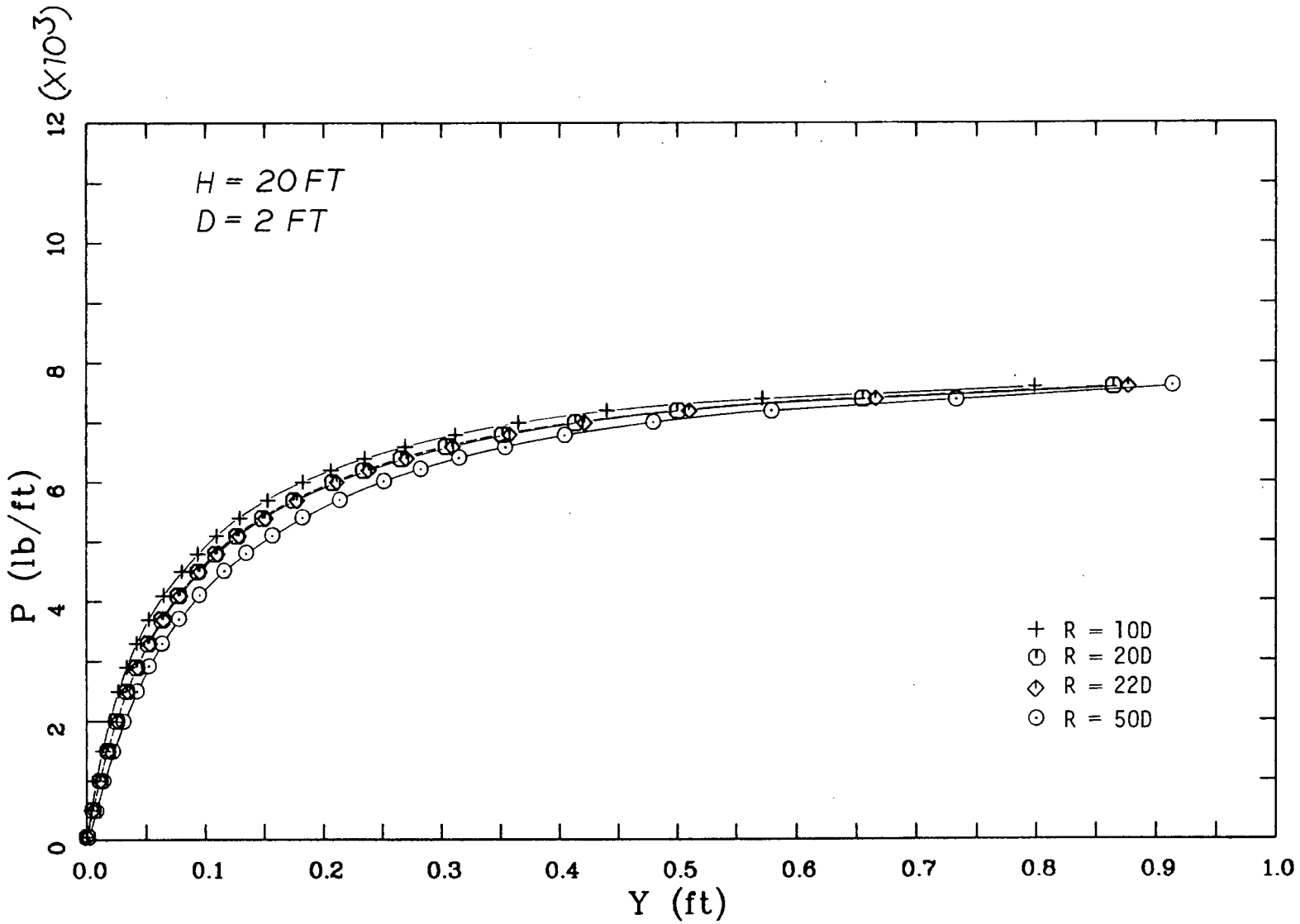

FIGURE 9.6: EFFECT OF MESH RADIUS ON PLANE STRAIN P-Y CURVE PREDICTIONS FOR UNDRAINED CLAY

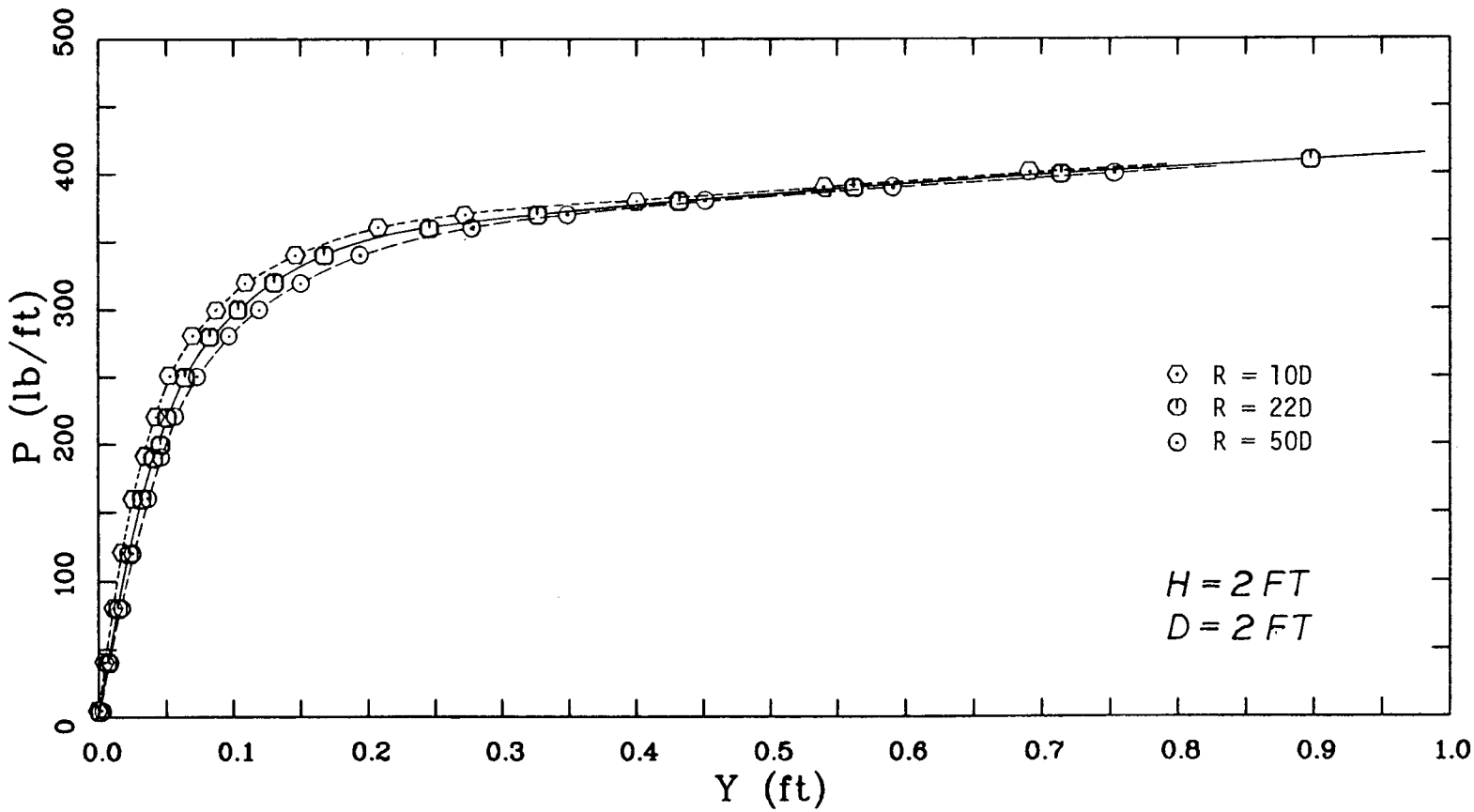

FIGURE 9.7: EFFECT OF MESH RADIUS ON PLANE STRESS P-Y CURVE PREDICTIONS FOR UNDRAINED CLAY

respectively, for plane stress analyses. R=22D was perviously determined as the appropriate mesh size for the given condition. Neither P_{ult} nor the shape of the curves appear to be overly sensitive to the value of R. In fact, only small differences exist between the R = 10D and R = 22D curves, and the R = 22D and R = 50D curves. Since R = 10D and R = 50D can be considered as approximate lower and upper bounds for the zone of influence, the curves predicted for R = 22D can be considered as good representations of actual P-Y relationships.

9.4 P-Y CURVES FOR SAND

Plane strain and plane stress P-Y curves were determined for a dense sand. The soil properties are summarized in Table 9.2. The values are identical to those used in the pressuremeter expansion analyses in Chapter 8.

As in the analyses for undrained clay, parameter values for the pile elements were 500 times greater than those of the soil elements. One exception was the internal friction angle, ϕ'. A constant value of 85° was used to ensure high strength.

To determine the insitu stresses, the following equations were used:

$$K_o = 1 - \sin\phi' \qquad 9.6$$

$$\phi' = \phi_1' - \Delta\phi' \log(\sigma_m'/P_a) \qquad 9.7$$

$$\sigma_m' = [(1 + 2K_o)/3]\ \sigma_v' \qquad 9.8$$

where

K_o = coefficient of lateral soil pressure at rest

TABLE 9.2

SOIL PARAMETERS FOR DENSE SAND

PARAMETER	VALUE
k_E	1000
n	0.5
k_B	600
m	0.5
R_f	0.8
μ_o	0.222
ϕ_1' (deg)	39.0
$\Delta\phi'$ (deg)	4.0
ϕ_{cv}' (deg)	33.0
D_r (%)	75
γ_{sat} (Pcf)	122.4
γ' (Pcf)	60.0
σ_{vo}' (Psf)	60.0 H
K_o	$1 - \sin\phi'$
ϕ' (deg)	$\phi_1' - \Delta\phi' \log(\sigma_m'/P_a)$
σ_{mo}' (Psf)	$(1 + 2K_o)\sigma_v'/3$

Note: H = depth (in feet)

ϕ' = internal friction angle

ϕ_1' = friction angle at P_a = 1 atm = 2116.2 Psf

$\Delta\phi'$ = change in ϕ' for a 10-fold increase in σ_m'

P_a = atmospheric pressure = 2116.2 Psf

σ_m' = mean normal effective stress

σ_v' = vertical effective stress

σ_m' was used as the initial overall confining pressure. The determination of σ_m' from Equations 9.6 to 9.8 involved an iterative process. A reasonable value for σ_m' was first estimated. Using this value in Equation 9.7, ϕ' was determined. K_o was then calculated from Equation 9.6 and a new value for σ_m' determined from Equation 9.8. The new σ_m' was substituted back into Equation 9.7 for a second iteration. Iterations proceeded until the new σ_m' was roughly equal to the old value.

9.4.1 Results

Figures 9.8 and 9.9 show the P-Y curves predicted for a pile diameter of 2 ft. The initial slopes for the plane strain curves range from $1.065E_i$ to $1.071E_i$, determined from $\Delta P/\Delta Y$ ratios for small load increments equal to about 0.5% of P_{ult}. For the plane stress analyses, initial slopes of $1.001E_i$ to $1.043E_i$ were obtained, using load increments of about 0.8% of P_{ult}. The slope values are tabulated in Table 9.3. Based on these figures, an initial slope of $1.08E_i$ can be reasonably assumed for both plane strain and plane stress P-Y curves predicted for any depths. For μ_o=0.222, this slope is equal to 1.32(2G), somewhat stiffer than the initial slope of

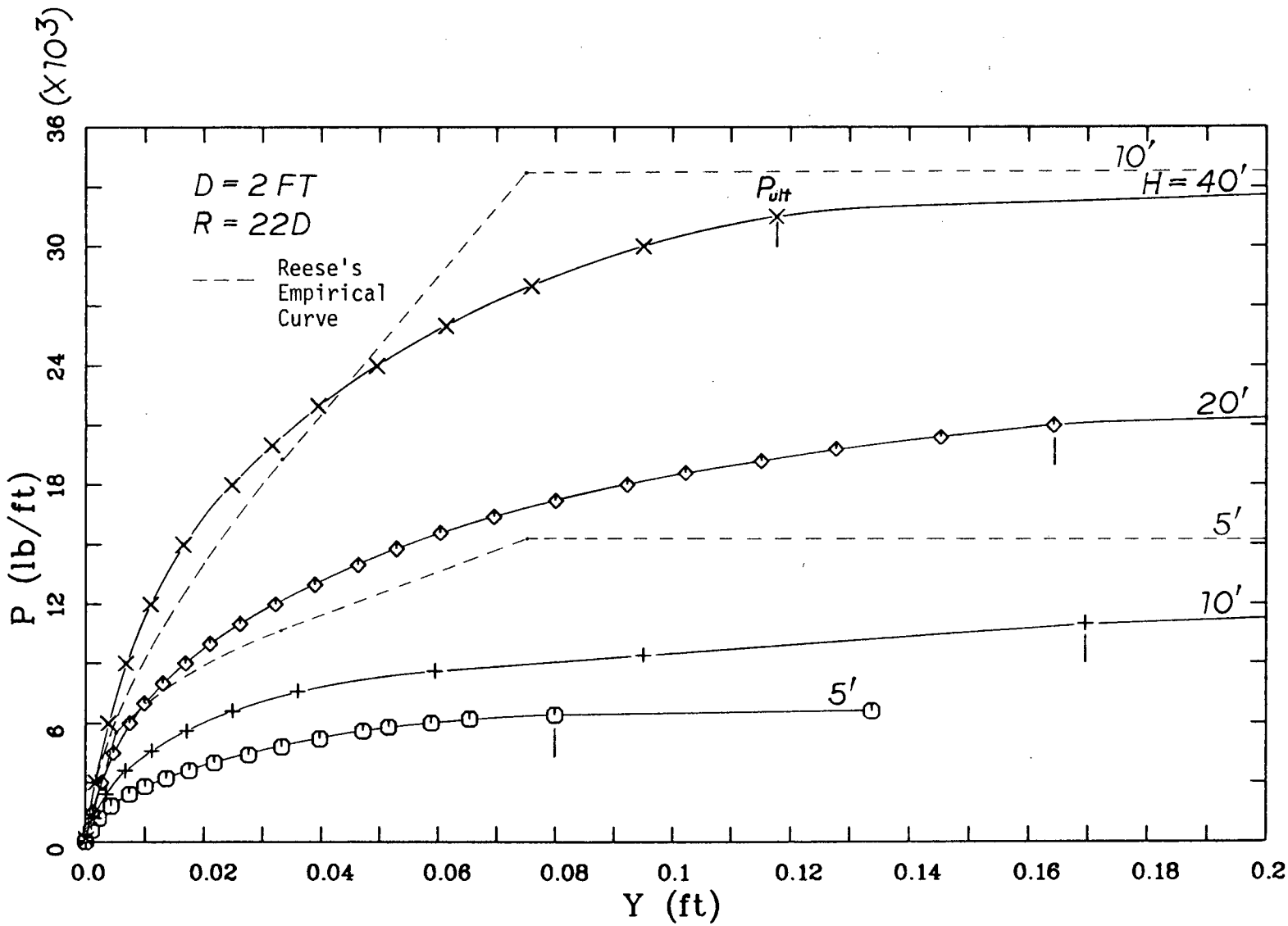

FIGURE 9.8: P-Y CURVES FOR DENSE SAND FROM PLANE STRAIN ANALYSES

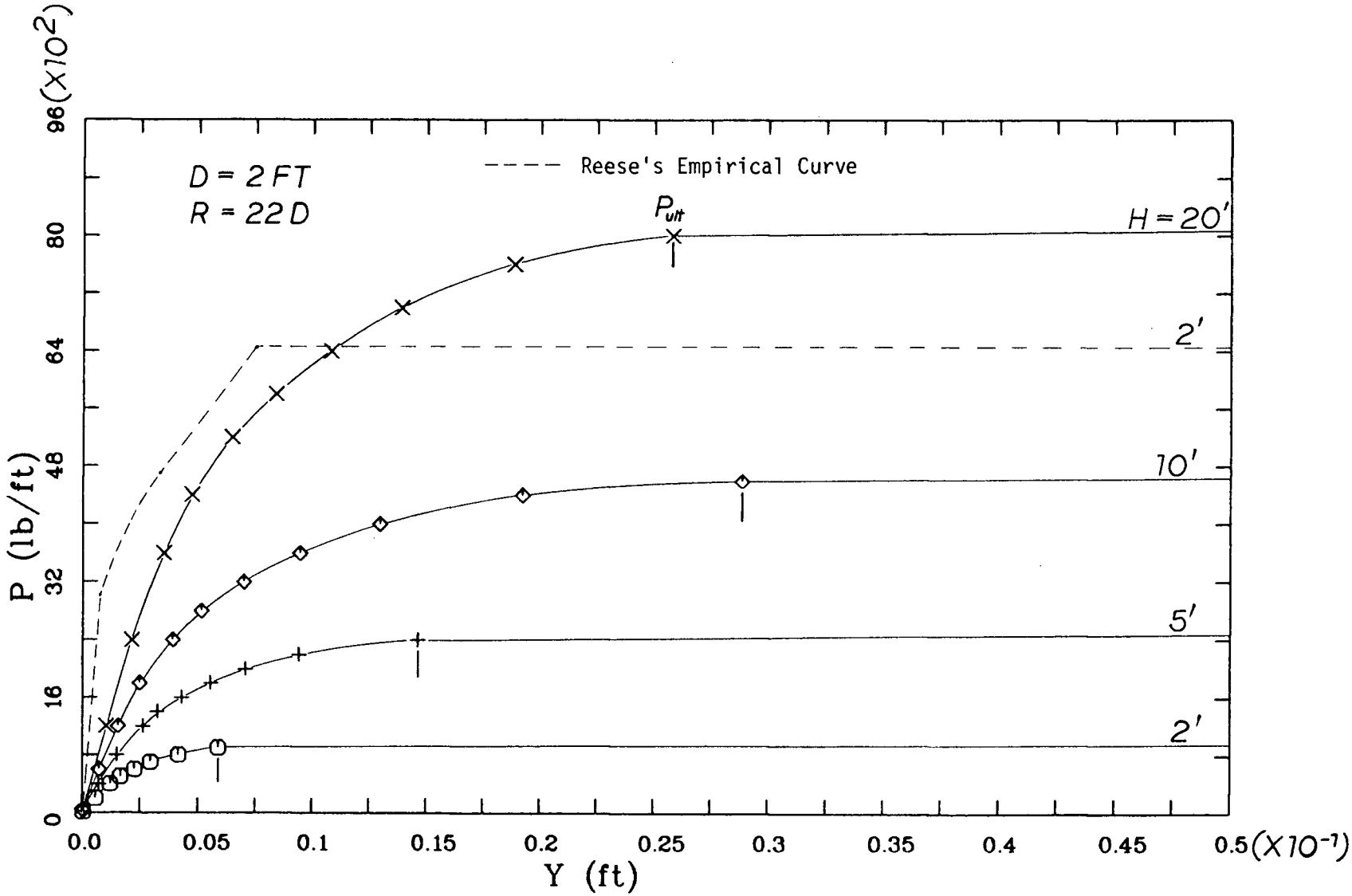

FIGURE 9.9: P-Y CURVES FOR DENSE SAND FROM PLANE STRESS ANALYSES

TABLE 9.3

RESULTS OF P-Y CURVE ANALYSES FOR DENSE SAND

DEPTH (ft)	PLANE STRAIN				PLANE STRESS			
	INITIAL SLOPE	LOAD INCREMENT	P_{ult} (lb/ft)	Y_c (ft)	INITIAL SLOPE	LOAD INCREMENT	P_{ult} (lb/ft)	Y_c (ft)
2	---	---	---	---	1.001 E_i	1.05% P_{ult}	950	0.0080
5	1.071 E_i	0.31% P_{ult}	6400	0.080	1.022 E_i	0.82% P_{ult}	2450	0.0225
10	1.065 E_i	0.45% P_{ult}	11000	0.170	1.043 E_i	0.65% P_{ult}	4600	0.0289
20	1.065 E_i	0.48% P_{ult}	21000	0.142	1.041 E_i	1.22% P_{ult}	8150	0.0365
40	1.066 E_i	0.48% P_{ult}	31500	0.118	---	---	---	---

0.98(2G) obtained for the pressuremeter curves in Chapter 8.

P_{ult} and the corresponding deflections, Y_c, for the P-Y predictions are also given in Table 9.3. As in the analyses for clay, none of the P-Y curves exhibit a peak value for P. Rather, slow linear increases in P with Y beyond the points of failure are observed. Accordingly, P_{ult} was taken as the load at which the linear load-deflection behaviour begins.

9.4.1.1 Comparison with Empirical P-Y Curves

Empirical P-Y curves for sand are also shown in Figures 9.8 and 9.9. The curves were determined according to the method recommended by Reese et al. (1974). Calculations are shown in Appendix B.

P_{ult} for the empirical curves were determined using a passive wedge failure mechanism at shallow depths, and a flow block model at large depths (see Figure 3.5). The equations derived from these models are given below:

Passive wedge:

$$P_{ult} = A\gamma' H\left[\frac{K_o H \tan\phi' \sin\beta}{\tan(\beta-\phi')\cos\alpha} + \frac{\tan\beta}{\tan(\beta-\phi')}(D + H\tan\beta\tan\alpha) + K_o H \tan\beta(\tan\phi' \sin\beta - \tan\alpha) - K_a D)\right] \qquad 9.9$$

Flow block:

$$P_{ult} = AD\gamma' H\,(K_a(\tan^8\beta - 1) + K_o \tan\phi' \tan^4\beta) \qquad 9.10$$

where

γ' = effective unit weight of the sand

H = depth

ϕ' = internal friction angle

$\alpha = \phi'/2$

$\beta = 45^{o} + \alpha$

K_o = coefficient of lateral earth pressure at rest

K_a = Rankine coefficient of active earth pressure

$= \tan^2(45^{o} - \alpha)$

A = adjustment factor to correct for differences between field and predicted results

Values of A determined by Reese et al. are shown in Figure B.2a.

Using Equations 9.9 and 9.10, theoretical P_{ult} values were calculated and compared with the finite element predictions. The results are shown in Table 9.4. Equating the theoretical and predicted P_{ult} values for plane strain analyses, A ranging from 0.0645 to 0.0697 were obtained. A constant value of A = 0.065 appears to be appropriate. For plane stress analyses, the calculated values of A decrease with depth. Such a trend is expected since the passive wedge failure mechanism is valid only for shallow depths, and P_{ult} predicted for large depths would be overestimated. A correction factor of about 0.35 would be appropriate for P-Y curve predictions at or near the ground surface.

9.4.2 Effects of Pile Diameter

Additional P-Y analyses were performed for the dense sand using pile diameters of 1 and 4 ft. Plane strain and plane stress conditions for the sand at a depth of 20 ft were considered. The radius of the finite element mesh was maintained at R=22D according to Equation 3.2.

TABLE 9.4

COMPARISON OF THEORETICAL

AND PREDICTED P_{ult} VALUES

DEPTH (ft)	ϕ' (deg)	σ_{mo}' (Psf)	K_o	K_a	P_{ult} from THEORY	P_{ult} from FEM	A [see note]
Plane Strain Analyses					(Eq. 9.10)		
5	43.5	162.5	0.31	0.18	98105 A	6400	0.0652
10	42.5	330.0	0.33	0.20	170467 A	11000	0.0645
20	41.0	675.0	0.34	0.21	286834 A	21000	0.0732
40	39.8	1370.0	0.36	0.22	484331 A	31500	0.0650
Plane Stress Analyses					(Eq. 9.9)		
2	45.1	63.5	0.29	0.17	3033 A	950	0.313
5	43.5	162.5	0.31	0.18	12217 A	2450	0.201
10	42.2	330.0	0.33	0.20	38426 A	4600	0.120
20	41.0	675.0	0.34	0.21	128448 A	8150	0.063

Note: γ' = 60.0 Pcf

D = 2 ft

P_{atm} = 2116.2 Psf

Values of A were determined by comparing P_{ult} obtained from the passive wedge and flow block models with P_{ult} obtained from the finite element analyses. The values are not those given by Reese (ie: Figure B.2a).

The results of the analyses are shown in Figures 9.10 and 9.11. As in the case of the undrained clay, changing D by a factor F_D resulted in changes in both P and Y by the same factor F_D. Consequently, plotting P/D vs. Y/D for any pile diameter would yield a unique curve for each of the plane strain and plane stress condition at a given depth.

9.4.3 Effect of Mesh Radius

To determine the sensitivity of the predicted P-Y responses to changes in the mesh radius, the problem was analysed using mesh radii of 10D, 20D, and 50D. The results for plane strain analyses are shown in Figure 9.12. Plane stress predictions are shown in Figure 9.13.

For plane strain analyses, the shape of the P-Y curve for loads approaching P_{ult} is sensitive to the mesh radius used. The R=50D curve shows a much softer response than the R=10D curve. The initial slope and the initial portion of the curve, however, are relatively insensitive to R, and only minor differences in P_{ult} were obtained for the various mesh radii used.

For plane stress analyses, neither the initial slope nor the shape of the P-Y curve are sensitive to the mesh radius. The curves differ only slightly from each other despite the wide range of mesh radius used in the analyses. Identical values for P_{ult} were also obtained from the four analyses.

Overall, the results show that the initial slope decreases with increasing mesh radius, but at a slow rate. The shape of the curves for loads less than about 1/2 P_{ult} was also insensitive to the mesh radius. Consequently, the curves can be considered as good

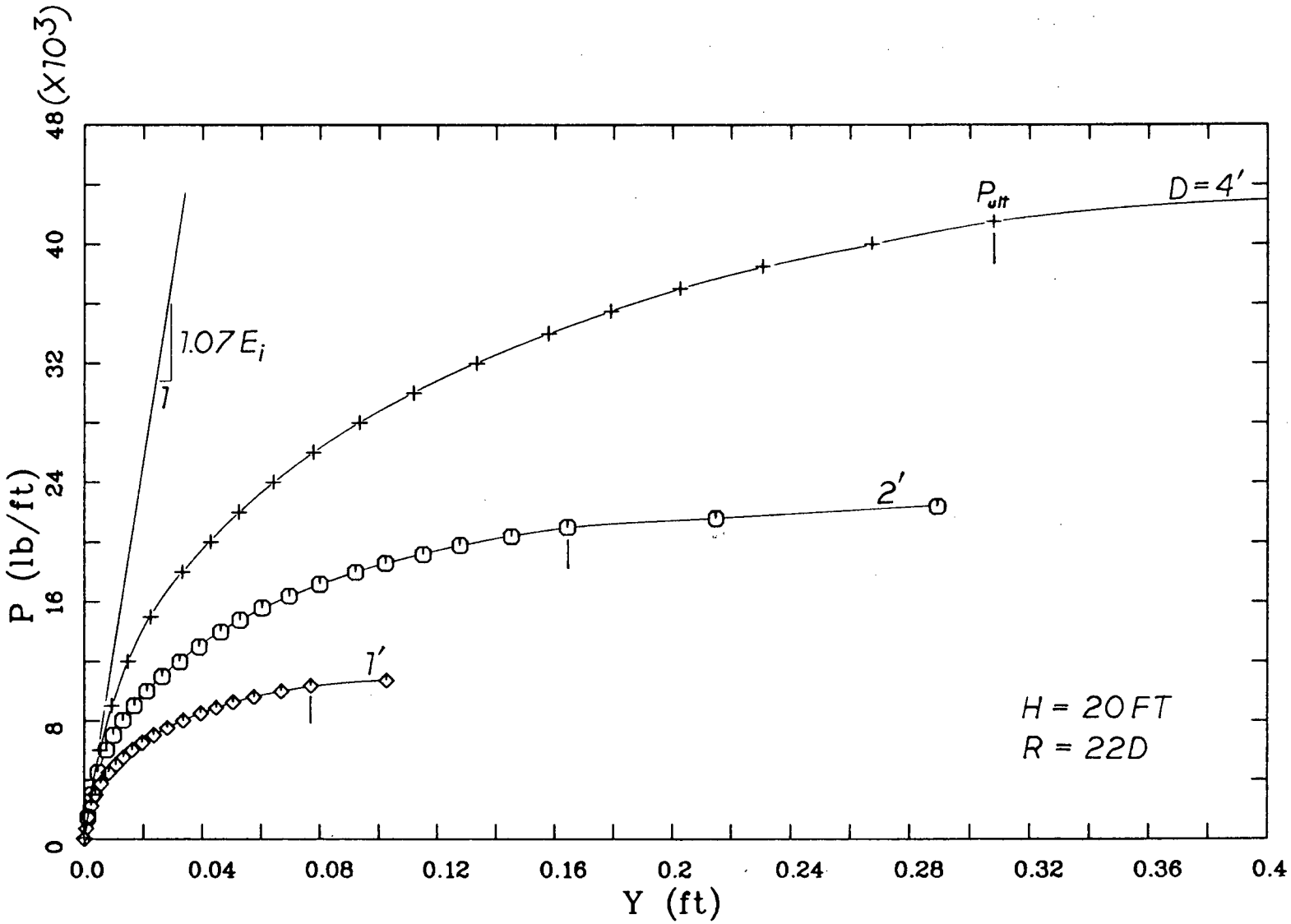

FIGURE 9.10: EFFECT OF PILE DIAMETER ON PLANE STRAIN P-Y CURVE PREDICTIONS FOR DENSE SAND

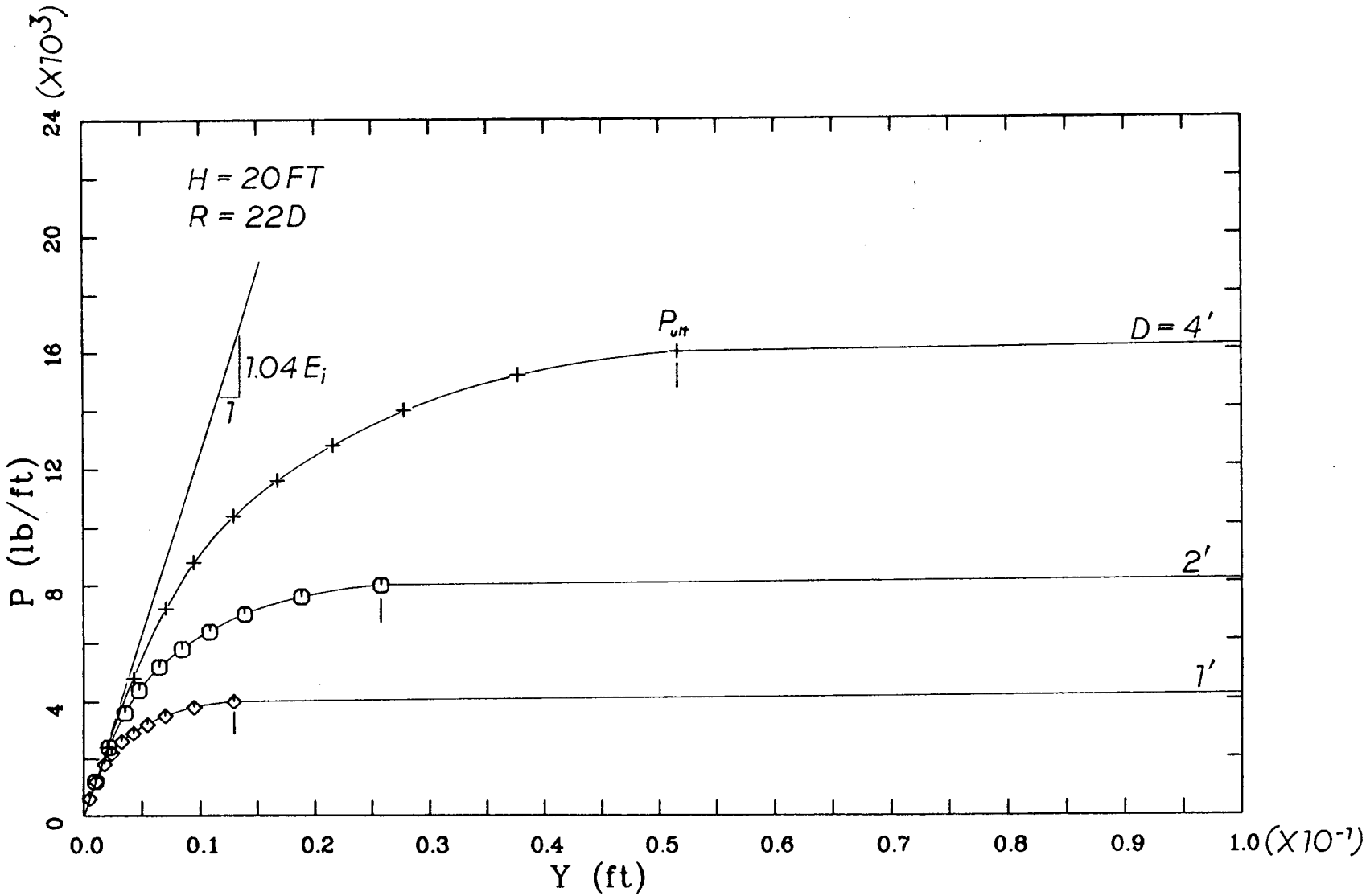

FIGURE 9.11: EFFECT OF PILE DIAMETER ON PLANE STRESS P-Y CURVE PREDICTIONS FOR DENSE SAND

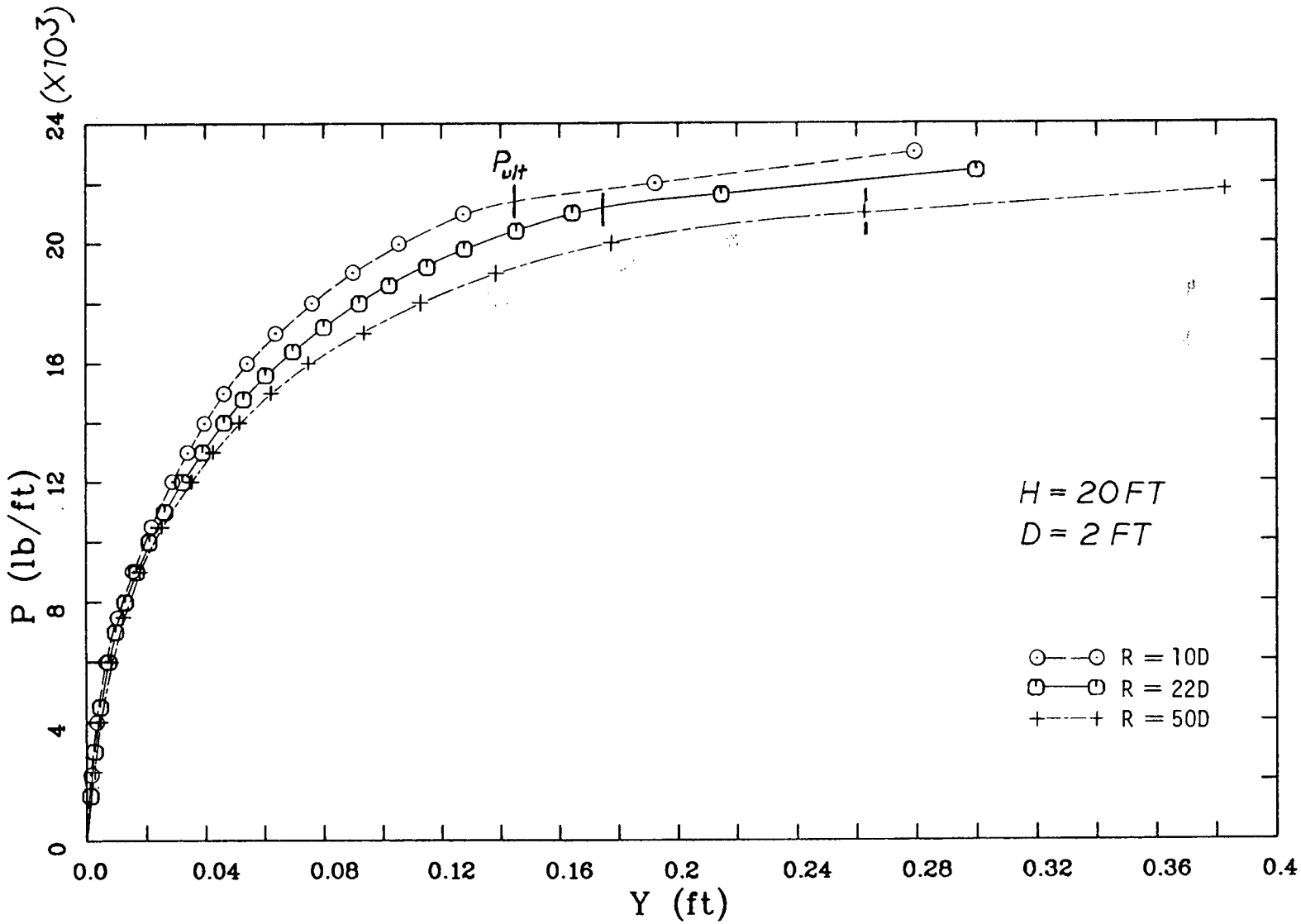

FIGURE 9.12: EFFECT OF MESH RADIUS ON PLANE STRAIN P-Y CURVE PREDICTIONS FOR DENSE SAND

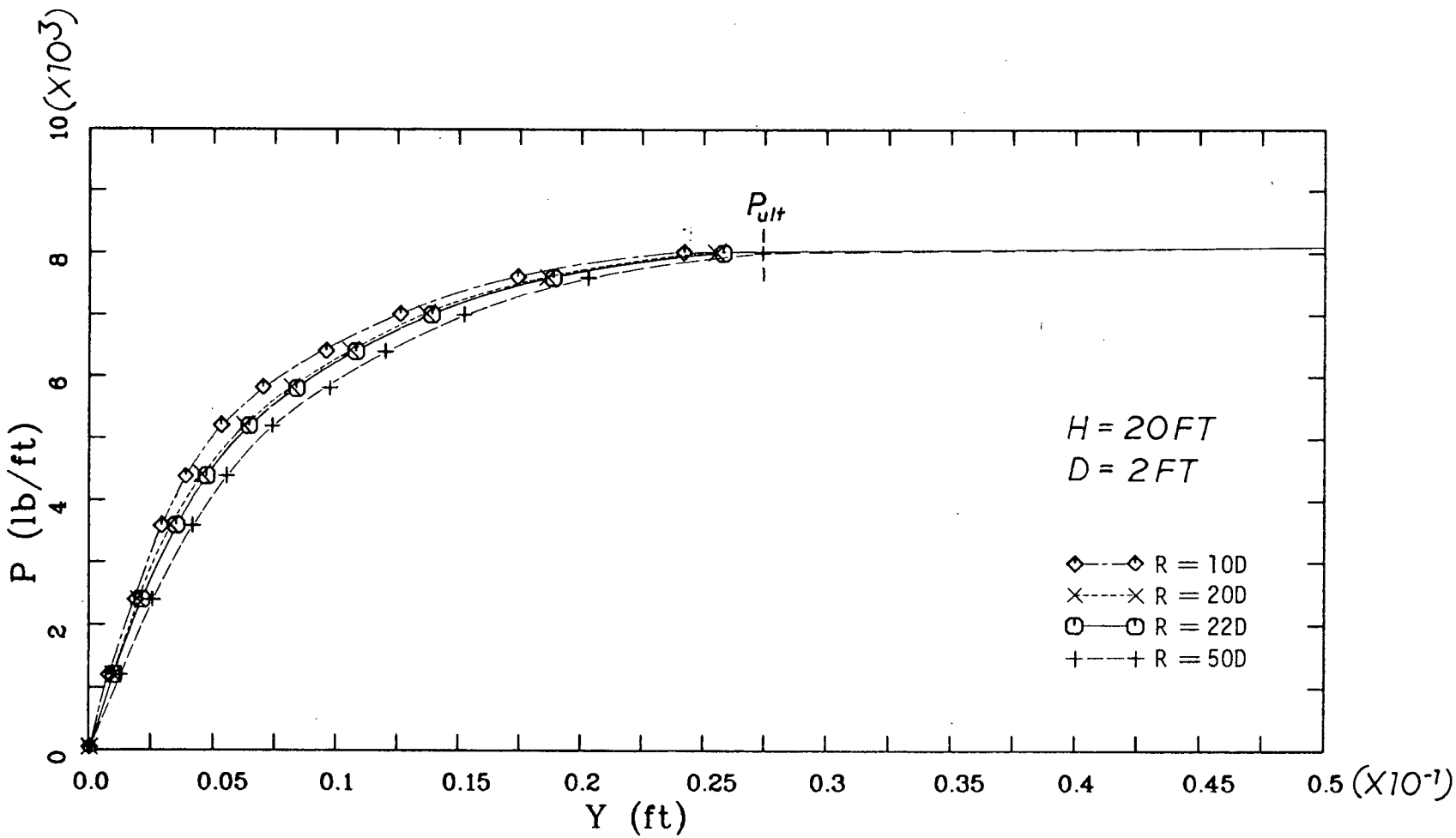

FIGURE 9.13: EFFECT OF MESH RADIUS ON PLANE STRESS P-Y CURVE PREDICTIONS FOR DENSE SAND

descriptions of the P-Y relationship for small loads. For larger loads near the failure condition, use of the plane strain P-Y curves may result in errors. However, since plane strain curves are applicable for load-deflection responses at large depths where the loading conditions are generally less severe, the errors are minimized.

CHAPTER 10

SIMPLIFIED METHOD FOR PREDICTING P-Y CURVES

10.1 INTRODUCTION

The prediction of P-Y curves from finite element analyses is both costly and time consuming. For many problems concerning laterally loaded piles, P-Y curves derived from empirical correlations are sufficient. Methods were recommended by Matlock (1970), and Reese et al. (1975, 1974) for determining P-Y curves for soft clay, stiff clay, and sand, respectively. These methods were subsequently adopted by the American Petroleum Institute for use in designing laterally loaded piles. Comparisons of these empirical curves with the finite element predictions are shown in Chapter 9.

The procedures recommended by Matlock and Reese et al. for determining P-Y curves are based on correlations with results of pile loading tests. However, load tests were performed at only one site for each of the three soil types. The resulting P-Y correlations may therefore be site specific, influenced by local soil characteristics or abnormalities not found in other soils. As an alternative to the empirical methods, simplified P-Y curves based on the finite element predictions were derived. The advantage of the finite element approach lies in its use of fundamental soil parameters and stress-strain relationship, and is therefore valid for general applications.

10.2 SIMPLIFIED P-Y CURVES FOR UNDRAINED CLAY

P-Y curves were predicted for an undrained normally-consolidated clay in Section 9.3. The effects of various parameters on

the P-Y predictions were examined and a method devised for normalizing the curves.

10.2.1 Normalized P-Y Curves

As discussed in Section 9.3.1, consistent values were obtained for the initial slopes and P_{ult} of the predicted P-Y curves. For plane strain analyses, P_{ult} = 12.1cD with an initial slope of $1.6E_i$. Values of 6.1cD and $1.0E_i$ were obtained for plane stress analyses. Moreover, in examining the effects of pile diameter in Section 9.3.2, plots of P/D vs. Y/D were shown to be identical for all values of D. Based on these observations, non-dimensional plots of P/cD vs. Y/D were drawn. The results are as expected. A unique curve was obtained for each of the plane strain and plane stress condition as shown in Figures 10.1 and 10.2. The normalized curves are compared in Figure 10.3.

The non-dimensional plots are useful for general design purposes. Using the curves shown in Figure 10.3, P-Y curves can be derived for circular piles of any diameter installed in a normally-consolidated clay with an undrained shear strength c. Care must be taken, however, to ensure that the curves are applied only to problems involving static loadings on single piles. Dynamic loadings and pile groups, or pile interaction effects, were not considered.

10.2.2 Simplified Method for Determining P-Y Curves

To further simplify P-Y curve predictions, the normalized curves in Figure 10.3 were divided into segments as illustrated in Figure 10.4. The steeply rising initial portions of the curves reflect

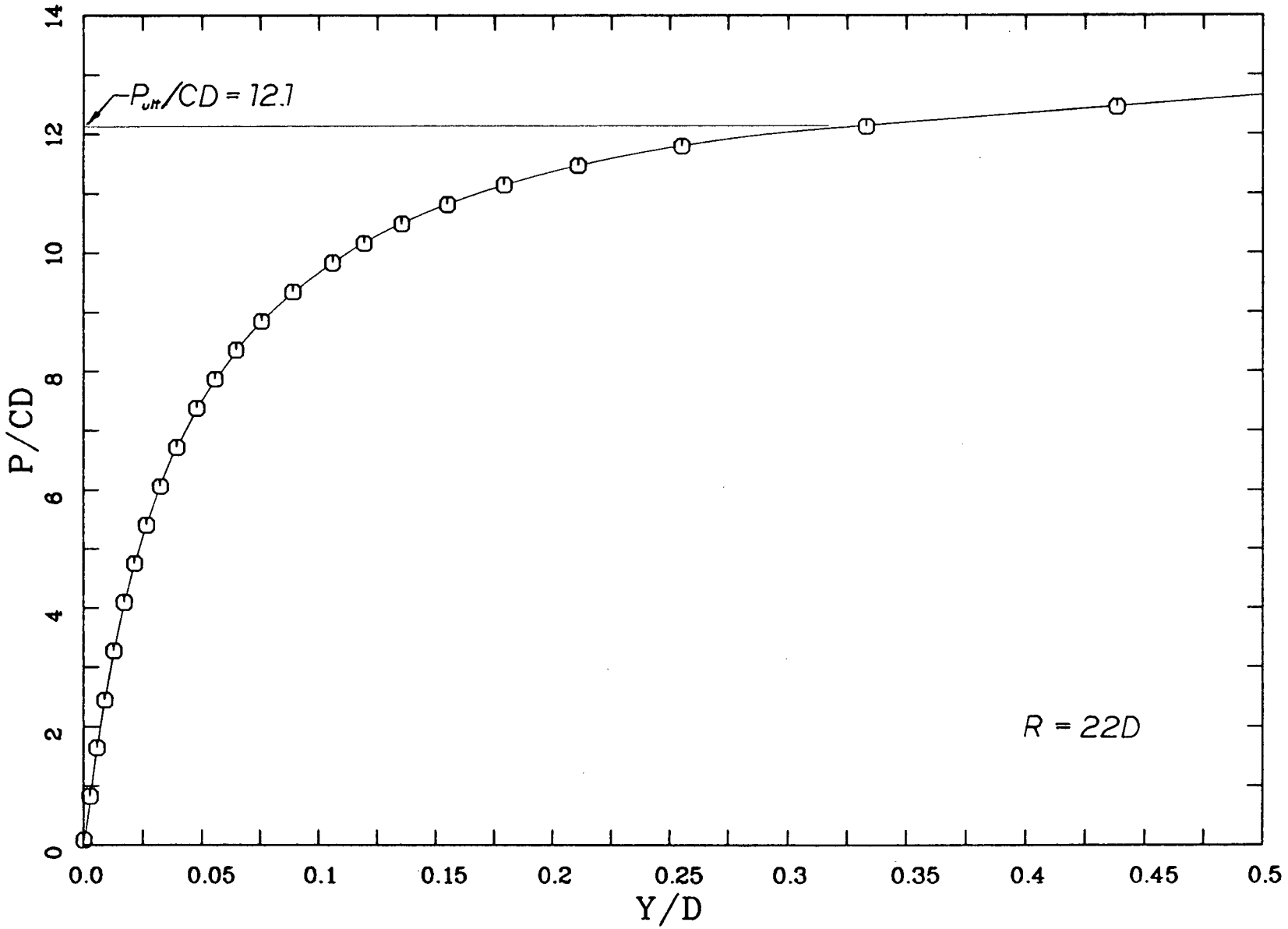

FIGURE 10.1: NORMALIZED P-Y CURVE FOR UNDRAINED CLAY FROM PLANE STRAIN ANALYSES

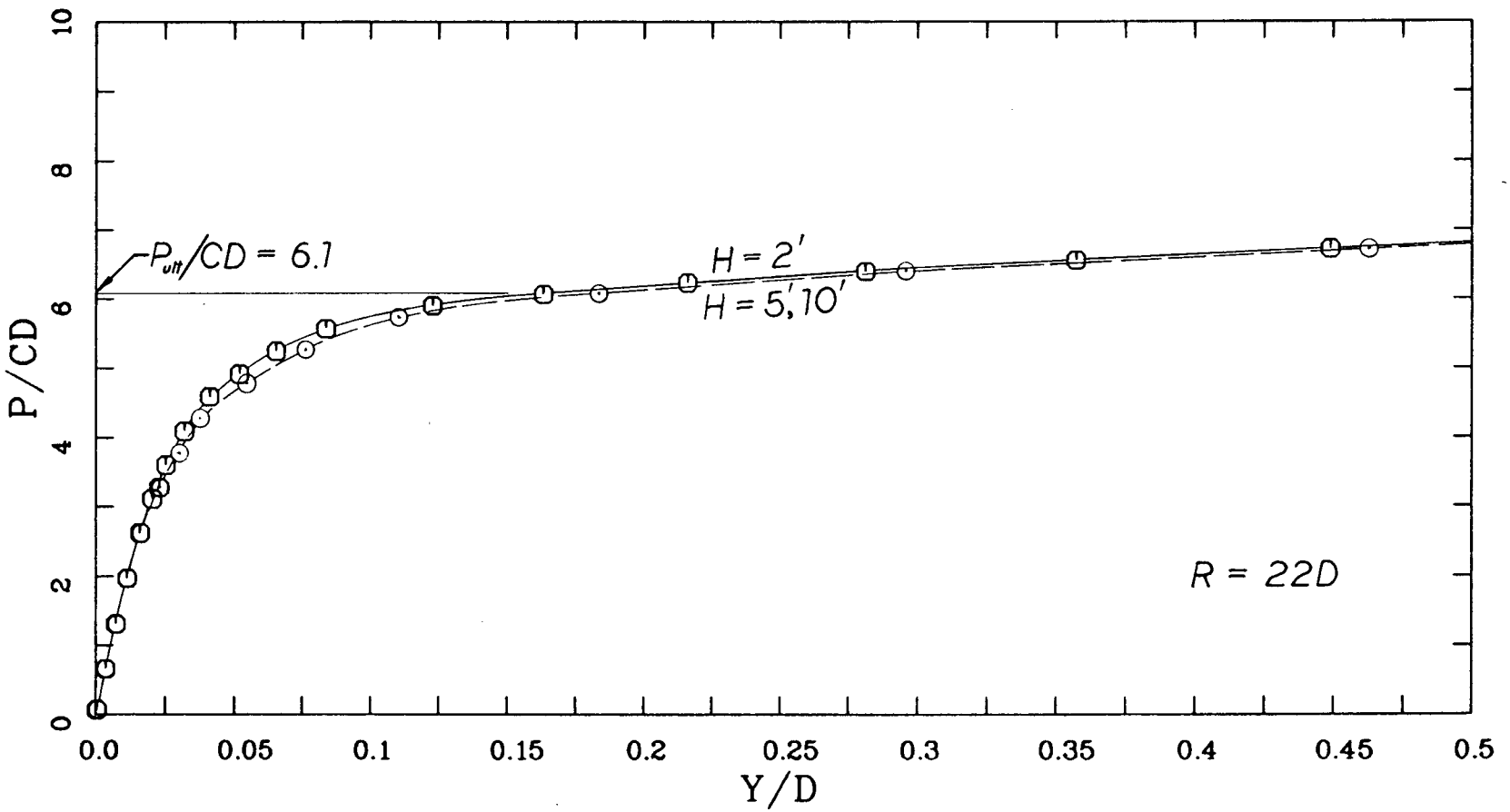

FIGURE 10.2: NORMALIZED P-Y CURVES FOR UNDRAINED CLAY FROM PLANE STRESS ANALYSES

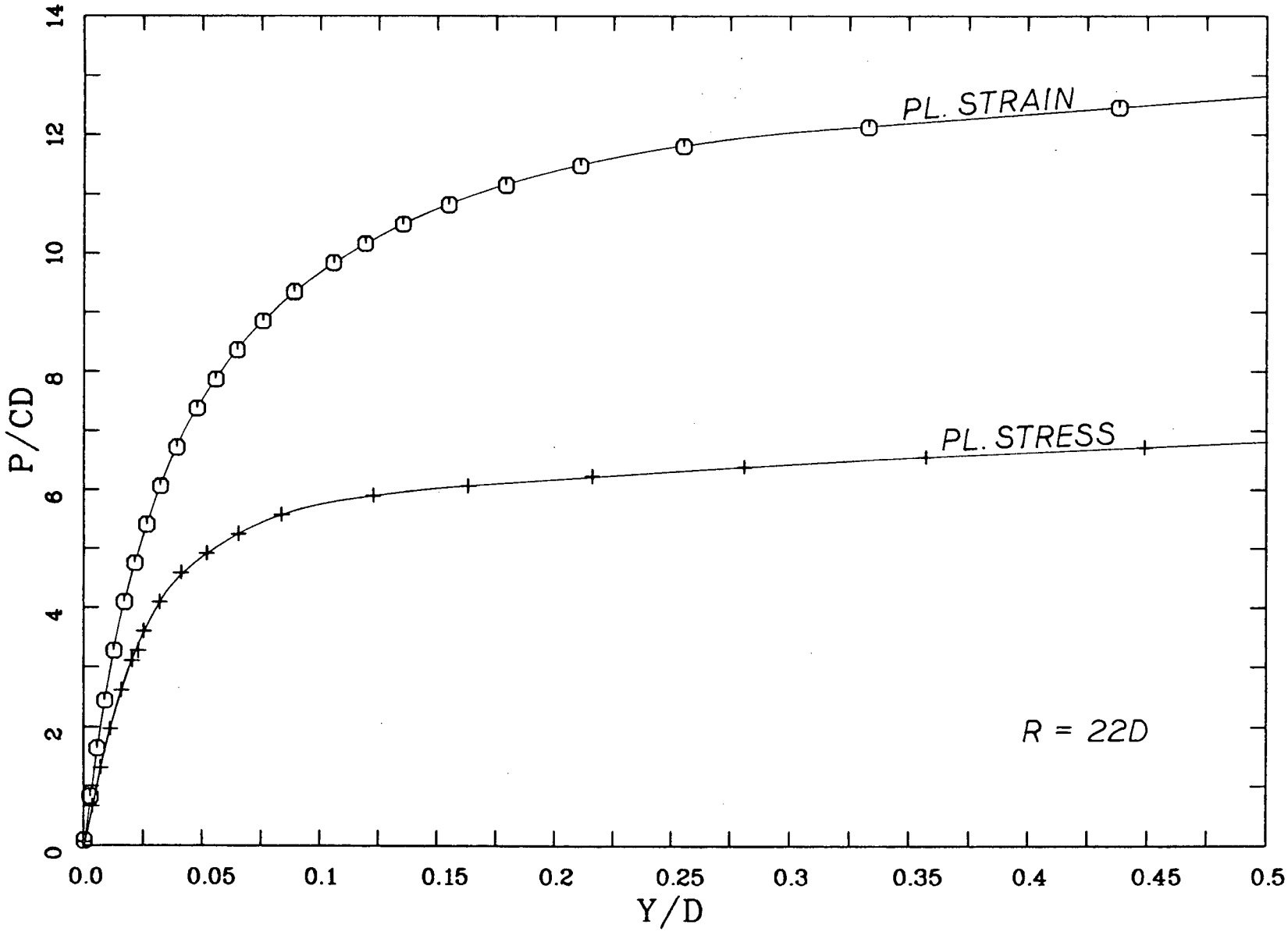

FIGURE 10.3: NORMALIZED P-Y CURVES FOR UNDRAINED CLAY

the stiff linear elastic soil response for small deformations. The curved middle portions describe progressive soil failure and consequently, the softening of the P-Y response. The final horizontal lines correspond to P_{ult}, at which soil failure is complete and the pile deflects at constant load.

The curves or curve segments shown in Figure 10.4 can be represented by simple mathematical equations. For the plane strain curve, the initial response and the curved centre portion can be described by a hyperbolic equation of the form

$$\frac{P}{cD} = \frac{Y/D}{a + R_a b(Y/D)} \qquad 10.1$$

a and b are constants related to the initial slope of the curve and the ultimate soil resistance:

$$a = 1/\text{initial slope}$$

$$b = 1/(P_{ult}/cD)$$

R_a is an adjustment factor applied to correct for cutting off the curve at $(P_{ult}/cD)=12.1$. In other words, the true ultimate resistance is at $(P_{ult}/cD)/R_a$, where R_a is less than 1. This value is reached, however, only at $Y/D=\infty$ and cannot be used for design purposes. The final segment of the normalized plane strain curve corresponding to complete soil failure is represented by a horizontal line.

To determine the value of R_a, a transformed plot of the plane

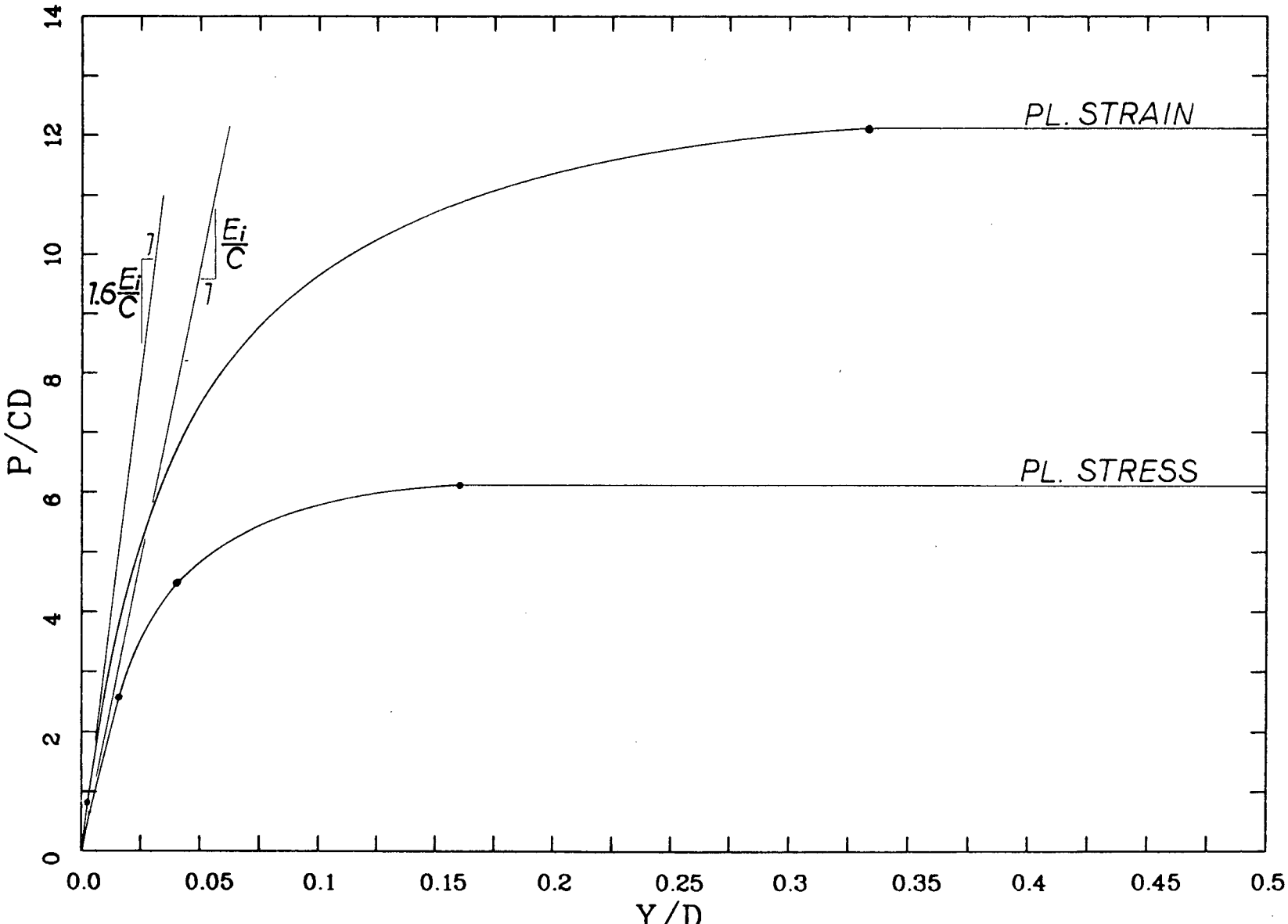

FIGURE 10.4: SIMPLIFIED NORMALIZED P-Y CURVES FOR UNDRAINED CLAY

strain curve was made. Equation 10.1 can also be written as

$$(Y/D)/(P/cD) = a + R_a b(Y/D) \qquad 10.1a$$

The plot of (Y/D)/(P/cD) vs. (Y/D) in Figure 10.5 shows the expected straight line with slope = $R_a b$ and vertical-axis intercept = a. Although the data for small values of Y/D corresponding to the initial segment of the normalized curve do not show a linear relationship, the assumption of a hyperbolic fit is nonetheless sufficient. The value of $R_a b$ determined from the plot is 0.0731. For $P_{ult}/cD = 12.1$, $R_a = 0.885$. The initial slope of the curve is $1.6E_i/c$. For $E_i/c = 200$ assumed for the P-Y analyses, the theoretical value of a is 0.003125. This value agrees well with a = 0.003 obtained from the transformed plot.

The plane stress curve is somewhat more complex. Aside from the straight lines describing the initial and failure responses, the curved portion is divided into two segments, a power function and a hyperbola. The hyperbola is given by a modified form of Equation 10.1:

$$\frac{P}{cD} = \frac{Y/D}{\alpha a + R_a b(Y/D)} \qquad 10.2$$

In Equation 10.1, a is defined as the inverse of the initial slope of the P/cD-Y/D curve. This is valid, however, only if the initial portion of the curve is hyperbolic. For the plane stress case, the initial segment of the curve is a power function. A correction factor, α, is therefore required for a.

The power function for the initial curve segment is given by the equation

$$P/cD = a'(Y/D)^{b'} \qquad 10.3$$

where

a', b' = constants

To determine the values of the constants for these equations, transformed plots of the P/cD and Y/D data were made. The plot in Figure 10.7 of (Y/D)/(P/cD) vs. (Y/D) for Equation 10.2 yields the expected straight line for the hyperbolic curve segment with slope = $R_a b$ and intercept = αa. For $R_a = 0.145$ and $P_{ult}/cD = 6.1$, $R_a = 0.885$ as for the plane strain curve. For an initial slope of $E_i/c = 200$ and $a = 0.0028$, $\alpha = 0.56$.

For the power function, Equation 10.3 can be expressed as

$$\log(P/CD) = \log a' + b'\log(Y/D) \qquad 10.3a$$

The plot of log(P/cD) vs. log(Y/D) in Figure 10.6 likewise yields a straight line with slope = b' and intercept = $\log(a')$. Values of $b' = 0.693$ and $a' = 45.31$ were obtained from the graph.

Equations for the fitted plane strain and plane stress curves are summarized in Table 10.1. The equations do not describe the curves perfectly and slight discontinuities may occur at the ends of the segments. For practical purposes, smoothening out the curves by hand is sufficient, and would not lead to significant errors.

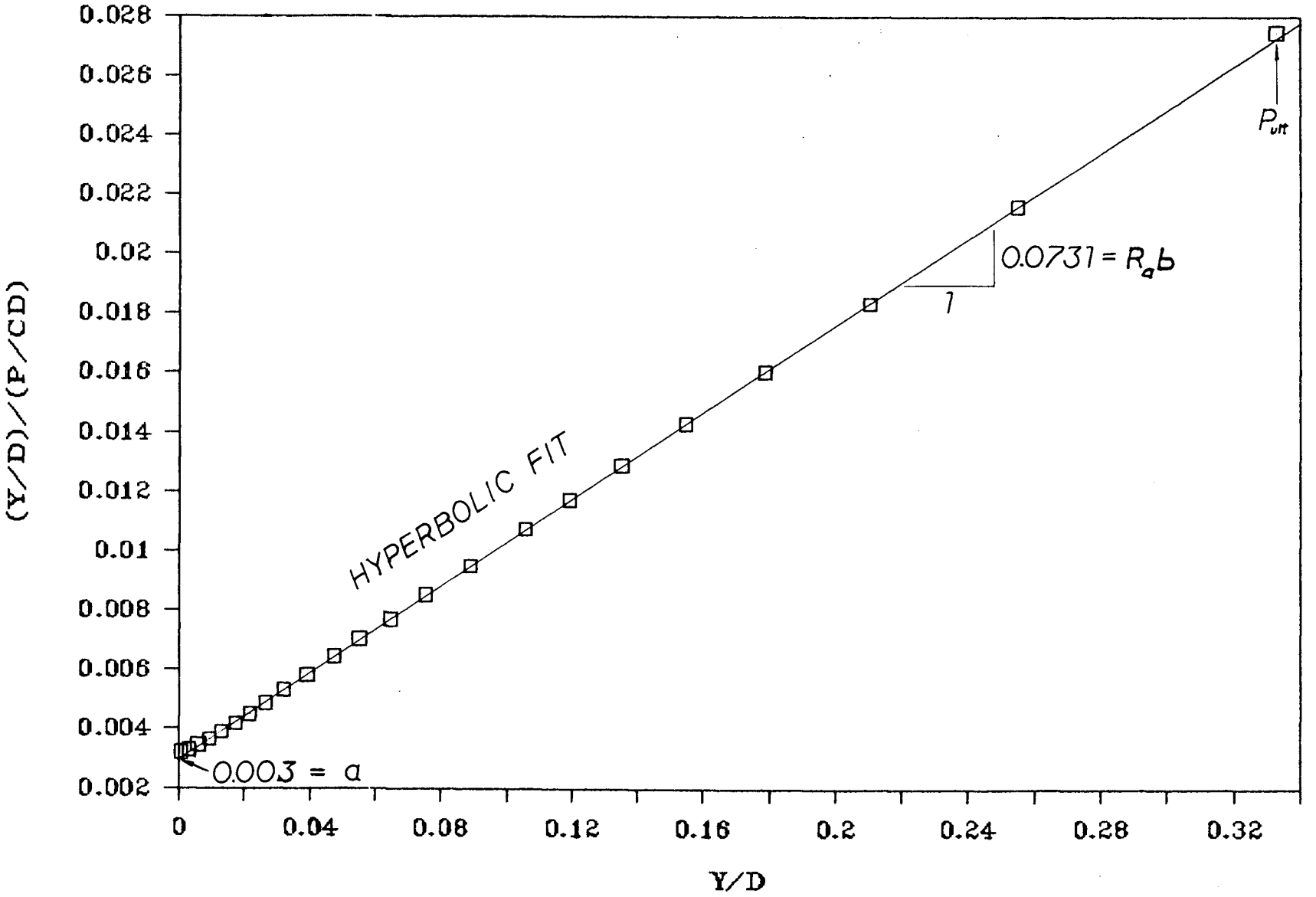

FIGURE 10.5: HYPERBOLIC FIT FOR PLANE STRAIN P-Y CURVES FOR UNDRAINED CLAY

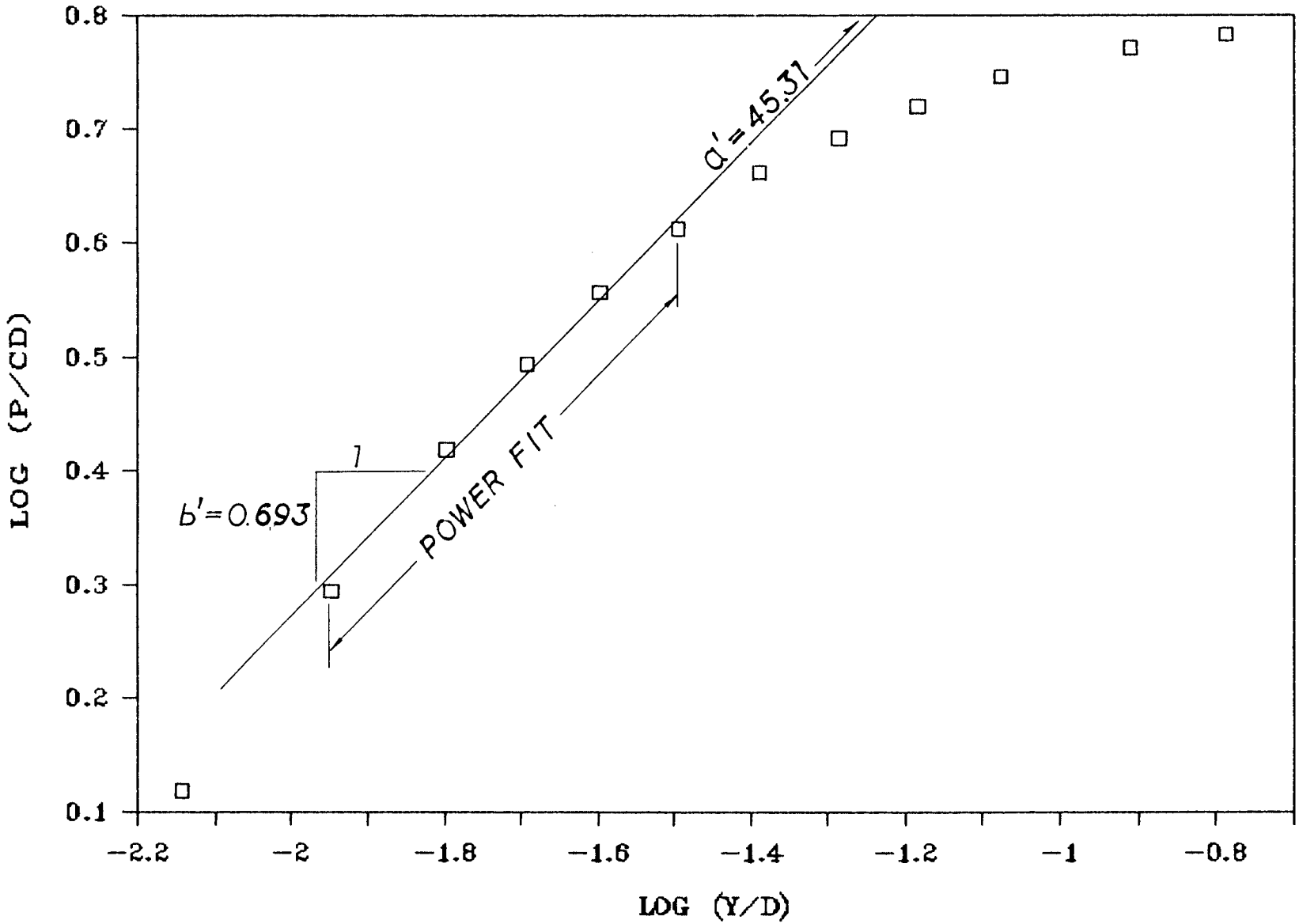

FIGURE 10.6: POWER FUNCTION FIT FOR PLANE STRESS P-Y CURVES FOR UNDRAINED CLAY

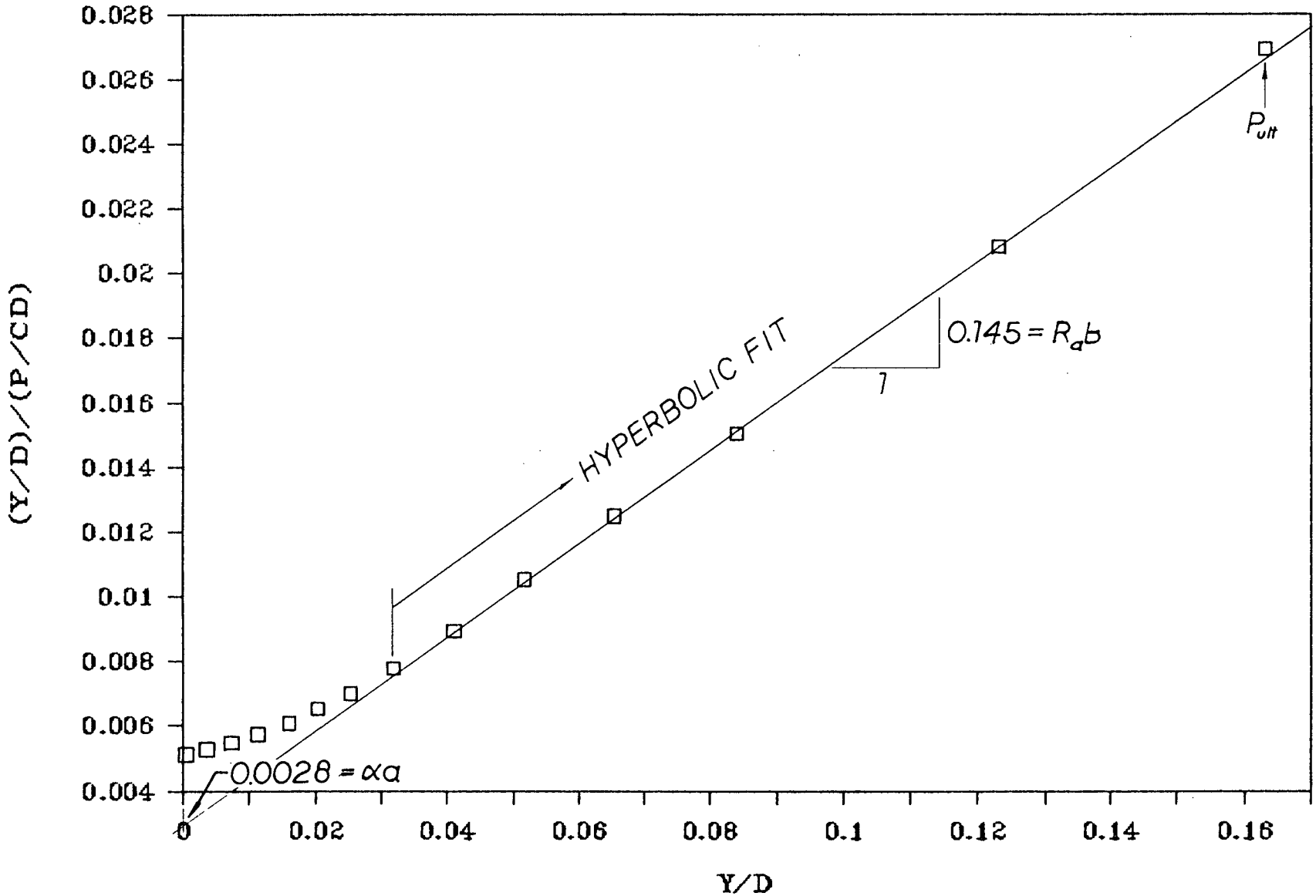

FIGURE 10.7: HYPERBOLIC FIT FOR PLANE STRESS P-Y CURVES FOR UNDRAINED CLAY

TABLE 10.1

SIMPLIFIED METHOD FOR DETERMINING

P-Y CURVES FOR N.C. CLAYS

PLANE STRAIN			PLANE STRESS		
FROM	TO	EQUATION	FROM	TO	EQUATION
(0, 0)	$(65.5c/E_i, 12.1)$	$\frac{P}{cD} = \frac{Y/D}{c/1.6E_i + 0.073(Y/D)}$	(0, 0)	$(1.59c/E_i, 1.59)$	$\frac{P}{cD} = \frac{E_i}{c}\frac{Y}{D}$
$(65.5c/E_i, 12.1)$	$(\infty, 12.1)$	Horizontal Line (P/cD = 12.1)	$(1.59c/E_i, 1.59)$	(0.035, 4.44)	$\frac{P}{cD} = 45.3(Y/D)^{0.693}$
			(0.035, 4.44)	$(29.6c/E_i, 6.1)$	$\frac{P}{cD} = \frac{Y/D}{0.56c/E_i + 0.145(Y/D)}$
			$(29.6c/E_i, 6.1)$	$(\infty, 6.1)$	Horizontal Line (P/cD = 6.1)

Note: Co-ordinates given are for (Y/D, P/cD)

10.3 SIMPLIFIED P-Y CURVES FOR DENSE SAND

Plane strain and plane stress P-Y curves were predicted for a dense sand using finite element analyses. The results are shown and discussed in Section 9.4. To facilitate the prediction of such curves for other depths and for different soil properties and pile diameters, a simplified method for predicting P-Y curves was developed.

10.3.1 Normalized P-Y Curves

The P-Y curves predicted for dense sand were shown to have similar initial slopes. A value of $1.08E_i$ for the initial slopes of both plane strain and plane stress curves at any depth is a good approximation.

In examining the effects of the pile diameter on predicted P-Y curves, P/D vs. Y/D plots at a given depth were shown to be identical, regardless of the pile diameter used.

The theoretical equations for P_{ult} given by Equations 9.9 and 9.10 are both functions of the pile diameter, D. In the plane strain equation (9.10), P_{ult} is directly proportional to D. In the passive wedge equation for plane stress deformations (9.9), D is contained in only two of the six terms in the equation.

For values of ϕ' used in the finite element analyses, the terms containing D in Equation 9.9 are relatively insignificant. However, for soil near the surface, H is small, and the four terms not containing D decrease in magnitude. At a depth of 2 ft, the "D terms" account for about half of the soil resistance. At H = 1 ft, the "D terms" account for roughly 2/3 of P_{ult}, and so on. Since the passive wedge equation is valid only for shallow depths, P_{ult} can be

considered as roughly proportional to D.

Based on the above conclusions, the P-Y curves can be normalized by plotting P/P_{ult} vs. Y/D. And since P_{ult} is proportional to D, the effects of pile diameter are also eliminated.

The normalized plots are shown in Figures 10.8 and 10.9. Although differences can be observed in the shapes of the curves for different depths, a single curve for each of the plane strain and plane stress condition can be estimated. These normalized curves are compared in Figure 10.10.

The normalized P-Y curves in Figure 10.10 are useful for design purposes. Given the basic soil parameters (ie: ϕ', E_i, γ', etc.), P_{ult} can be calculated using Equation 9.9 or 9.10 and the adjustment factor A. Values of A determined by comparing P_{ult} predicted from the flow block and passive wedge models with P_{ult} obtained from the finite element analyses in Chapter 9 are given in Table 9.4 and graphed in Figure 10.14. P-Y curves can then be derived for sand at any depth and for any pile diameter. A simplified method for determining these P-Y curves is presented in the following sections.

10.3.2 Simplified Method for Determining P-Y Curves

The normalized P-Y curves shown in Figure 10.10 can be divided into four sections as shown in Figure 10.11. Soil response prior to failure is represented by three curves to best fit the results predicted by finite element analyses. The strain-softening behaviour of the sand is clearly illustrated. At P_{ult}, or $P/P_{ult} = 1$, the sand is assumed to fail completely. The P-Y relationship is represented by a horizontal straight line, ignoring the small increases in soil

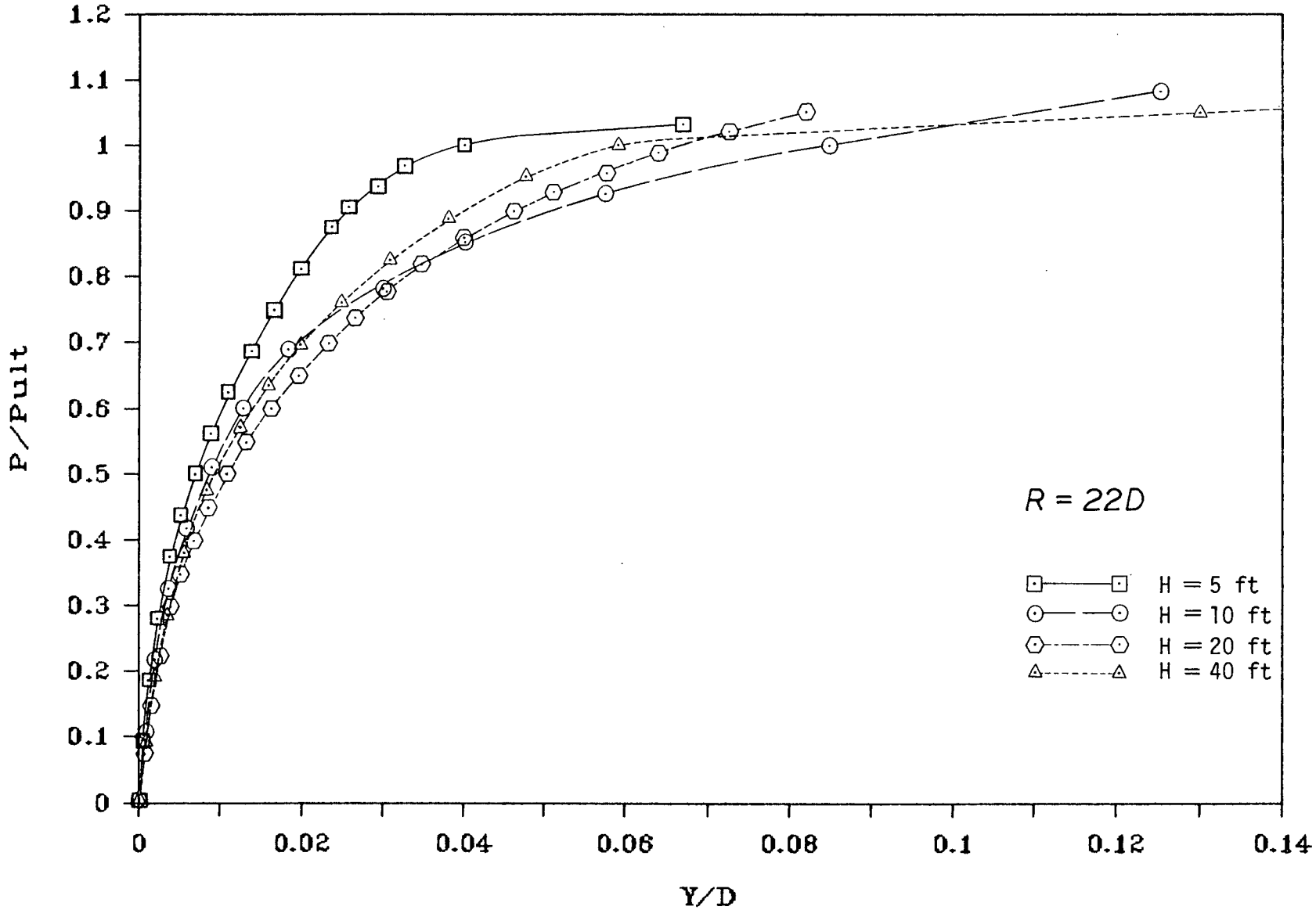

FIGURE 10.8: NORMALIZED P-Y CURVES FOR DENSE SAND FROM PLANE STRAIN ANALYSES

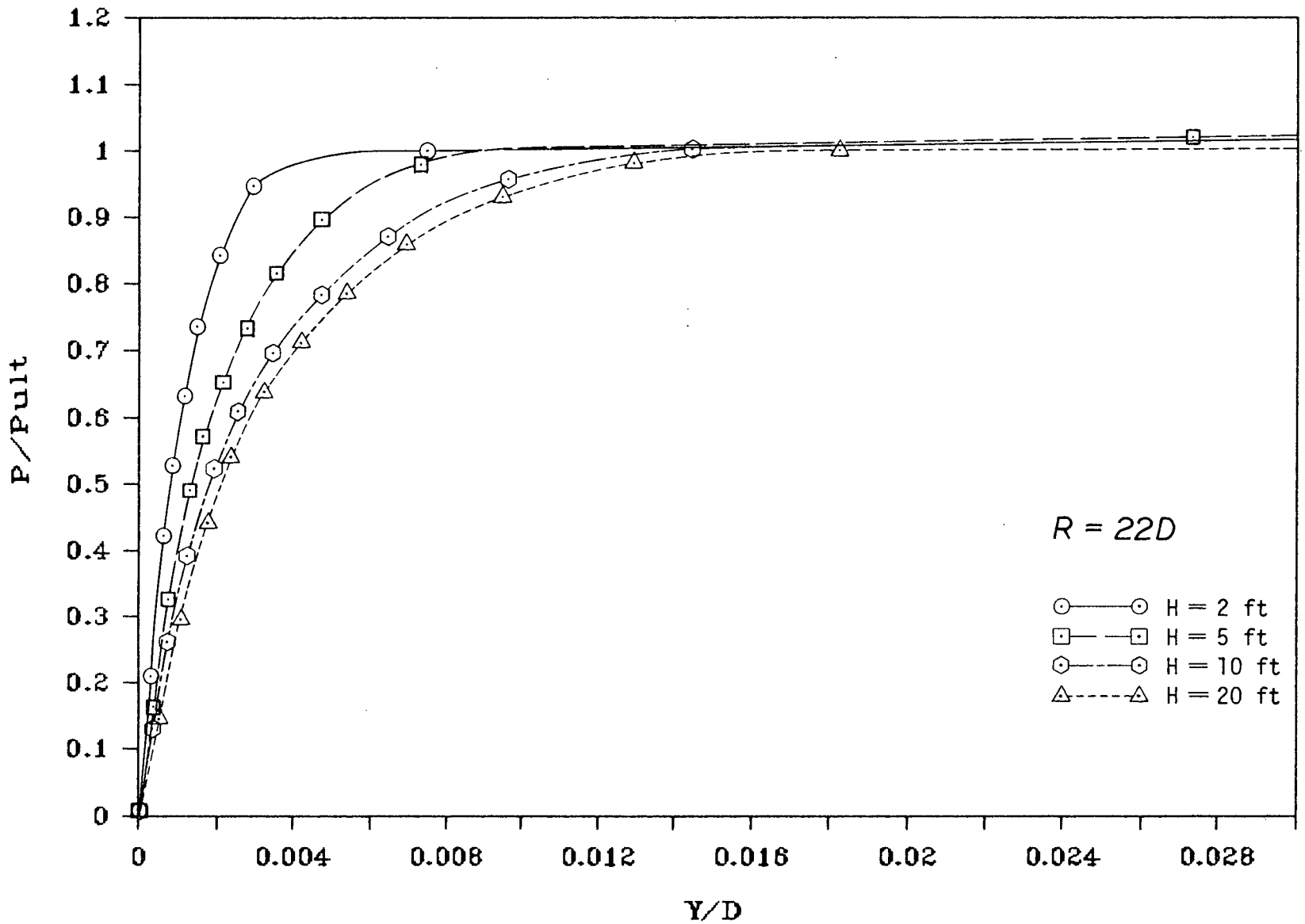

FIGURE 10.9: NORMALIZED P-Y CURVES FOR DENSE SAND FROM PLANE STRESS ANALYSES

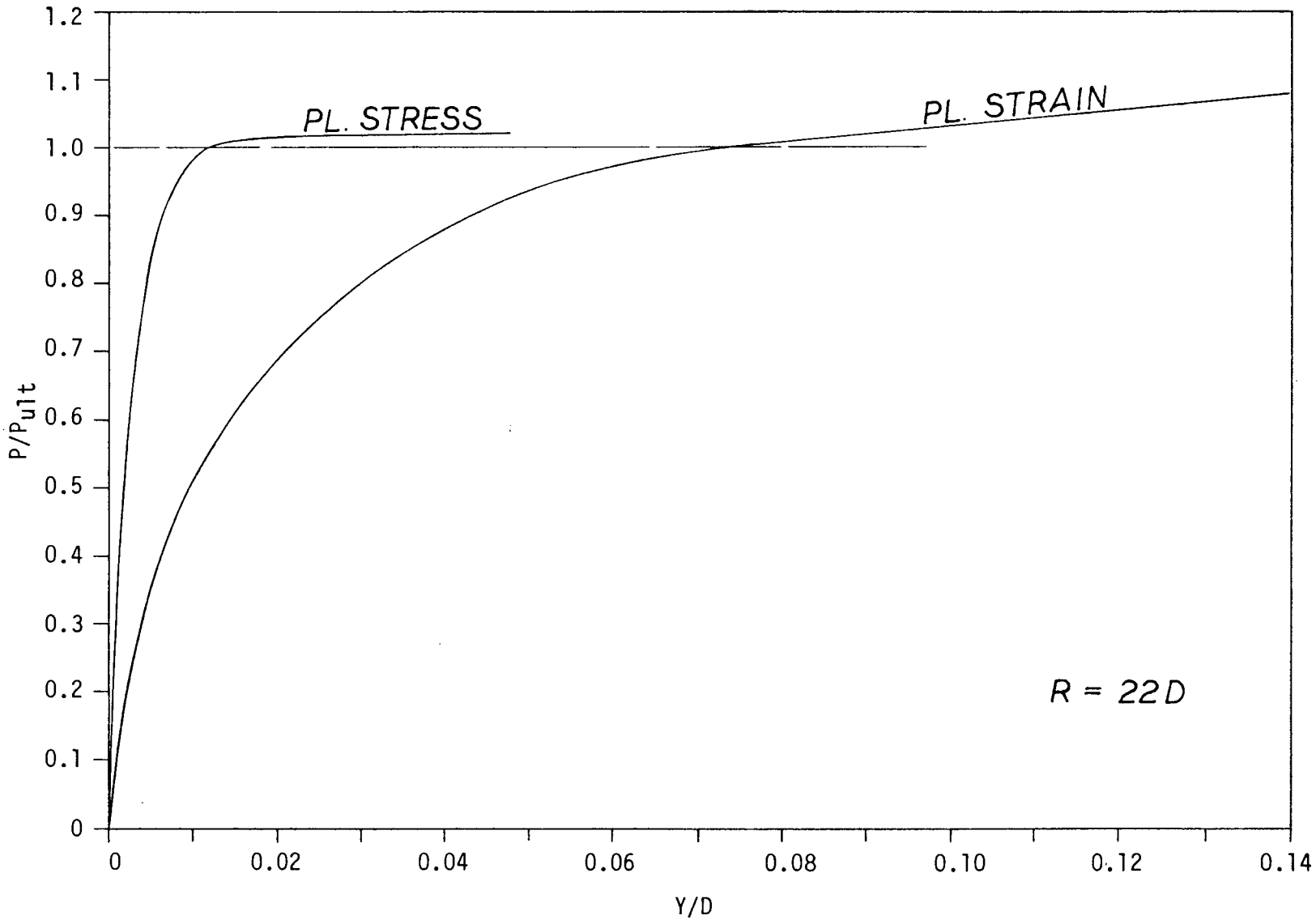

FIGURE 10.10: NORMALIZED P-Y CURVES FOR DENSE SAND

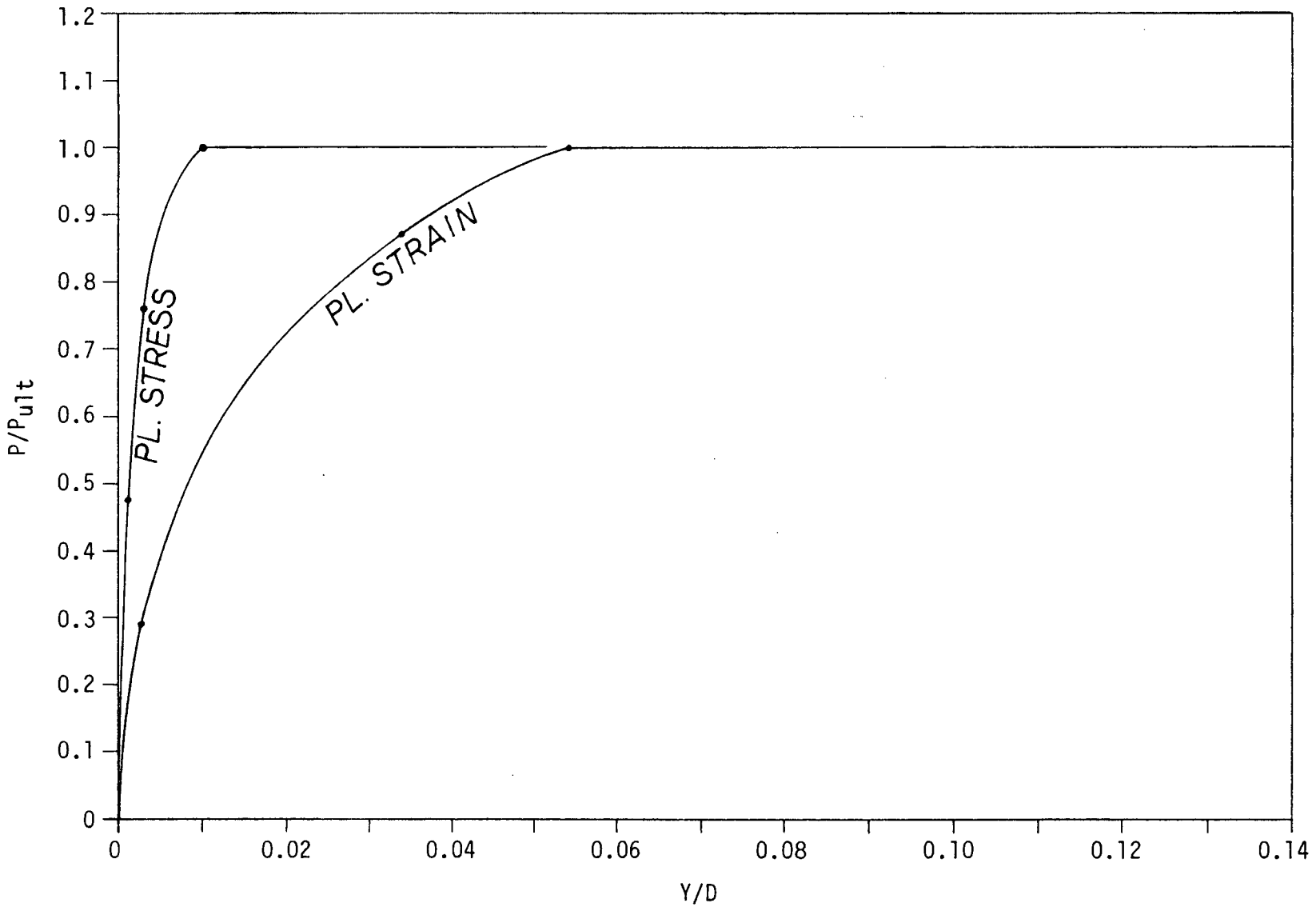

FIGURE 10.11: SIMPLIFIED NORMALIZED P-Y CURVES FOR DENSE SAND

resistance beyond P_{ult}. The modelling of soil behaviour after failure by the finite element method is questionable, and hence, the omission of the post-failure soil resistances predicted in the analyses.

The curved portions of the normalized P-Y responses can be described by power functions of the form

$$P/P_{ult} = a'(Y/D)^{b'} \qquad 10.4$$

As in Section 10.2.2, plotting $\log(P/P_{ult})$ vs. $\log(Y/D)$ yields a straight line with a slope = b' and a $\log(P/P_{ult})$-axis intercept of log(a'). The log-log plots for the plane strain and plane stress curves are shown in Figures 10.12 and 10.13, respectively. The equations for the curves obtained from these plots, along with the method for determining the P-Y curves, are summarized in Table 10.2.

10.4 APPLICATION OF THE P-Y CURVES

Using the simplified methods recommended in Sections 10.2.2 and 10.3.2, P-Y curves can be predicted for plane strain and plane stress conditions at any depth. For laterally loaded pile analyses, plane strain P-Y curves can be applied to the problem at large depths. Near the surface (ie: $H < 2$ ft), plane stress curves can be used. In the intermediate zone where both stresses and strains are three-dimensional, combinations of the plane strain and plane stress curves are appropriate. Thompson (1977) concluded that a linear increase in the value of P_{ult} with depth, from the plane stress value at the surface to the plane strain value at large depths, is an adequate

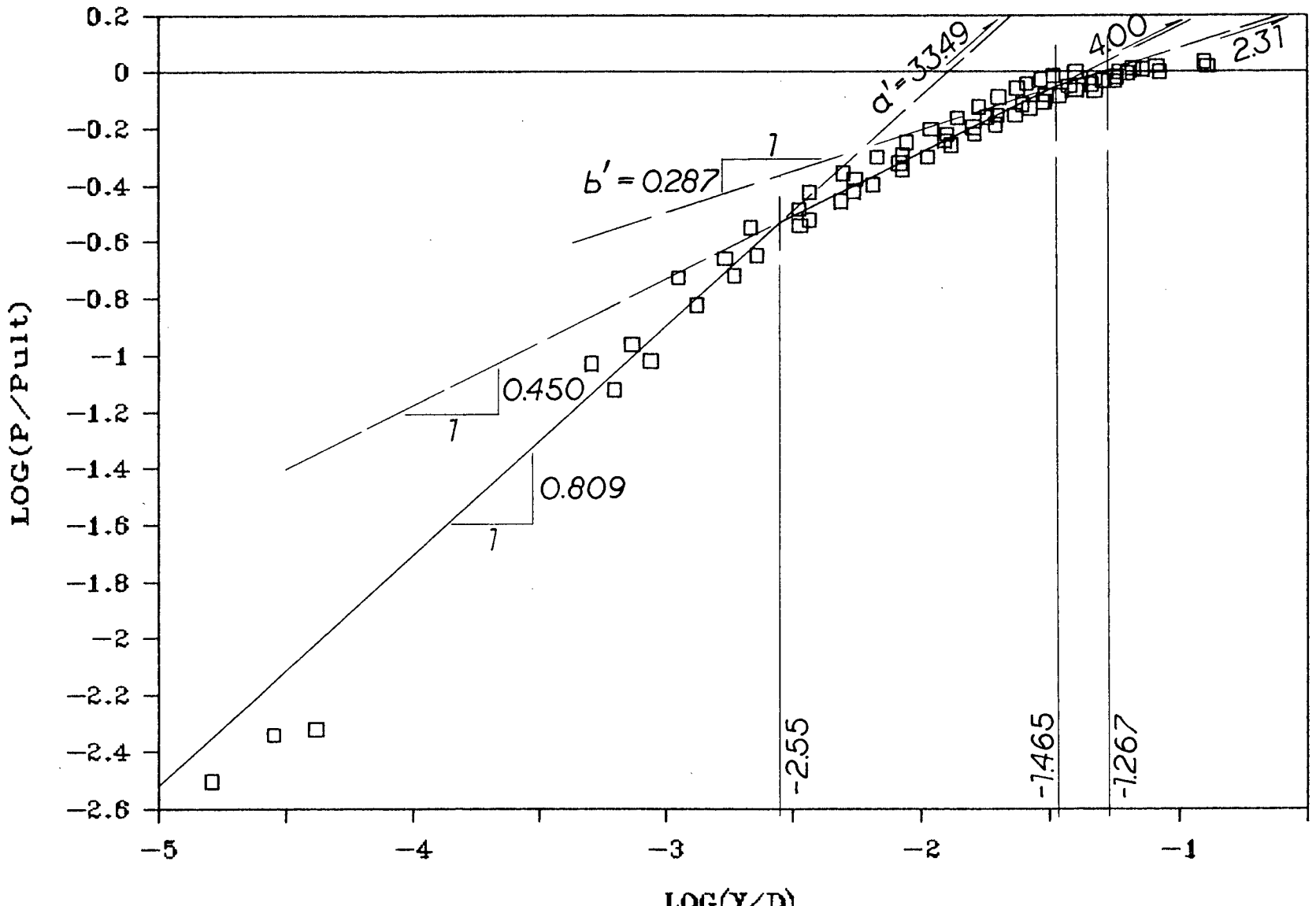

FIGURE 10.12: POWER FUNCTION FITS FOR PLANE STRAIN P-Y CURVES FOR DENSE SAND

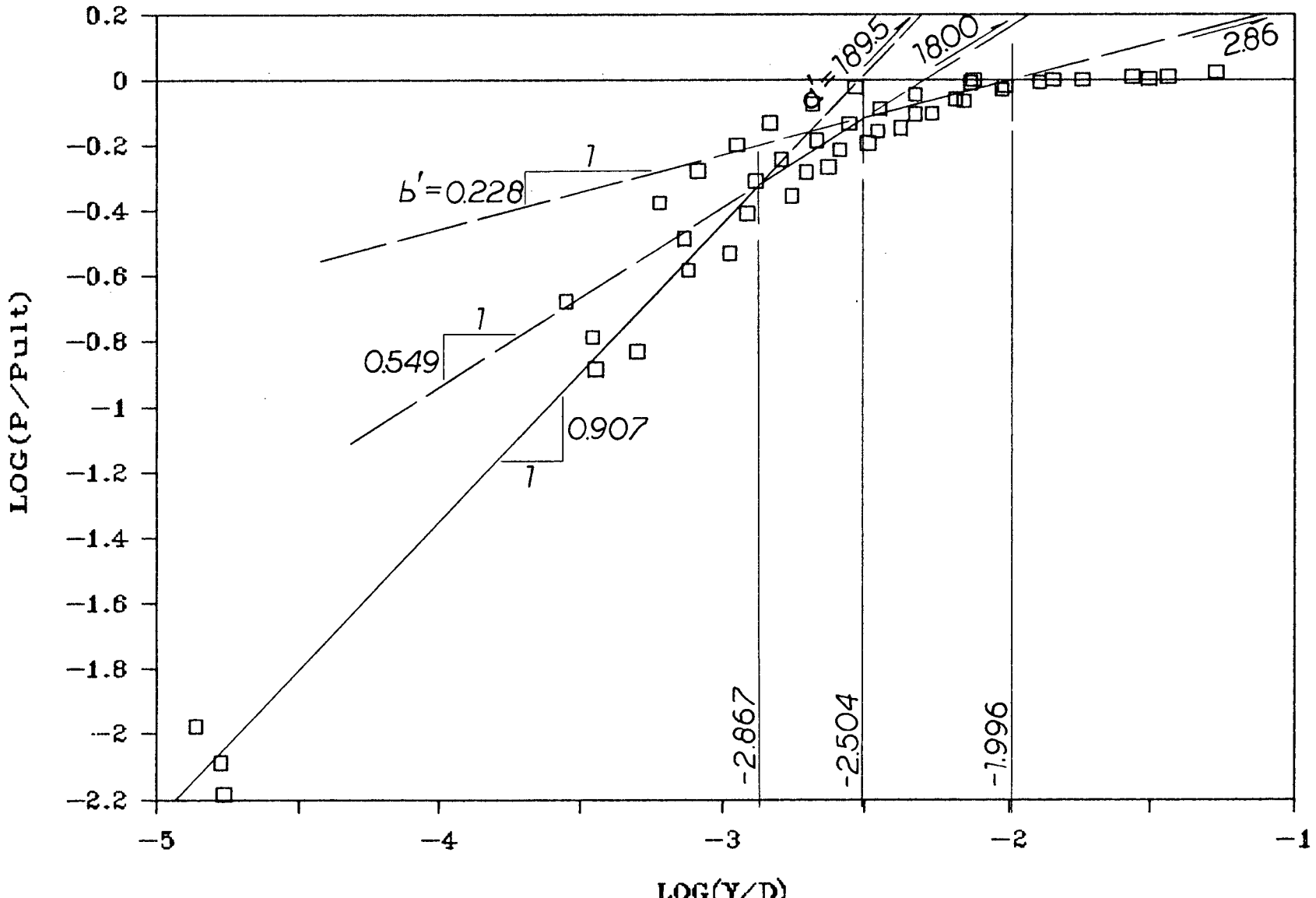

FIGURE 10.13: POWER FUNCTION FITS FOR PLANE STRESS P-Y CURVES FOR DENSE SAND

TABLE 10.2

SIMPLIFIED METHOD FOR DETERMINING

P-Y CURVES FOR DENSE SAND

PLANE STRAIN			PLANE STRESS		
FROM	TO	EQUATION	FROM	TO	EQUATION
(0, 0)	(0.0028, 0.29)	$P/P_{ult} = 33.5(Y/D)^{0.81}$	(0, 0)	(0.00136, 0.48)	$P/P_{ult} = 190(Y/D)^{0.91}$
(0.0028, 0.29)	(0.034, 0.87)	$P/P_{ult} = 4.0(Y/D)^{0.45}$	(0.00136, 0.48)	(0.00313, 0.76)	$P/P_{ult} = 18(Y/D)^{0.55}$
(0.034, 0.87)	(0.054, 1.0)	$P/P_{ult} = 2.31(Y/D)^{0.29}$	(0.00313, 0.76)	(0.01, 1.0)	$P/P_{ult} = 2.86(Y/D)^{0.23}$
(0.054, 1.0)	(∞, 1.0)	Horizontal Line: $P/P_{ult}=1$	(0.01, 1.0)	(∞, 1.0)	Horizontal Line: $P/P_{ult}=1$

Note: Co-ordinates given are for $(Y/D, P/P_{ult})$
P_{ult} calculated from Equations 9.9 for plane stress and Equation 9.10 for plane strain. Values for the adjustment factor A in the equations are given in Table 9.4 or can be estimated from Figure 10.14.
The initial slopes of the curves derived from the above equations should be modified to the value of $1.08E_i(D/P_{ult})$.

approximation for real soil behaviour. Extending this method to all values of P, plane strain and plane stress curves can then be added linearly to produce P-Y approximations for intermediate soil depths. This method is illustrated in Figure 10.15 for undrained clay at a hypothetical depth of 5 ft with H_c = 7.5 ft.

For undrained normally-consolidated clays, the zone of three-dimensional stresses and strains extends to a depth given by Equation 9.5:

$$H_c = \frac{6D}{\sigma_v' D/cH + J}$$

For dense sand, the limit of the transition zone can be estimated from Figure 10.14. The inverse of the adjustment factor, 1/A (see Table 9.4), for plane stress analyses is shown to increase with depth until the plane strain condition takes over. Accordingly, H_c = 19 ft can be taken as the limit of the transition zone. The value of H_c, however, is not constant, but is a function of soil properties and pile diameter.

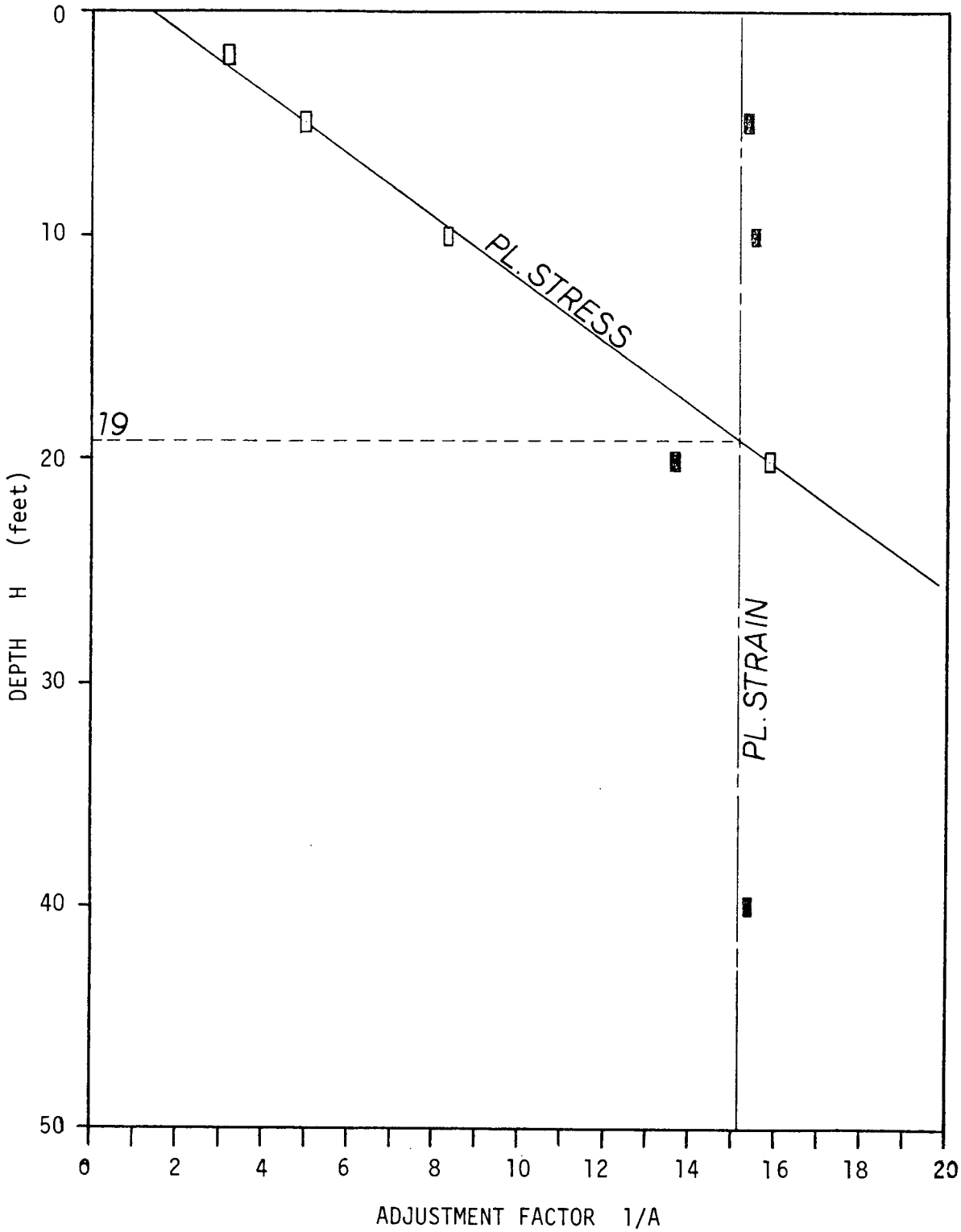

FIGURE 10.14: PLANE STRESS - PLANE STRAIN TRANSITION ZONE FOR DENSE SAND

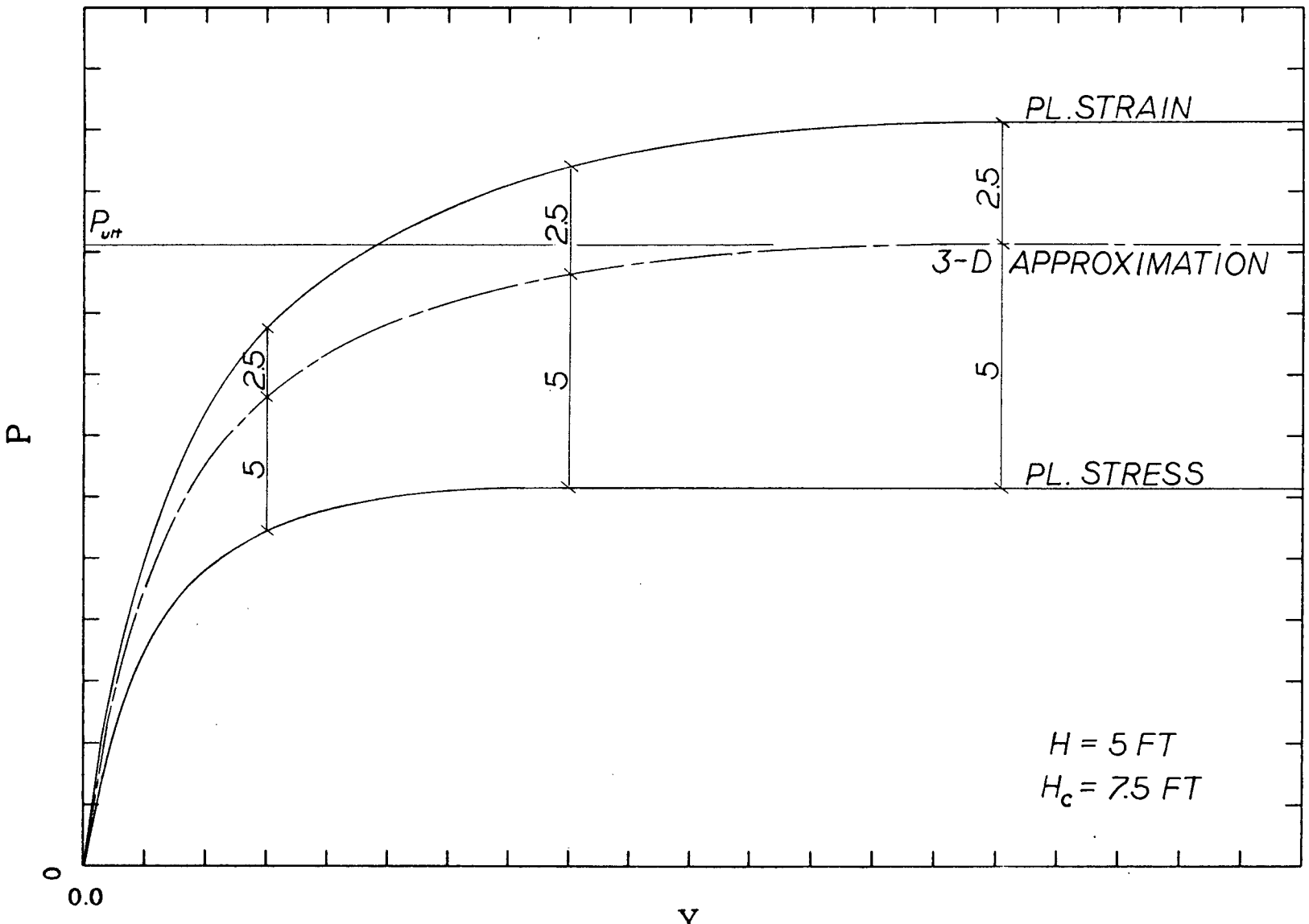

FIGURE 10.15: P-Y CURVE FOR 3-DIMENSIONAL STRESS AND STRAIN CONDITION

CHAPTER 11

PREDICTION OF P-Y CURVES FROM PRESSUREMETER EXPANSION CURVES

11.1 INTRODUCTION

In recent years, with the refinement of testing techniques and the increased sophistication of both the instrument and the data acquisition system, the pressuremeter has seen increased use as a design tool. One obvious application of the pressuremeter test is the design of laterally loaded piles. Since loads are applied to the surrounding soil in much the same manner for both the pressuremeter and the lateral pile problem, similarities are expected in their load-deformation characteristics. Various researchers have attempted to predict or derive P-Y curves from pressuremeter expansion curves. In most instances, the authors have suggested increasing the load component of the pressuremeter curves by some factor to yield P-Y curves for piles (Robertson et al. (1983), Atukorala & Byrne (1984), and Robertson et al. (1985)). Factors ranging from 1.9 to 2.6 were suggested for clays, and 1.4 to 1.7 for sands.

Having thus determined conversion factors for the load component of the curves, uncertainties still existed as to the initial slopes of the two curves. Using cavity expansion theory, the slope of the pressuremeter curve was assumed to equal 2G. The initial slope of the P-Y curve, however, was essentially unknown. Values as low as $0.48E_i$ (Broms, 1964) and as high as $2.0E_i$ (Pyke & Beikae, 1984) were suggested by various researchers.

Another uncertainty lies in the difference in size, or

diameter, between the pressuremeter cell and the piles. The validity of applying pressuremeter curves obtained from 3-inch diameter probes to problems involving piles with diameters often in excess of 2 ft was questionable and warranted investigation.

To ascertain the initial slopes of the curves and to determine the effects of large pile diameters on the load conversion factors, pressuremeter and P-Y curves predicted from finite element analyses were compared. The methods of analysis are as discussed in Section 8.2 for pressuremeter expansion, and in Sections 3.2 and 9.2 for laterally loaded piles.

11.2 COHESIVE SOIL

Pressuremeter and P-Y curves were predicted for a normally-consolidated undrained clay. Soil properties used in the analyses are given in Tables 8.1 and 9.1. Comparisons were made for curves obtained for the clay at depths of 10 and 20 ft.

11.2.1 Pressuremeter Expansion Curves

The predicted pressuremeter curves are shown in Figure 8.1. The initial slopes of the two curves are approximately 0.99(2G). As discussed in Section 8.3, the shape of the curves are similar, and the 20-foot curve is, in fact, simply a scaled-up version of the 10-foot curve. The scaling factor of 2.0 suggests that a "family" of such curves for different soil depths can be normalized to produce a unique curve for the soil. Normalizing of the curves are discussed in Section 11.2.3.1.

11.2.2 P-Y Curves

The P-Y curves predicted in Chapter 9 were compared with the pressuremeter results. Both plane strain and plane stress P-Y curves were employed in the comparisons. The curves are shown in Figures 9.2 and 9.3. As noted in Section 9.3.2, the initial slopes and ultimate resistances of the curves are $1.6E_i$ and 12.1cD for the plane strain curves, and $1.0E_i$ and 6.1cD for the plane stress curves.

11.2.3 Comparison of Pressuremeter and P-Y Curves

In order to compare directly the results of pressuremeter expansion and lateral pile loading, the pressuremeter curves must be converted to equivalent P-Y plots. Since "P" in the lateral pile problem represents soil resistance per unit length of pile, pressuremeter curves must be converted to plots of ΔPD vs. Δr, where D is the diameter of the probe. To be correct, the current probe diameter, equal to $D_o + 2\Delta r$ (D_o = initial probe diameter), should be used. However, for convenience in converting pressuremeter results to P-Y curves, D is taken as the initial diameter. The modified pressuremeter curves and P-Y curves are compared in Figures 11.1 and 11.2.

11.2.3.1 Normalized Curves

The plots in Figures 11.1 and 11.2 are valid for comparison only if the pile diameter is equal to the size of the pressuremeter cell (ie: about 3 inches). To account for the size difference, normalized plots must be compared. In Section 8.5, size effects for pressuremeters were eliminated by plotting strains, $\Delta r/r_o$, instead

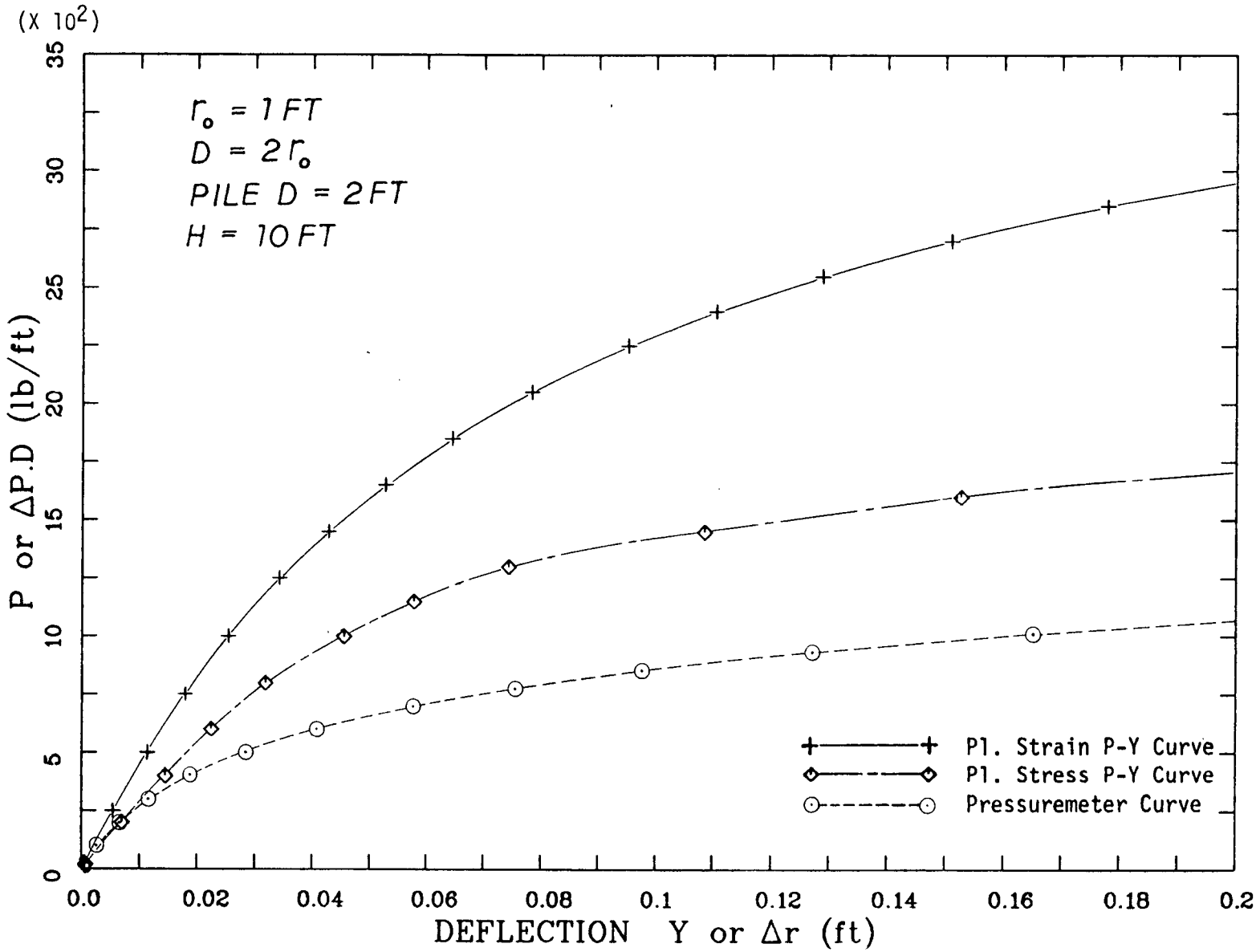

FIGURE 11.1: COMPARISON OF PRESSUREMETER AND P-Y CURVES FOR NORMALLY-CONSOLIDATED UNDRAINED CLAY

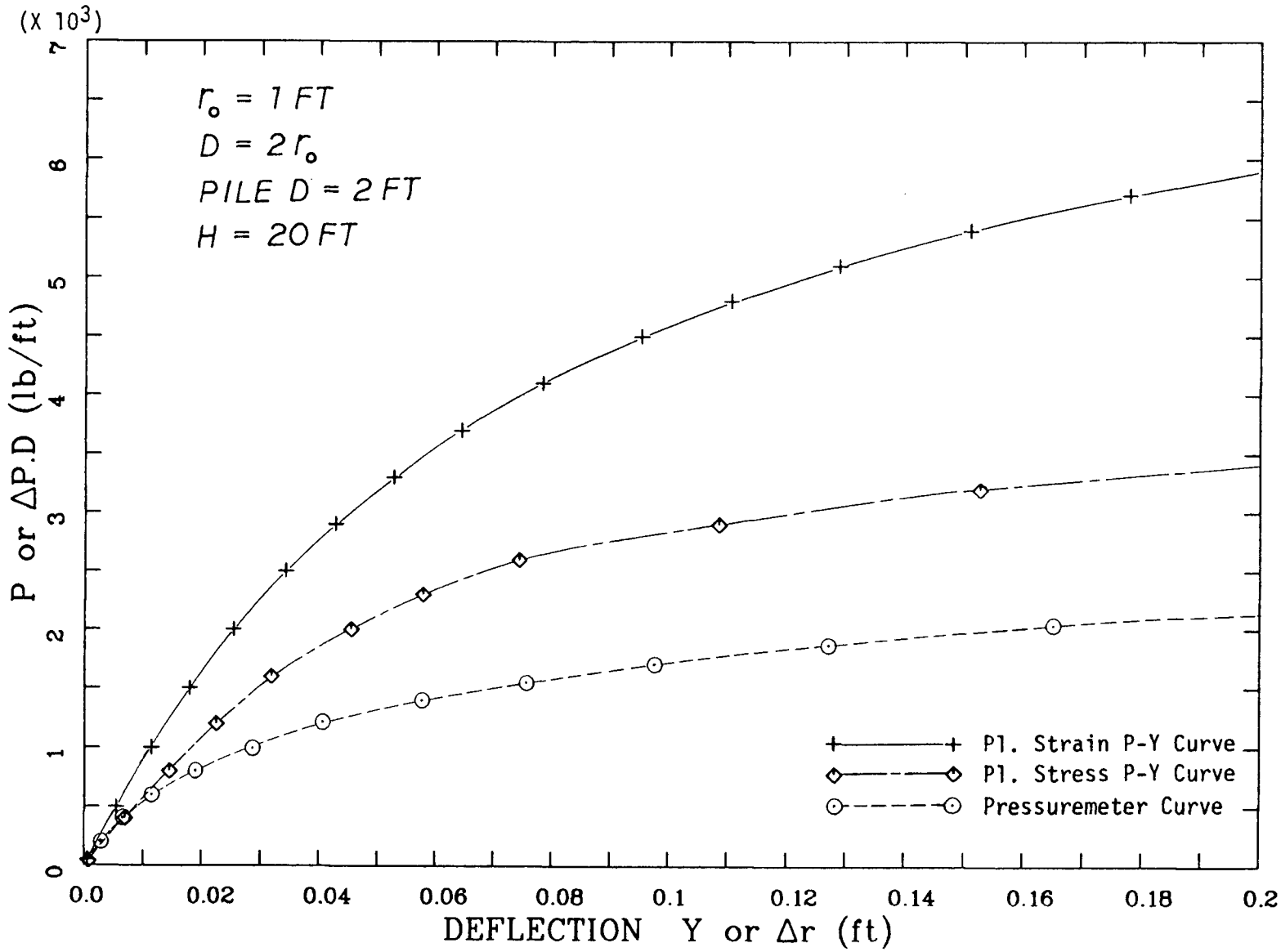

FIGURE 11.2: COMPARISON OF PRESSUREMETER AND P-Y CURVES FOR NORMALLY-CONSOLIDATED UNDRAINED CLAY

of displacements, Δr. Since $r_o = D/2$, plotting $\Delta r/D$ will likewise eliminate size effects. Similarly, size effects for P-Y curves were eliminated in Section 9.3.3 through the use of P/D vs. Y/D plots (D is the pile diameter).

To further simplify analysis, fully normalized plots of P/cD vs. Y/D for the lateral pile problem, and $\Delta P/c$ vs. $\Delta r/D$ for pressuremeter expansion were made. The curves are presented in Figure 11.3. As shown in Section 10.2.1 and discussed in Section 11.2.1, the resulting curves are valid for the normally-consolidated clay at any depth and for any value of D.

11.2.3.2 Conversion Factors

Conversion factors were determined for the normalized curves shown in Figure 11.3. The use of normalized curves is ideal since entire "families" of P-Y curves for different depths can be generated from the results of a single pressuremeter test.

In converting pressuremeter curves to P-Y curves, care must be taken to ensure that the correct initial slopes are obtained. The slopes obtained from the finite element analyses are as follows:

Plane strain P-Y curves: $P/Y = 1.6E_i$

Plane stress P-Y curves: $P/Y = 1.0E_i$

Pressuremeter curves from 3-D analysis: $\Delta P/(\Delta r/r_o) = 1.0(2G_i)$

To convert these values to slopes for the normalized curves, the following relationships were used:

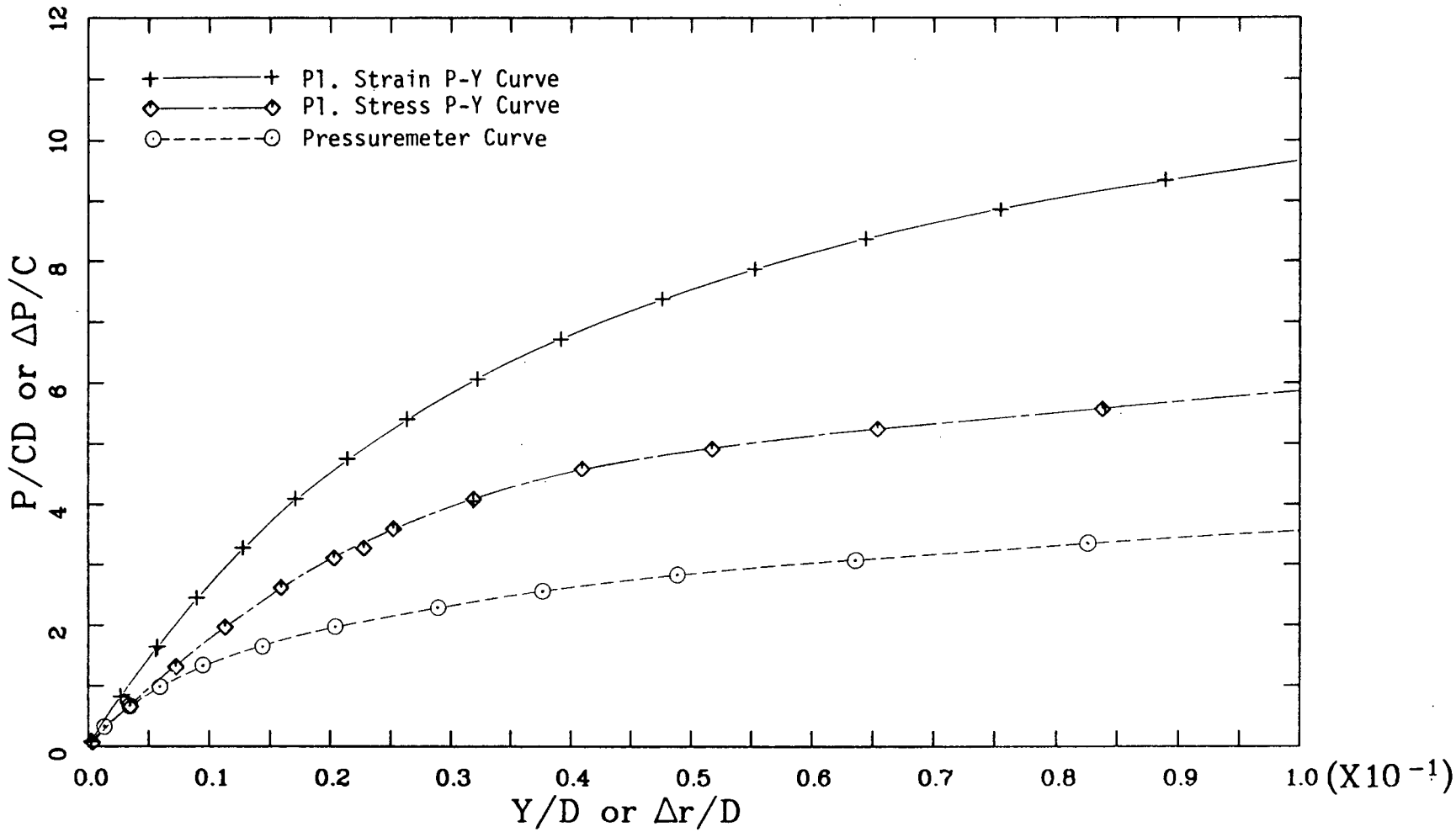

FIGURE 11.3: COMPARISON OF NORMALIZED PRESSUREMETER AND P-Y CURVES FOR NORMALLY-CONSOLIDATED UNDRAINED CLAY

$E_i = 200c$ (previous assumption)

$G_i = E_i/[2(1 + \mu)]$

$\mu = 0.498$

Initial slopes for the normalized curves were thus calculated, yielding the following values:

Plane strain P-Y curves: $\frac{P/cD}{Y/D} = \frac{1.6E_i}{c} = 320$

Plane stress P-Y curves: $\frac{P/cD}{Y/D} = \frac{1.0E_i}{c} = 200$

Pressuremeter curves: $\frac{\Delta P/c}{\Delta r/D} = \frac{2(1.0)(2G_i)}{c} = 267$

Conversion factors for the initial slopes are therefore 1.20 for plane strain P-Y curves, and 0.75 for plane stress P-Y curves.

Load factors were determined by simply taking the ratios of the normalized loads for various values of the normalized displacement. The factors are summarized in Table 11.1. For practical purposes, a plane strain P-Y curve load factor of 2.72 and a plane stress factor of 1.66 can be assumed for $Y/D \geqslant 0.07$ without significant errors.

11.3 COHESIONLESS SOIL

Pressuremeter and P-Y curves were predicted for a dense sand using the soil properties summarized in Tables 8.2 and 9.2. The method for determining K_o, ϕ', and σ_{mo}' for the analyses are described in Section 9.4.1. Curves obtained for the soil at depths of 10 and 20 ft were compared to determine factors for converting pressuremeter curves to P-Y curves.

TABLE 11.1

CONVERSION FACTORS FOR

NORMALLY-CONSOLIDATED CLAYS

Y/D or $\Delta r/D$	PLANE STRAIN P-Y CURVES		PLANE STRESS P-Y CURVES	
Initial Slope	1.20		0.75	
0.005	1.70		1.12	
0.01	1.96		1.31	
0.02	2.32		1.59	
0.03	2.53		1.72	
0.04	2.60		1.74	
0.05	2.65		1.72	
0.06	2.69		1.69	
0.07	2.72	Assume 2.72	1.68	Assume 1.66
0.08	2.73		1.66	
0.09	2.71		1.65	
0.10	2.72		1.65	

11.3.1 Pressuremeter Expansion Curves

The predicted pressuremeter curves are shown in Figure 8.2. The initial slopes of the curves are approximately 0.98(2G). As discussed in Section 8.4, the 20-ft curve is a scaled-up version of the 10-ft curve. A scaling factor of 1.66 was calculated.

11.3.2 P-Y Curves

Plane strain and plane stress P-Y curves were predicted in Chapter 9. The initial slopes of the P-Y curves are approximately $1.08E_i$. For the value of $\mu = 0.222$ calculated from the given soil parameters, this is equivalent to 1.32(2G), slightly higher than the value of 2G for the pressuremeter curves. The curves are compared in Figures 11.4 and 11.5.

11.3.3 Comparison of Pressuremeter and P-Y Curves

As discussed in Section 11.2.3, pressuremeter curves were converted to plots of $\Delta P.D$ vs. Δr to allow for proper comparisons with P-Y curves. These curves are shown in Figures 11.4 and 11.5.

11.3.3.1 Normalized Curves

To facilitate the direct comparison of pressuremeter and P-Y curves, the influences of the pile and pressuremeter diameters must be eliminated. This can be accomplished by normalizing the P-Y plots to give P/P_{ult} vs. Y/D as shown in Figures 10.8 and 10.9. For the pressuremeter situation, size effect can be eliminated by plotting ΔP vs. $\Delta r/r_o$, as illustrated in Figure 8.4, or ΔP vs. $\Delta r/D$ ($D = 2r_o$). To normalize the load component of the pressuremeter

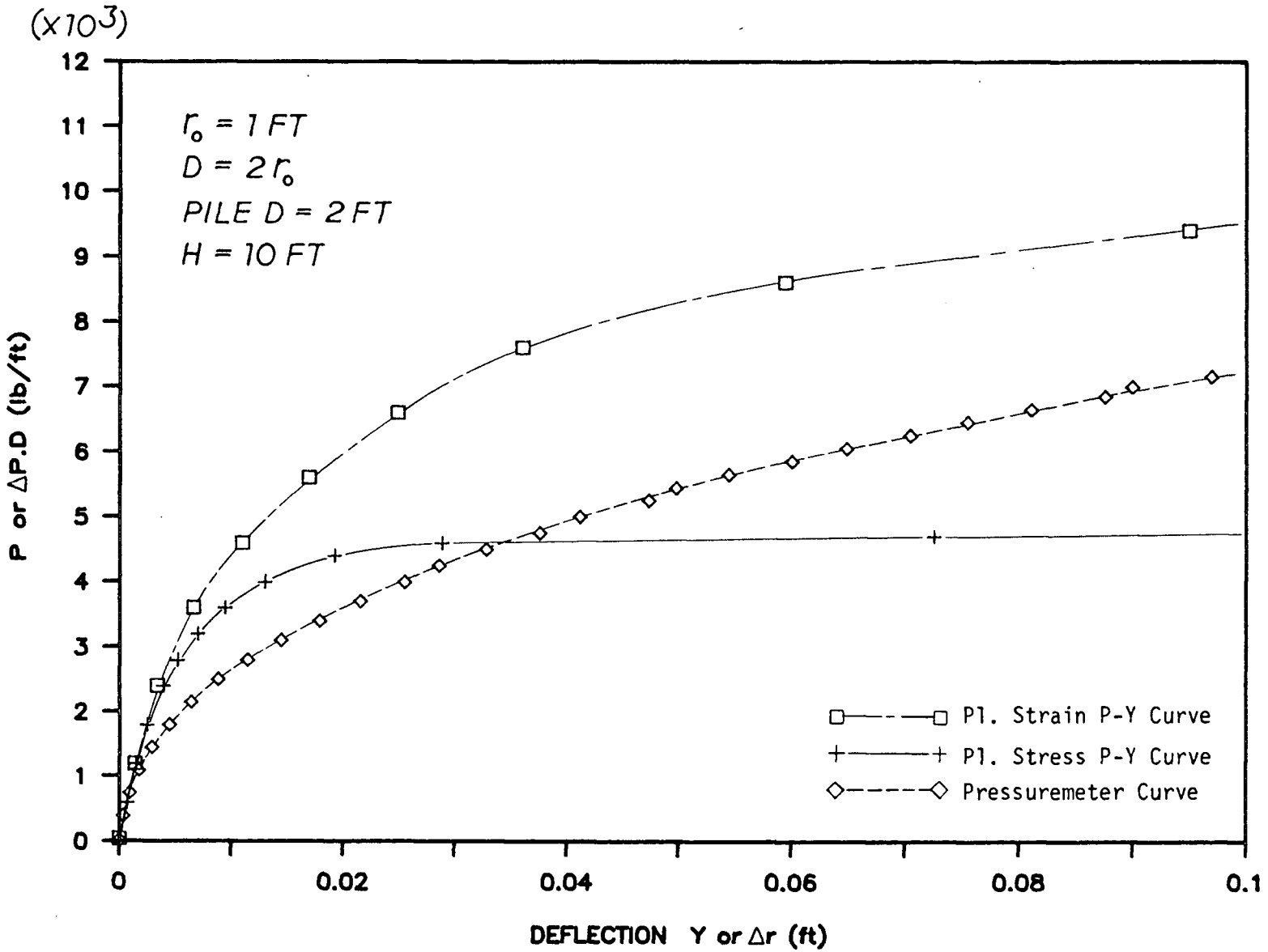

FIGURE 11.4: COMPARISON OF PRESSUREMETER AND P-Y CURVES FOR DENSE SAND

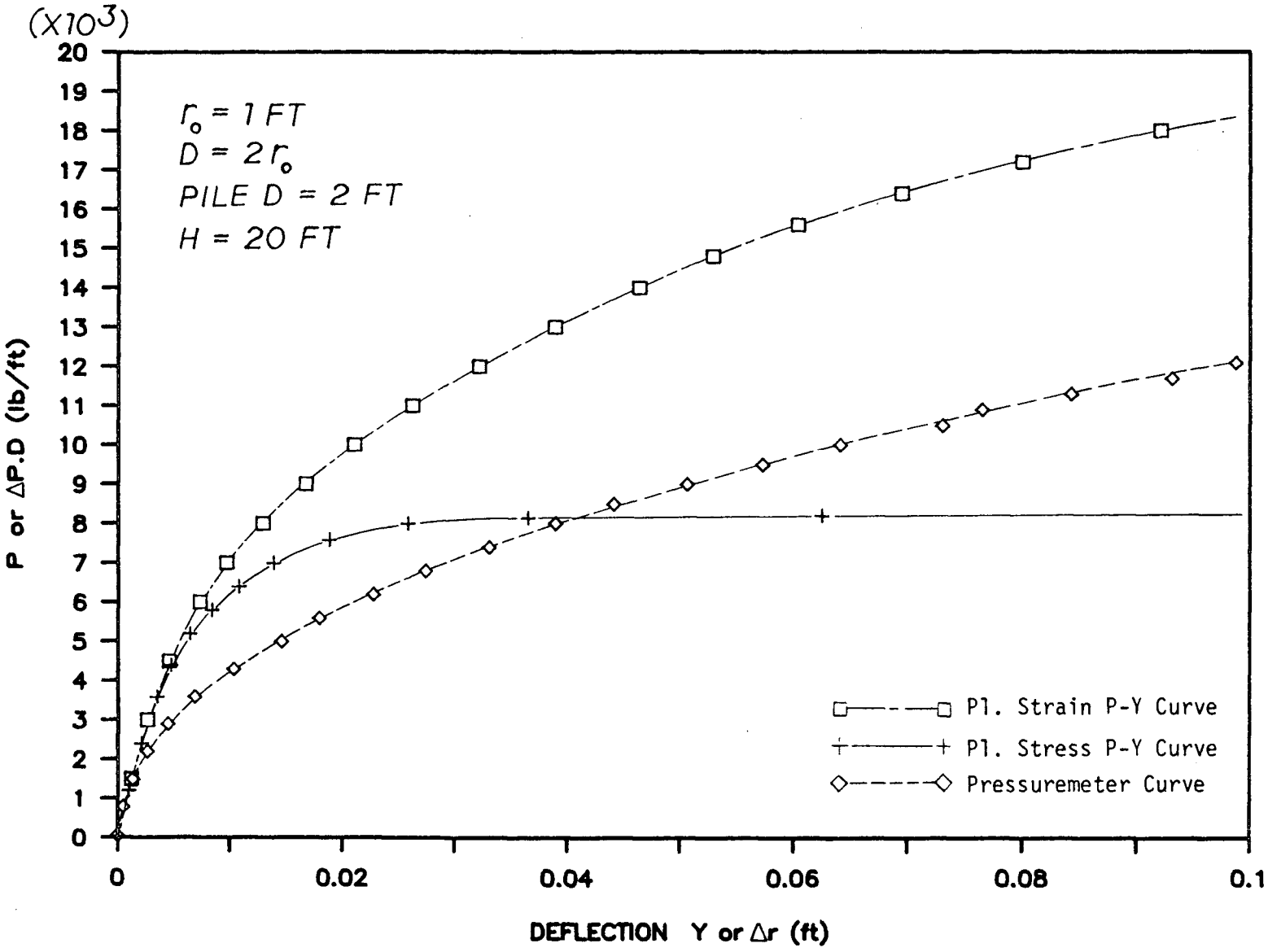

FIGURE 11.5: COMPARISON OF PRESSUREMETER AND P-Y CURVES FOR DENSE SAND

curves, an arbitrary reference value, P_{10}, corresponding to a strain of 10%, was selected. P_{10} values of 3625 Psf and 6075 Psf were estimated from the 10-ft and 20-ft curves shown in Figure 8.2. Fully normalized pressuremeter curves are thus given by plots of $\Delta P/P_{10}$ vs. $\Delta r/D$. The normalized curves are shown in Figures 11.6 and 11.7.

11.3.3.2 Conversion Factors

Factors for converting pressuremeter curves to "P-Y" curves were determined using the normalized plots. The recommended values for the conversion factors are given in Table 11.2.

The initial slopes of the normalized curves are as follows:

P-Y curves: $$\frac{P/P_{ult}}{Y/D} = \frac{1.38(2G)(D)}{P_{ult}} = \frac{2.76(2G)}{P_{ult}}$$

Pressuremeter curves: $$\frac{P/P_{10}}{r/D} = \frac{P/P_{10}}{r/2r_o} = \frac{2(2G)}{P_{10}}$$

For the values of P_{ult} and P_{10} obtained from the analyses, the conversion factors, given by the ratio of the slopes above as $1.38P_{10}/P_{ult}$, are listed in Table 11.2.

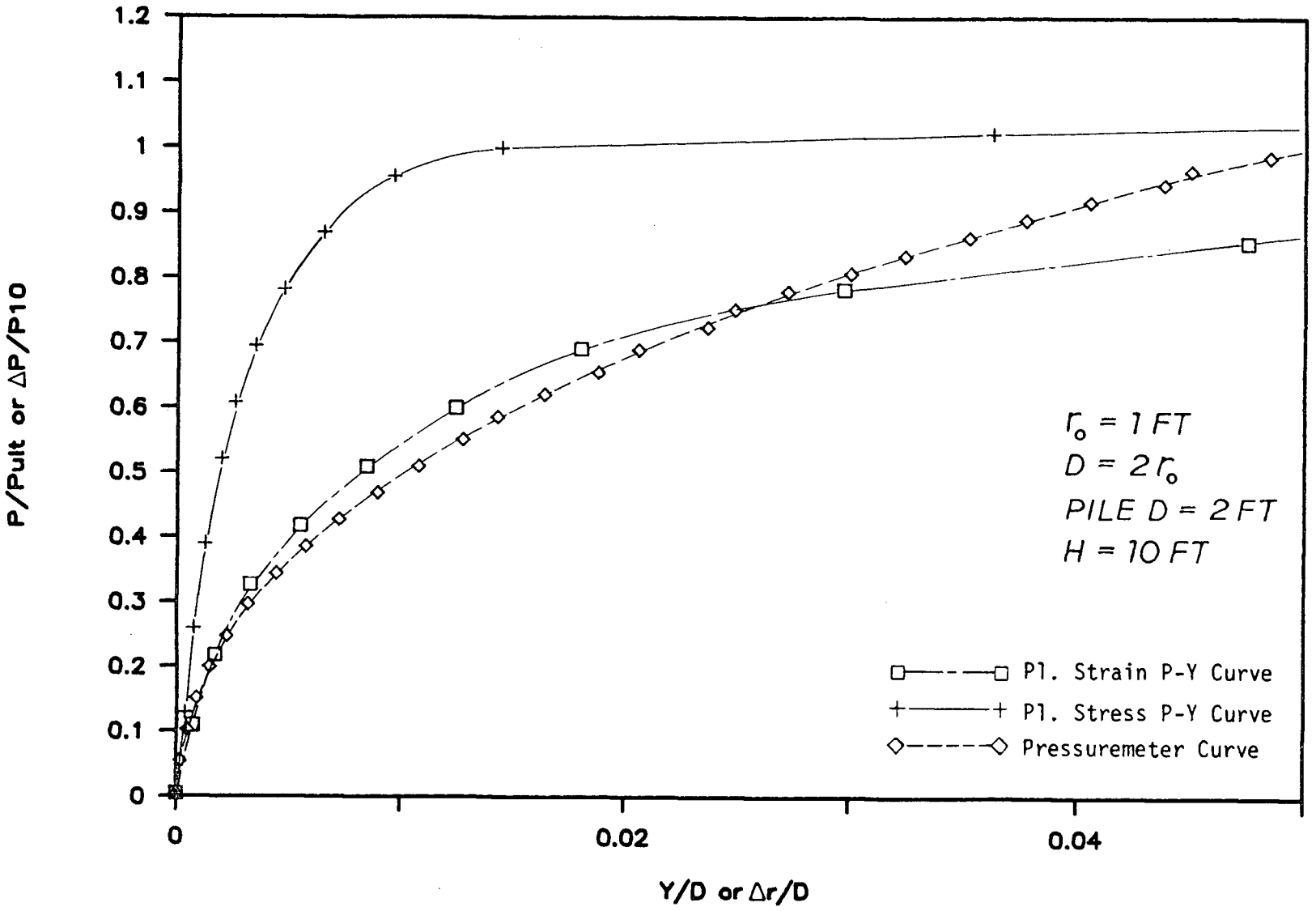

FIGURE 11.6: COMPARISON OF NORMALIZED PRESSUREMETER AND P-Y CURVES FOR DENSE SAND

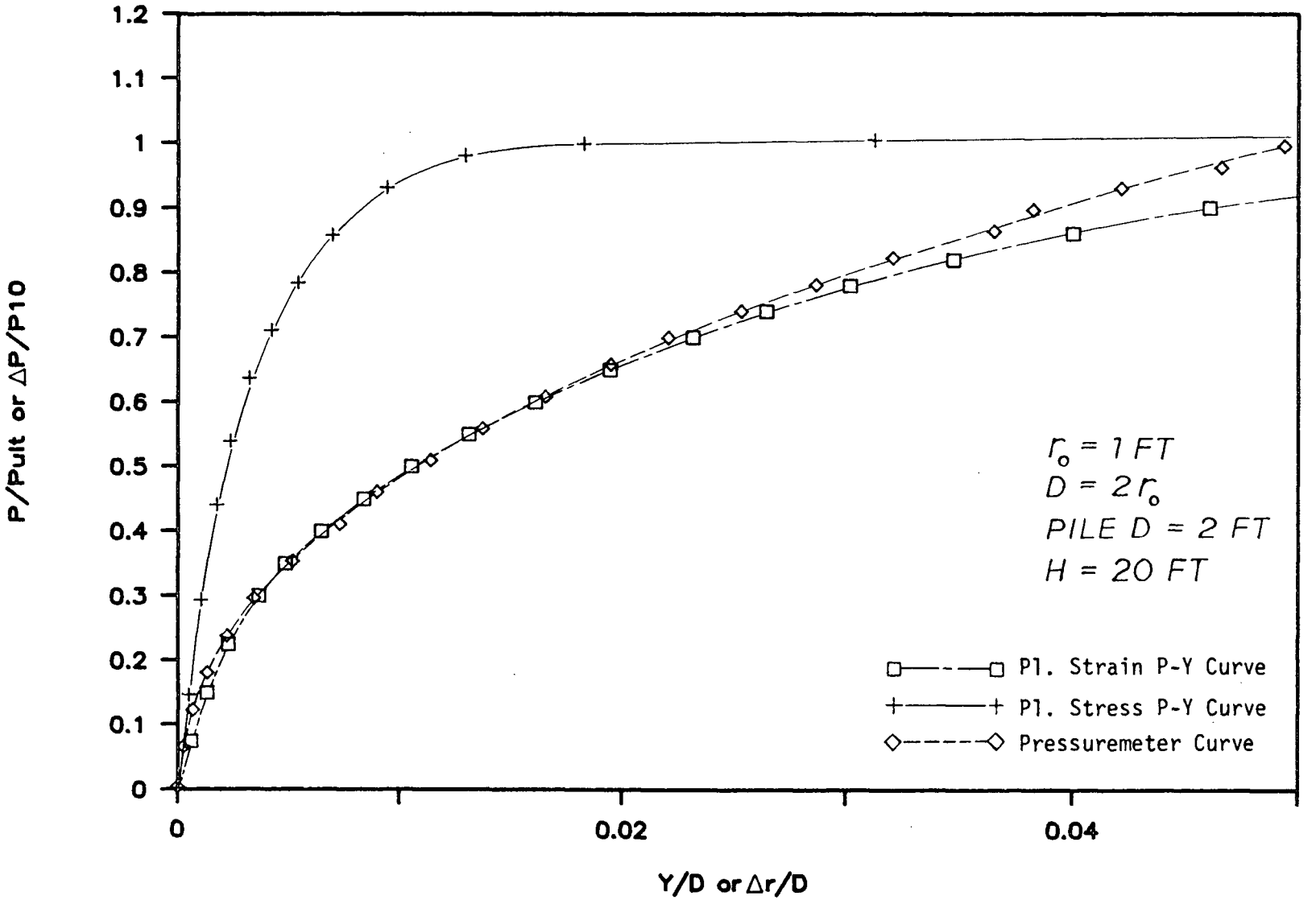

FIGURE 11.7: COMPARISON OF NORMALIZED PRESSUREMETER AND P-Y CURVES FOR DENSE SAND

TABLE 11.2

CONVERSION FACTORS FOR DENSE SAND

Y/D or	PLANE STRAIN P-Y CURVES				PLANE STRESS P-Y CURVES			
$\Delta r/D$	H=10FT	H=20FT	RECOMMENDED		H=10FT	H=20FT	RECOMMENDED	
Initial Slope	0.455	0.419	0.44		1.088	1.029	1.06	
0.002	1.057	0.909	0.98	Assume 1.00	2.216	2.091	2.15	Assume 2.15
0.004	1.085	1.000	1.04		2.233	2.202	2.22	
0.006	1.100	1.002	1.05		2.145	2.116	2.13	
0.008	1.100	1.004	1.05		2.048	2.031	2.04	
0.010	1.102	1.004	1.05		1.940	1.946	1.94	
0.015	1.081	1.000	1.04		1.679	1.700	1.69	
0.020	1.046	0.989	1.02		1.479	1.500	1.49	
0.025	1.010	0.979	0.99		1.352	1.360	1.36	
0.030	0.967	0.974	0.97		1.256	1.256	1.26	
0.035	0.932	0.966	0.95		1.182	1.179	1.18	
0.040	0.903	0.950	0.93		1.123	1.109	1.11	
0.045	0.882	0.934	0.91		1.074	1.053	1.06	
0.050	0.867	0.917	0.89		1.032	1.010	1.02	

CHAPTER 12

SUMMARY AND CONCLUSIONS

The prediction of P-Y curves based on the results of finite element analyses was examined. Methods for determining the P-Y relationships for undrained clay and sand are presented.

A new higher-ordered finite element program, CONOIL, was used in the analyses. The use of 6-noded linear strain triangular (LST) elements, coupled with the program's ability to handle Poisson's ratios as high as 0.499, permitted the accurate modelling of the undrained soil condition. Comparisons of the finite element predictions with closed form solutions for the cylindrical cavity expansion problem showed excellent agreements.

The pressuremeter problem was analysed using the plane strain formulation for cavity expansion. Pressuremeter load-deflection curves were predicted for an undrained normally-consolidated clay and a dense sand.

Having validated the finite element program's ability to model the cavity expansion problem, which bears some similarities to the laterally loaded pile situation, plane strain and plane stress P-Y curves were predicted for both undrained clay and sand. The initial slopes of the plane strain and plane stress curves were confirmed to be approximately $1.6E_i$ and $1.0E_i$, respectively, for clay, and $1.1E_i$ for sand. P_{ult} values of 12.1cD and 6.1cD were also obtained for plane strain and plane stress loading in undrained clay. The value of 12.1cD is in reasonably good agreement with the value of 10.82cD obtained from plasticity theory. P_{ult} for sand was shown to be

fractions of the theoretical values determined from assumed failure mechanisms. Normalized plots of the P-Y relationships, P/cD vs. Y/D for clay, and P/P_{ult} vs. Y/D for sand, were also shown to reduce families of curves for all pile diameters (D) and soil depths to unique curves for each of the plane strain and plane stress conditions.

Finite element results for the pressuremeter and laterally loaded pile problems were also compared. Scaling factors were determined from the comparison of normalized curves to convert pressuremeter curves to P-Y curves. Factors ranging from 1.70 to 2.72 were obtained for plane strain curves, and 1.12 to 1.66 for plane stress curves for undrained clay. For dense sand, conversion factors of 0.89 to 1.00 were determined for plane strain P-Y curves, and 1.02 to 2.15 for plane stress curves.

BIBLIOGRAPHY

Atukorala, U., and Byrne, P.M., "Prediction of P-Y Curves from Pressuremeter Tests and Finite Element Analyses", Soil Mechanics Series No. 66, Dept. of Civil Eng., U.B.C., July, 1984

Baguelin, F., Frank, R., and Said, Y.H., "Theoretical Study of Lateral Reaction Mechanism of Piles", Géotechnique, Vol. 27, No. 3, Sept., 1977, pp. 405-434

Barton, Y.O., Finn, W.D.L., Parry, R.G.H., and Towhata, I., "Lateral Pile Response and P-Y Curves from Centrifuge Tests", Proceedings, 15th O.T.C., Houston, Texas, 1983, Vol. 1, pp. 503-508

Briaud, J.-L., Smith, T.D., and Meyer, B.J., "Using the Pressuremeter Curve to Design Laterally Loaded Piles", Proceedings, 15th O.T.C., Houston, Texas, 1983, Vol. 1, pp. 495-502

Broms, B.B., "Lateral Resistance of Piles in Cohesive Soils", JSMFD, ASCE, Vol. 90, SM2, March, 1964, pp. 27-63

Byrne, P.M., and Cheung, H., "Soil Parameters for Deformation Analysis of Sand Masses", Soil Mechanics Series No. 81, Dept. of Civil Eng., U.B.C., June, 1984

Byrne, P.M., and Eldridge, T.L., "A Three Parameter Dilatant Elastic Stress-Strain Model for Sand", Proceedings, International Symposium on Numerical Models in Geomechanics, Rotterdam, Sept., 1982, pp. 73-80

Byrne, P.M., and Grigg, R.F., "OILSTRESS: A Computer Program for Nonlinear Analysis of Stresses and Deformations in Oilsands", Soil Mechanics Series No. 42, Dept. of Civil Eng., U.B.C., July, 1980

Byrne, P.M., and Grigg, R.F., "Documentation for LATPILE.G", Civil Engineering Program Library, Dept. of Civil Eng., U.B.C., 1982

Byrne, P.M., Vaid, Y.P., and Samarasekera, L., "Undrained Deformation Analysis Using Path Dependent Material Properties", Soil Mechanics Series No. 58, Dept of Civil Eng., U.B.C., May, 1982

Campanella, R.G., and Robertson, P.K., "Applied Cone Research", Soil Mechanics Series No. 46, Dept. of Civil Eng., U.B.C., May, 1981

Craig, R.F., Soil Mechanics, 2nd ed., Van Nostrand Reinhold Co., New York, 1978

Denby, G.M., "Self-Boring Pressuremeter Study of the San Francisco Bay Mud", Ph.D. Thesis, Dept of Civil Eng., Stanford University, California, July, 1978

Duncan, J.M., Byrne, P.M., Wong, K.S., and Mabry, P., "Strength, Stress-Strain and Bulk Modulus Parameters for Finite Element Analysis of Stresses and Movements in Soil Masses", Report No. UCB/GT/80-01, Dept. of Civil Eng., Univ. of Calif., Berkeley, Aug. 1980

Duncan, J.M., and Chang, C.Y., "Nonlinear Analysis of Stress and Strain in Soils", JSMFD, ASCE, Vol. 96, SM5, Sept., 1970, pp. 1629-1653

Eldridge, T.L., "Pressuremeter Tests in Sand: Effects of Dilation", M.A.Sc. Thesis, Dept. of Civil Engineering, U.B.C., Feb., 1983

Focht, J.A., Jr., and McClelland, B., "Analysis of Laterally Loaded Piles by Difference Equation Solution", The Texas Engineer, Texas Section, ASCE, 1955

Gibson, R.E., and Anderson, W.F., "In-Situ Measurement of Soil Properties with the Pressuremeter", Civil Eng. and Public Works Review, Vol. 56, No. 658, May, 1961, pp. 615-618

Goodman, R.E., Taylor, R.L., and Brekke, T.L., "A Model for the Mechanics of Jointed Rock", JSMFD, ASCE, Vol. 94, SM3, May, 1968, pp. 637-659

Hughes, J.M.O., "Pressuremeter Testing", Lecture Notes for C.E. 577, Dept. of Civil Eng., U.B.C., Nov., 1979

Hughes, J.M.O., Wroth, C.P., and Windle, D., "Pressuremeter Tests in Sand", Géotechnique, Vol. 27, No. 4, Dec., 1977, pp. 455-477

Janbu, N., "Soil Compressibility as Determined by Oedometer and Triaxial Tests", Proceedings, European Conference on Soil Mechanics and Foundation Engineering, Wiesbaden, Germany, Vol. 1, 1963, pp. 19-25

Matlock, H., "Correlations for Design of Laterally Loaded Piles in Soft Clay", Proceedings, 2nd OTC, Houston, Texas, 1970, Vol. 1, pp. 577-594

Peck, R.B., Hanson, W.E., and Thornburn, T.H., Foundation Engineering, 2nd ed., John Wiley & Sons, New York, 1974

Potyondy, J.G., "Skin Friction Between Various Soils and Construction Materials", Géotechnique, Vol. 11, No. 4, Dec., 1961, pp. 339-353

Pyke, R., and Beikae, M., "A New Solution for the Resistance of Single Piles to Lateral Loading", ASTM, STP 835, 1984, pp. 3-20

Randolph, M.F., and Houlsby, G.T., "The limiting Pressure on a Circular Pile Loaded Laterally in Cohesive Soil", Géotechnique, Vol. 34, No. 4, Dec., 1984, pp. 613-623

Reese, L.C., Discussion on "Soil Modulus for Laterally Loaded Piles", by McClelland, B., and Focht, J.A., Jr., Transactions, ASCE, Vol. 123, 1958, pp. 1071-1074

Reese, L.C., "Laterally Loaded Piles: Program Documentation," JGED, ASCE, Vol. 103, GT4, April, 1977, pp. 287-305

Reese, L.C., Cox, W.R., and Koop, F.D., "Analysis of Laterally Loaded Piles in Sand", Proceedings, 6th OTC, Houston, Texas, 1974, Vol. 2, pp. 459-472

Reese, L.C., Cox, W.R., and Koop, F.D., "Field Testing and Analysis of Laterally Loaded Piles in Stiff Clay", Proceedings, 7th OTC, Houston, Texas, 1975, Vol. 2, pp. 671-690

Reese, L.C., and Sullivan, W.R., "Documentation of Computer Program COM624", Dept. of Civil Eng., Univ. of Texas, Austin, 1980.

Robertson, P.K., "In-Situ Testing of Soil With Emphasis on Its Application to Liquefaction Assessment", Ph.D. Thesis, U.B.C., December, 1982

Robertson, P.K., Campanella, R.G., Brown, P.T., Grof, I., and Hughes, J.M.O., "Design of Axially and Laterally Loaded Piles Using In-Situ Tests: A Case History", Preliminary Draft, May, 1985

Robertson, P.K., Hughes, J.M.O., Campanella, R.G., and Sy, A., "Design of Laterally Loaded Displacement Piles Using a Driven Pressuremeter", Soil Mechanics Series No. 67, Dept. of Civil Eng., U.B.C., May, 1983

Scott, R.F., Foundation Analysis, Prentice-Hall Inc., Englewood Cliffs, N.J., 1981

Stevens, J.B., and Audibert, J.M.E., "Re-Examination of P-Y Curve Formulations", Proceedings, 11th OTC, Houston, Texas, 1979, Vol. 1, pp. 397-403

Terzaghi, K., and Peck, R.B., Soil Mechanics in Engineering Practice, 2nd ed., John Wiley & Sons, New York, 1967

Thompson, G.R., "Application of the Finite Element Method to the Development of P-Y Curves for Saturated Clays", M.S. Thesis, Univ. of Texas, Austin, May, 1977

Vaid, Y.P., "Effect of Consolidation History and Stress Path on Hyperbolic Stress-Strain Relations", Soil Mechanics Series No. 54, Dept. of Civil Eng., U.B.C., Dec., 1981

Vaziri, H., Ph.D. Thesis, Dept. of Civil Eng., U.B.C., 1985

Yan, L., Forthcoming M.A.Sc. Thesis, Dept. of Civil Eng., U.B.C., 1986

Yegian, M., and Wright, S.G., "Lateral Soil Resistance-Displacement Relationships for Pile Foundations in Soft Clays", Proceedings, 5th OTC, Houston, Texas, 1973, Vol. 2, pp. 663-676

APPENDIX A

DERIVATION OF STRESS-STRAIN RELATIONSHIPS FOR UNIAXIAL LOADING

A.1 PLANE STRAIN CONDITION

The general stress-strain relationship for soil is given by the equations

$$\varepsilon_y = \frac{\sigma_y - \mu\sigma_x - \mu\sigma_z}{E_s} \qquad \text{A.1a}$$

$$\varepsilon_z = \frac{\sigma_z - \mu\sigma_x - \mu\sigma_y}{E_s} \qquad \text{A.1b}$$

where

μ = Poisson's ratio

E_s = secant elastic modulus

For plane strain analyses, $\varepsilon_z = 0$. Hence,

$$\sigma_z = \mu(\sigma_x + \sigma_y) \qquad \text{A.2}$$

Using σ and ε to represent changes in stress and strain, $\sigma_x = 0$ for the uniaxial loading condition considered (see Figure 6.1). Therefore,

$$\sigma_z = \mu\sigma_y \qquad \text{A.3}$$

and

$$\varepsilon_y = \frac{\sigma_y - \mu(\mu\sigma_y)}{E_s} = \frac{\sigma_y(1 - \mu^2)}{E_s} \qquad \text{A.4}$$

For a homogeneous, isotropic non-linear elastic material, μ varies with the elastic (E) and bulk (B) modulii according to

$$\mu = \frac{3B - E}{6B} \qquad \text{A.5}$$

Substituting E_s for E,

$$1 - \mu^2 = \frac{(9B - E_s)(3B + E_s)}{36B^2} \qquad \text{A.6}$$

Finally,

$$\varepsilon_y = \frac{(9B - E_s)(3B + E_s)}{36B^2 E_s} \sigma_y \qquad \text{A.7}$$

In the hyperbolic stress-strain model for soil given by Duncan & Chang (1970), the secant elastic modulus can be expressed as

$$E_s = E_i[1 - R_f(\sigma_d/\sigma_{df})] \qquad \text{A.8}$$

where

E_i = initial elastic modulus

R_f = failure ratio

σ_d = deviator stress = σ_y for uniaxial loading in the Y-direction

σ_{df} = deviator stress at failure

The initial elastic modulus given by Janbu (1963) is

$$E_i = k_E P_a (\sigma_3/P_a)^n \qquad \text{A.9}$$

where

k_E = elastic modulus number

n = elastic modulus exponent

P_a = reference pressure = atmospheric pressure = 2116.2 Psf

σ_3 = minor principal stress

And lastly, according to the Mohr-Coulomb failure criterion,

$$\sigma_{df} = \frac{2c \cos\phi + 2\sigma_3 \sin\phi}{1 - \sin\phi} \qquad \text{A.10}$$

For undrained clay, $\phi = 0$ and $n = 0$. Equations A.9 and A.10 reduce to

$$E_i = k_E P_a \qquad \text{A.9a}$$

and $$\sigma_{df} = 2c \qquad \text{A.10a}$$

For sand, $c' = 0$ and

$$\sigma_{df} = \frac{2\sigma_3' \sin\phi'}{1 - \sin\phi'} \qquad \text{A.10b}$$

The complete stress-strain relationship for the plane strain uniaxial loading condition is therefore given by Equations A.7 to A.10

A.2 PLANE STRESS CONDITION

The derivation of the stress-strain relationship for plane stress loading is similar to that of the plane strain condition. Using the same general stress-strain equation as before,

$$\varepsilon_y = \frac{\sigma_y - \mu\sigma_x - \mu\sigma_z}{E_s} \qquad \text{A.1a}$$

For the plane stress condition, $\sigma_z = 0$, and for uniaxial loading, $\sigma_x = 0$, and $\sigma_d = \sigma_y$. Therefore,

$$\varepsilon_y = \frac{\sigma_y}{E_s} = \frac{\sigma_y}{E_i[1 - R_f(\sigma_y/\sigma_{df})]} \qquad \text{A.11}$$

E_i and σ_{df} are as given by Equations A.9 and A.10.

APPENDIX B

EMPIRICAL P-Y CURVES

B.1 MATLOCK'S EMPIRICAL CURVES FOR CLAY

The empirical curves shown in Figures 9.2 and 9.3 were determined according to the method proposed by Matlock (1970) for static loading of single piles. The curves are defined by two parameters, P_{ult} and Y_c, given by

$$P_{ult} = N_p cD \ , \quad N_p = 3 + \sigma_v'/c + J\,H/D \qquad \text{B.1}$$

and

$$Y_c = 2.5\,\varepsilon_{50} D \qquad \text{B.2}$$

The value of N_p lies between 3 and 9.

Using recommended values of $\varepsilon_{50} = 0.010$ and $J = 0.35$ for the soil properties used in the finite element analyses (Table 9.1), the following values were determined for a pile diameter of 2 feet:

Depth H (ft)	N_p	P_{ult} (lb/ft)	Y_c (ft)
2	7.35	448	0.05
5	7.88	1202	0.05
10	8.75	2669	0.05
20	9.00	5490	0.05
40	9.00	10980	0.05

The empirical curve, as defined by the above parameters, is shown in Figure B.1. The equation for the curved portion of the P-Y

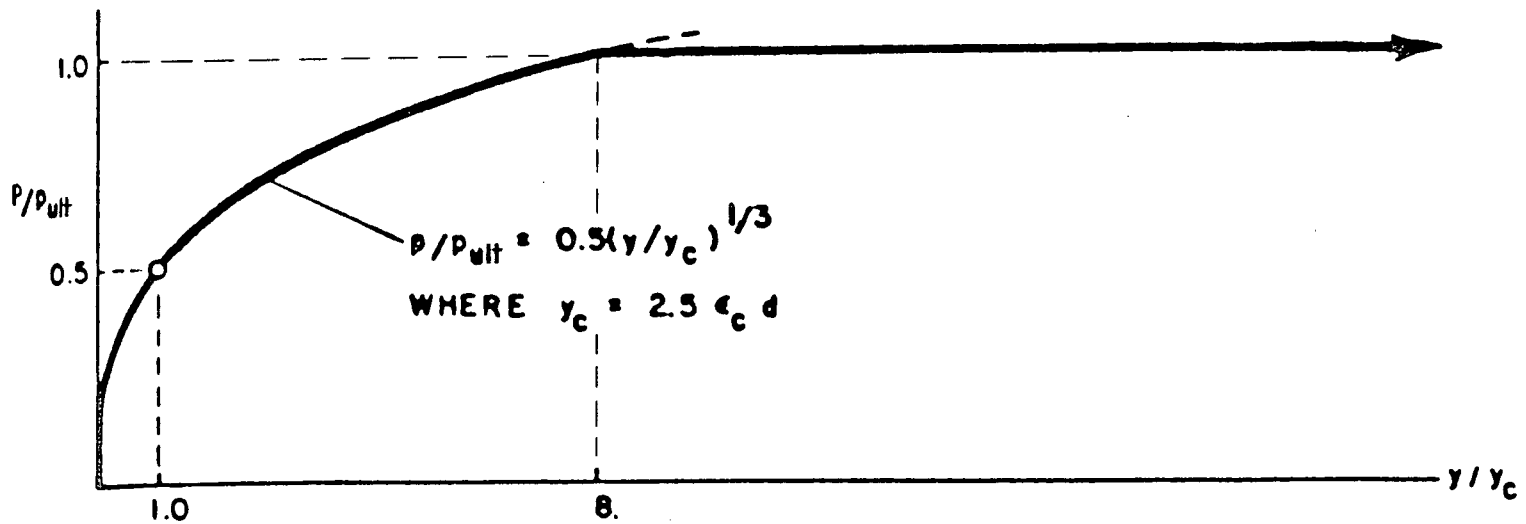

FIGURE B.1: MATLOCK'S EMPIRICAL P-Y CURVE FOR STATIC LOADING OF PILES IN UNDRAINED CLAY

(After Matlock, 1970, p. 591)

relationship is

$$P/P_{ult} = 0.5(Y/Y_c)^{0.333} \qquad \text{B.3}$$

B.2 REESE'S EMPIRICAL CURVES FOR SATURATED SAND

The empirical P-Y curves shown in Figures 9.8 and 9.9 were determined according to the method recommended by Reese at al. (1974) for static loading of single piles.

The curves are defined by three points, k, m, and u, as shown in Figure B.3. Point u is given by

$$P_u = P_{ult} = A\ P_c \qquad \text{B.4}$$

where P_c is the theoretical ultimate soil resistance determined according to Equation 2.2 or 2.3. The smaller of the two values is used. Values for the adjustment factor, A, determined by comparing theoretical values with experimental results, are given in Figure B.2a. The corresponding deflection at point u is 3D/80.

Point m is given by

$$P_m = B\ P_c \qquad \text{B.5}$$
$$Y_m = D/60$$

Values for B were also determined experimentally and are given in Figure B.2b.

Point k is defined by the intersection of the initial linear segment and the parabolic portion of the P-Y relationship. The

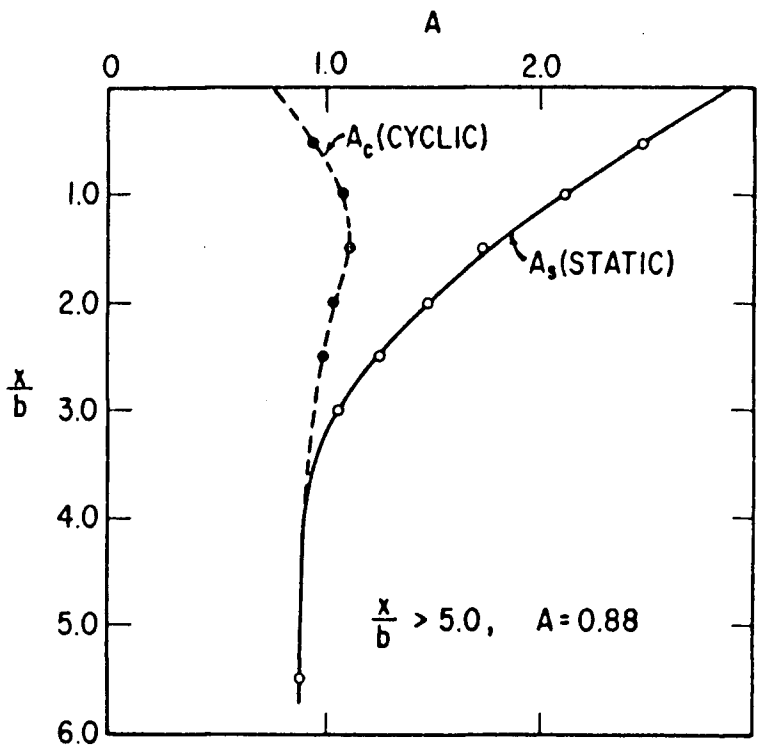

a) Non-Dimensional Coefficient A for Ultimate Soil Resistance

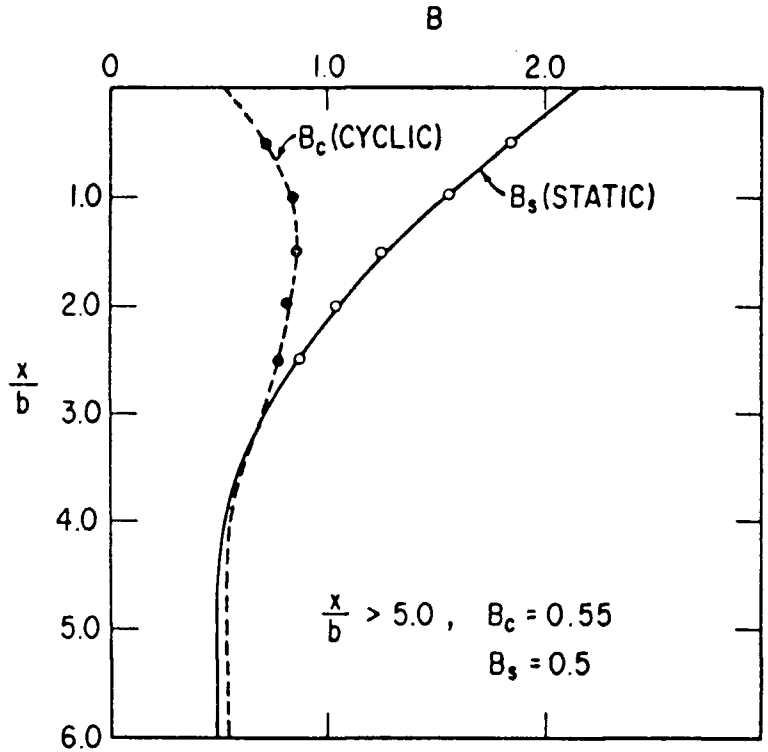

b) Non-Dimensional Coefficient B for Soil Resistance

Note: x = depth
b = pile diameter

FIGURE B.2: NON-DIMENSIONAL COEFFICIENTS FOR SOIL RESISTANCE

(After Reese et al., 1974, p. 482)

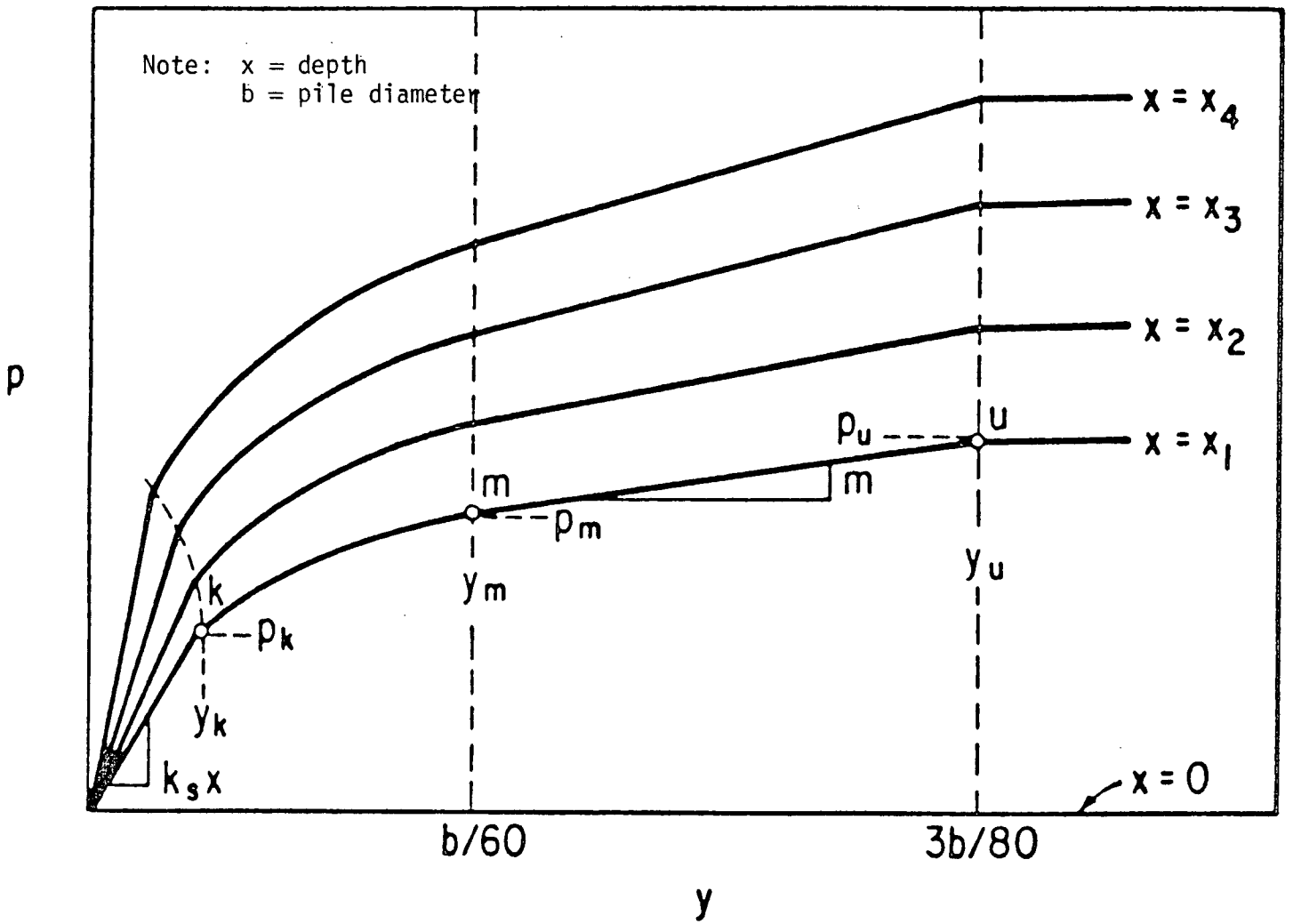

FIGURE B.3: EMPIRICAL P-Y CURVES FOR STATIC LATERAL LOADING OF PILES IN SATURATED SAND

(After Reese et al., 1974, p. 482)

equation of the parabola is

$$P = C\ Y^{1/n} \qquad \text{B.6}$$

$$n = P_m/mY_m$$

$$C = P_m/Y_m^{\ 1/n}$$

m = slope of line between points m and u

$$= (P_u - P_m)/(Y_u - Y_m)$$

The slope of the initial portion of the curve is k_sH. Values recommended for k_s are 20, 60, and 125 lb/in^3 for loose, medium, and dense sand, respectively.

Using the soil properties listed in Table 9.2 for the dense sand, values for P_c were calculated:

Depth H (ft)	P_{ct} (Eq.2.2) (lb/ft)	P_{cd} (Eq.2.3) (lb/ft)	A	B
2	3033	--	2.13	1.55
5	12217	98105	1.25	0.87
10	38426	170467	0.88	0.50
20	128448	286834	0.88	0.50
40	--	484331	0.88	0.50

Values for A and B estimated from Figure B.2 for a pile diameter of 2 feet are also tabulated above. The P-Y curves determined from the above equations are shown in Figures 9.8 and 9.9.